WERF

Water Environment Research Foundation
Collaboration. Innovation. Results.

Conveyance Systems

FINAL REPORT

Assessment of Grease Interceptor Performance

(Supplemental Report to 03-CTS-16T)

Co-published by

IWA
Publishing

03-CTS-16TA

ASSESSMENT OF GREASE INTERCEPTOR PERFORMANCE

Supplemental Report to 03-CTS-16T

by:

Joel J. Ducoste
North Carolina State University

Kevin M. Keener
Purdue University

John W. Groninger
Southern Illinois University

Leon M. Holt
Town of Cary

2008

WERF

WERF

ACKNOWLEDGEMENTS

Report Preparation

Principal Investigators:
Joel J. Ducoste, Ph.D., *North Carolina State University*
Kevin M. Keener, Ph.D., *Purdue University*
John W. Groninger, Ph.D., *Southern Illinois University*

Project Subcommittee

Mary Lappin, P.E. RC Liaison, *Kansas City Water Services Department*
Mark Kawamoto, P.E. PSC Chair, *Orange County Sanitation District*
Philip Friess, *County Sanitation Districts of Los Angeles County*
Gayle Tupper, *East Bay Municipal Utility District*
Kevin Sherman, *Florida Onsite Wastewater Association*
Hugh T. Garrison, *Metro Water Services, Nashville*
Charles Vanderlyn, P.E., *U.S. EPA*

Steering Subcommittee

Frank Brockman, *Cobb County*
Ben Horenstien, *East Bay Municipal Utilities District*
Mike Dunbar, *South Coast Water District*
John Redner, PE, *County Sanitation Districts of Los Angles County*
Jim Peters, PE, DEE, *Florida Water Environment Association Utility Council*
Quyen Tram, PE, *Toho Water Authority*
Brian Wheeler, *Toho Water Authority*
Nick Arhontes, PE *Orange County Sanitation District*
Terrie Mitchell, *Sacramento Regional County Sanitation District*
Drew Mihocko, *City of Philadelphia Water Department*
Tim McKim, PE, *Reedy Creek Energy Services*
Adel Hagekhalil, *City of Los Angeles*
Christine Mikulice, *County of San Francisco Water Pollution Control*
Gail Chester, Ph.D., PE, *Central Contra Costa Sanitary District*
Brett Goodman, *Gainesville Regional Utility*
Rick Oliver, *Jensen Precast*

Water Environment Research Foundation

Director of Research   Daniel M. Woltering, Ph.D.
Senior Program Director: Amit Pramanik, Ph.D., BCEEM
Program Director: Lauren Fillmore
Program Manager: Jane Casteline

WERF

Abstract:

Fat, oil, and grease (FOG) is generated everyday by food preparation and cleaning activities conducted at commercial establishments and, on a smaller scale, by residential sewer usage. FOG accumulations in the sanitary sewer collection system result in reduced capacity that may lead to sanitary sewer overflows (SSO) if not periodically removed. The primary means of controlling FOG blockages is to capture and retain FOG materials before discharge into sewer systems through the use of passive grease interception devices.

Limited scientific studies have evaluated the performance of these devices. Many claims of enhanced performance made by manufacturers of grease and oil interception devices need to be verified by objective and unbiased research protocols. This report presents the evaluation of field grease interceptors through their separation and cleaning cycles. In addition, researchers performed controlled laboratory scale grease interceptor tests and numerical simulations to assess removal efficiency by grease interceptors (GI) at different residence times and under different geometric configurations

Numerical simulations included a 3-D multi-phase flow model of a grease interceptor to evaluate design changes, and operation and maintenance conditions on the removal of FOG from foodservice waste streams. The results from experimental tests performed on lab-scale grease interceptors were used to validate the model results.

Benefits:

♦ Determines the optimal design, sizing, and operations and maintenance criteria for grease interceptors to help control problems with FOG in centralized and decentralized systems.

♦ Develops an alternative design methodology for grease interceptors that can be submitted to the International Association of Plumbing & Mechanical Officials (IAPMO) for consideration for inclusion into the Uniform Plumbing Code (UPC).

Keywords: Fats, oils, grease, FOG, grease interceptors, residence time, scouring, accumulation, performance, percent removal, globule, droplet size.

TABLE OF CONTENTS

WERF

LIST OF FIGURES

WERF

EXECUTIVE SUMMARY

Objectives:

♦ Determine the optimal design, sizing, and operations and maintenance (O&M) criteria for grease interceptors to help control problems with FOG in sewer collection systems.

♦ Propose an alternative grease interceptor design methodology that can be submitted to the International Association of Plumbing & Mechanical Officials (IAPMO) for consideration for inclusion into the Uniform Plumbing Code (UPC).

Current Situation

Currently, federal regulations require municipal utility and sewer collection entities to properly manage, operate, and maintain the collection system (40CFR 122.41(e)). Because of the severity of the FOG problem, cities, states, and the U.S. Environmental Protection Agency (U.S. EPA) regulate the discharge of oil and grease into sanitary sewer collection and treatment systems. The prevention of FOG blockages is a primary focus of many capacity management operations maintenance (CMOM) regulations. Since no past research has examined the effectiveness of technologies—such as grease interceptors—to prevent blockages, control of these blockages has been difficult.

Performance of Field Grease Interceptors

Researchers performed a significant number of tests on field grease interceptors to characterize the food service establishment (FSE) waste stream flow rate, FOG and solids layer thickness, and bulk temperature profile. Researchers performed these tests with different inlet tee configurations. Flow measurements at several grease interceptors suggest that more than 90% of the flow range fell below 10 gallons per minute (gpm) with the exception of three restaurants, which fell below 20 gpm. Grease interceptor sizes at these measurement sites varied between 1000 to 2000 gallons. These results suggest that the FSE waste stream experiences long average residence times, exceeding 2 hours, albeit under highly intermittent influent flow conditions. The ratio of the 90% flow rate from the cumulative distribution curve to the maximum recorded flow rate was found to be 1/3 for 70% of the sampled restaurants. Alternate inlet tee configurations displayed inconsistent accumulation of FOG and solids in the first and second compartments of the grease interceptor. Researchers found an increased accumulation of FOG and solids in the first compartment when the distributed inlet tee was used, since it allows for lower inlet jet velocity and possibly better solids and FOG separation performance. However, transport of FOG between compartments occurred with some cases displaying a high degree of FOG accumulation in the second compartment.

The shift in FOG layer thickness from compartment 1 to 2 is likely a temperature-driven event causing a buoyant plume to occur between the measurement periods. This buoyant plume would not significantly influence the solids layer. These observations suggest that interceptors

are highly dynamic, transferring FOG and solids between the first and second compartment (and likely out of the system) quite frequently between cleanings. Solids and FOG loading to an interceptor should be monitored, as standard cleaning cycles may not be sufficient. In addition, any flow condition that may impact the FOG layer, such as high temperature discharge from dishwashers, should be cooled to the temperature of the bulk grease interceptor to reduce the potential for buoyant plumes.

Analysis and Design of Grease Interceptors

In this study, the removal of the baffle wall from the standard configuration resulted in a six percent increase in performance. Currently, design guidelines for grease interceptors (IAPMO, 2004; NPCA, 2007) suggest the use of at least one baffle wall configuration, citing improved grease separation. As the results of the experimental work suggest, the inclusion of the baffle wall may produce detrimental results. In the no-baffle straight-pipe configurations, removing the baffle wall improved performance. The improved performance is not universal, however, as the distributive inlet configuration with no baffle displayed a significant decrease in performance (69% removal) compared to the inclusion of the baffle wall (87% removal).

Shifts in the flow pattern as a result of the distributive style inlet resulted in a poorer performing grease interceptor. Examination of the velocity vectors for the distributive configuration using computational fluid dynamics (CFD) simulations revealed high local velocities along the walls of the grease interceptor in the first compartment. This high near wall velocity continued all the way to the outlet unless a mid-baffle wall broke the velocity profile. Inclusion of the hanging baffle did not increase the performance beyond the standard no baffle, or short pipe no baffle configuration. The hanging baffle experimental results suggest that even the minor constriction resulting from the hanging baffle opening may still have a negative effect on the overall grease interceptor performance compared to the no baffle configuration.

Analysis of different inlet configurations and no mid-baffle wall indicate little difference using different lengths for the straight inlets. The results show that the distributed configuration is significantly impacted by the absence of the mid-baffle. When the distributed mid-baffle was used with distributed inlet/outlet configuration, researchers found comparable removal results with the standard configuration or short inlet configuration without a mid-baffle wall. The results of tests performed with the standard configuration at two residence times—20 minutes and 1 hour—suggest that a minimum residence time to achieve better than 80% removal is 20 minutes. Better than 90% removal is possible with one hour detention time, but this is only a slight (10%) increase in oil removal.

The research team explored the effects of basic design modifications to "conventional" grease interceptor designs, such as the rectangular foot-print, baffled interceptor most commonly seen in the field. Mo difications, such as decreases in the inlet pipe length, the use of inlet and outlet pipe expansions, distributive tees, and other fittings, can be easily added to existing grease interceptors and may result in significant improvements. Field evidence suggests potentially enhanced first compartment FOG and solids separation with such devices.

Researchers performed numerical simulations of different grease interceptor configurations to evaluate not only the effectiveness of using these simulations to model these processes but also to explore "what if" design scenarios that may result in improved separation performance. Researchers concluded that high local velocities in the grease interceptor fluid may result in reduced separation performance. The standard grease interceptor configuration had the

WERF

poorest performance (57% predicted removal) due to high local velocities near the inlet pipe, baffle wall pipe, and outlet pipe regions, creating regions of short circuiting through the unit. Simulations performed with the flared, short inlet pipe, and distributed designs under identical residence times displayed less short circuiting and clearly allowed for greater separation (82%, 89.3%, and 96% predicted removal, respectively). As expected, the model also displayed an increase (up 20%) in separation performance with the standard configuration, when residence increased from 20 minutes to 1 hour. In addition to these designs, which were all experimentally tested, a distributed plane jet design displayed a higher percent removal (93%) compared to the standard configuration.

In general, model predictions were generally within 10% of the experimental results. Exceptions include the standard configuration (21% difference) and the distributed no baffle configuration (25% difference). The difference between the simulated and experimental distributed design is due to slight variations in the actual model configuration of the inlet pipe and the physical inlet pipe design. Currently, there is no explanation for the difference between the simulated and experimental standard configuration tests.

The numerical results of this study suggest great promise in utilizing CFD for simulating grease interceptors. Although the 3D simulations performed to date do not incorporate drop coalescence and breakup, they still display similar trends in the removal of oil from a given reactor. The absence of droplet coalescence and breakup, and the reasonable agreement between the model and experimental results, suggest that the influent size distribution is fairly stable and that these mechanisms did not significantly enhance separation with the flow field developed in the grease interceptor. Researchers need to perform more sophisticated experimental measurements to verify the importance and contribution of oil droplet coalescence and breakup in these systems.

Need for Future Research

Analytical Techniques for FOG Concentration Measurements

As an indirect outcome of this study, the FOG concentration measurement results showed that the EPA Method 1664 displayed significant variability when measuring known concentrations of total oil and grease. Variability in the measured concentration was approximately 40%, making it impossible to confirm or refute whether the grease interceptor is properly achieving the required effluent limit. Without a reliable experimental approach, it is impossible for a municipality to enforce a discharge limit. Consequently, a research study needs to develop an alternative, reliable, total oil and grease analytical measurement technique that can be performed relatively quickly, potentially at the field site.

Alternative Approaches for FOG Reduction in Grease Interceptors

The results of this study revealed that, while increases in grease interceptor removal performance can be achieved with geometric modifications to the inlet and outlet pipe configuration as well as modifications to the mid-baffle wall, FOG removal performances were still limited to approximately 80-90%. The modifications studied were limited to designs that still allowed for ease of pump out maintenance. Consequently, alternative approaches for enhancing total oil and grease removal may be necessary to help achieve better than two log removal (i.e., 99%). Other technologies that could be investigated include the generation of

micro-bubbles by super-saturation of a portion of the influent flow stream or chemical demulsifying agents.

Inclusion of Solids Modeling in CFD Simulations of Grease Interceptors

In this study, researchers performed the CFD simulations of grease interceptors with only the FOG and water phase. This was due to computational requirements of the 3D model. Actual grease interceptors also function to remove solids that are discharged along with FOG. These solids may impact the FOG removal process and change the fluid flow pattern within the grease interceptor. More advanced models should include three phases: FOG, water, and solids.

WERF

CHAPTER 1.0

INTRODUCTION

1.1 Background

Fat, oil, and grease (FOG) blockages are the primary cause in 40-50% of all sanitary system overflows (SSOs) (Southerland, 2002). Sewer collection utilities are required to properly manage, operate, and maintain the collection system (Code of Federal Regulations, 2002). Currently, the primary means of controlling FOG blockages is to capture and retain FOG materials through passive and mechanized grease interceptor devices (Figure 1-1).

The performance of these devices in real-world environments is being questioned and needs further examination. Limited scientific studies have been done evaluating these devices, and many claims of enhanced performance made in marketing strategies by manufacturers of grease and oil interception devices need to be verified by objective and unbiased research protocols. Visual observation of grease interceptors has shown numerous occurrences of hydraulic short circuiting due to either high FOG concentration discharges from the kitchen or high temperature FOG discharges. Recent discussions with a variety of grease interceptor manufacturers indicate a lack of consistency in design geometry and considerations (i.e., tank sizing variability, effect of depth, width, and length ratios). Moreover, grease interceptor manufactures were unable to support their design configurations with scientific data or research study results.
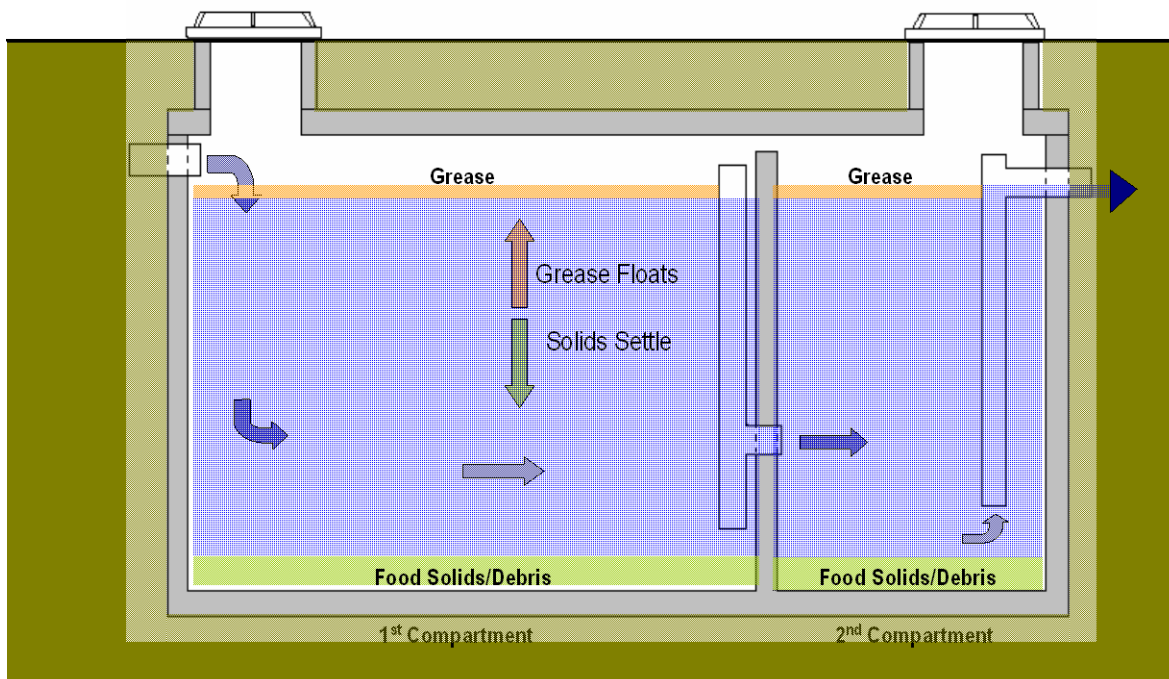
Figure 1-1. Standard Configuration of Grease Interceptor.

1.2   Significance to Wastewater Utilities

This research will greatly benefit the wastewater community by being the first to develop a link between how the influent and effluent designs impact the food solids and grease separation thickness. This research will also be the first to develop a 3-D two-phase (fat/oil and water) flow model of a grease interceptor. This model will be used to evaluate design changes, and operation and maintenance (O&M) conditions on the removal of FOG from foodservice waste. The model will be validated using a laboratory-scale grease interceptor. The results of this research will then be used to develop an alternative grease interceptor sizing methodology that can be used by the International Association of Plumbing and Mechanical Officials (IAPMO) for inclusion to the Uniform Plumbing Code (UPC).

1.3   Literature Review

1.3.1   Grease Interceptor Design

Current grease interceptor evaluations use animal fat as a test medium for finding minimum retention time. These tests do not consider that many restaurants use detergents, sanitizers, and vegetable oils. These factors can influence emulsification characteristics (e.g. droplet size) of FOG discharges, and thus influence separation efficiencies.

Per the American Society of Plumbing Engineers, "grease interceptors are sized according the volume of effluent expected, the retention time necessary for separation at the temperature of the waste, the frequency of cleaning, and the quantity of emulsified grease (ASPE, 1999). "Grease" is being referred to as a "catch-all" phrase by the utility industry for FOG and include some waxes and paraffin. Each of these categories of FOG exhibit different chemical and physical properties.

Presently, the universal plumbing standards are based solely on effluent measurements. These standards do not consider chemical composition of FOG, baffle arrangement, maintenance, and geometry criteria. For example, the Uniform Plumbing Code (UPC) requires one baffle. However, jurisdictions such as Austin, Texas recommend two baffles, citing increased grease interceptor efficiency. The geometry criterion for interceptors also varies significantly among regulating authorities. Many authorities believe length of the interceptor is more significant for separation than depth. In the case of cleaning frequency, the U.S. EPA recommends cleaning of interceptors when the volume is at 75% of maximum. However, many cities recommend cleaning frequencies between 60 and 120 days (Fankel, 2004).

Stoll and Gupta (1997) developed management strategies for FOG collection, treatment, and disposal. In their work, Stoll and Gupta mentioned that grease interceptors could achieve higher FOG and solids removal efficiencies by assuring the following:

♦ Avoid the use of emulsions, and use cleaning agents sparingly.
♦ Drain surfactant-laden food wastes only at the end of the day to provide longer periods in the grease interceptor and improve separation.
♦ Encourage intermediate machine cleaning to working surfaces and floors with hot water at high pressure, without cleaning agents, and drain scalding and boiling containers slowly after cooling first.
♦ Train and keep an eye on kitchen staff.

WERF

Although Stoll and Gupta assumed that grease interceptors have 80% separation efficiency, no research was presented or cited. Moreover, if 80% separation efficiency were realizable, it would be necessary to state the operating conditions, influent waste characteristics, and grease interceptor size.

Chu and Ng (2000) investigated the use of installing tube settlers in a traditional grease interceptor design to determine whether this design modification would enhance performance. In their research, Chu and Ng used a synthetic wastewater, which contained peanut oil and measured the amount of oil/grease and chemical oxygen demand (COD) in the effluent. Chu and Ng (2000) showed that an 8% improvement in the removal efficiency can be achieved for oil/grease with the addition of tube settlers. They also found that a 70% COD removal efficiency can be achieved with a reduction in hydraulic retention time (HRT) by 60%. The reduction in HRT was true when the overall HRT was less than 30 minutes. However, when the HRT was above 30 minutes, the addition of tube settlers did not show any significant improvement in COD removal. Moreover, Chu and Ng did not discuss the impact of tube settlers on the maintenance of grease interceptors (i.e., the periodic cleaning that is required for proper performance). The scientific literature on grease interceptors design is limited. There is a need to perform research on the design of grease interceptors.

1.3.2 Characterization of Grease Interceptor Performance

In a recent study, Lesikar et al. (2006) performed the field analysis of grease interceptors for 28 restaurants ranging in size of the restaurant, fast food versus full fare, and cuisine types. Five day biochemical oxygen demand (BOD_5), total suspended solids (TSS), FOG concentration, and flow (in the form of total gallons accumulated per day) measurements were performed for six consecutive days around the same time per day. A second set of BOD_5, TSS, FOG, and flow measurements were performed at the same sites after a two week break. All samples were collected in the grease interceptor effluent.

Lesikar et al. found higher BOD_5 and average flow values found previously in the literature. As shown in the Table 1-1, mean values for BOD_5, TSS, FOG, and flow were 1040 mg/L, 358 mg/L, 123 mg/L, and 68 L/(day-seat), respectively. A large variance was found for all the parameters measured suggesting significant variability over the operation period of the restaurants investigated. The BOD_5, TSS, and FOG variability is likely to be larger in the influent stream of the grease interceptor. However, no measurements were made in the grease interceptor influent. Moreover, Lesikar et al. made no mention of when the grease interceptor was last cleaned prior to the sampling time.

Table 1-1. Grease Interceptor Effluent Measurements (Lesikar et al., 2006).

Wastewater Parameter	Mean	Standard deviation
BOD_5 (mg/L)	1040	690
TSS (mg/L)	358	430
FOG (mg/L)	123	107
Flow (L/(seat-day))	68	39

Lesikar and coworkers (Garza et al., 2005) also investigated how these measurement parameters were influenced by the restaurant's management practices and cuisine type. In Garza et al., a multiple regression with backward elimination (MRBE) statistical analysis was used to determine the degree that the specific management practice or parameter can be used as a predictor for the change in magnitude of the grease interceptor effluent TSS, BOD_5, FOG, and

flow data. If the parameter passed the MRBE test, a follow up repeated measure analysis with stepwise elimination (RMASE) test was performed to determine the final degree of correlation between the parameter and the effluent grease interceptor measurements. The restaurant management practices were collected using a self reported survey sent out by Garza et al. Parameters that were investigated are displayed in Table 1-2. The highlighted values in Table 1-2 display the highest degree of correlation after the RMASE test.

Table 1-2. Analysis of Garza et al. (2005) Surveyed Variables Tested with MRBE and RMASE.

Parameter	Significant under MRBE (i.e. $p < 0.05$)	Significant under RMASE
After hours cleanup(AHC)	Yes	No
AHC chemicals used	Yes	No
Automatic flush fixtures	Yes	No
Buffet style facility	Yes	No
Cuisine type (Full service, Mexican, Asian, Single service, Seafood)	**Yes**	**Yes**
Food defrosting	Yes	No
Full service alcohol bar	Yes	No
Garbage disposal use	Yes	No
Ice cream/yogurt machines	Yes	No
Kitchen laundry	Yes	No
Lawn irrigation system	Yes	No
Low flow fixtures	Yes	No
Oil type (liquid)	Yes	No
Oil type (solid)	Yes	No
Self serve salad bar	**Yes**	**Yes**
Service type (full or single)	Yes	No
Self serve fountain drinks	Yes	No
Number of seats	**Yes**	**Yes**
Restaurant sq footage	Yes	No
Meals served	Yes	No
Hours of operation	Yes	No

Garza et al. results suggest that several factors provided the greatest impact on the grease interceptor effluent TSS, BOD_5, FOG, and average flow values. These factors are: cuisine type (in particular Mexican, Asian, seafood, single-service and full-service American); the operation of self service salad bars; and the number of seats. As discussed in Garza et al. (2005), the use of seat number in the sizing of grease interceptors seems appropriate due to the degree of importance from the RMASE results. In addition, Garza et al. concluded that self service salad bars are a likely source of uncontrolled patron usage of salad dressing with a range of FOG content as well as a higher disposal rate of unconsumed salad. However, no information was provided about the extent of variety that the salad bar offers (i.e., anti pasta salads, vegetable salads, range of salad dressings, meat toppings, etc.). In addition, Garza et al. (2005) did not include other variables such as detergent types and dishwashing methods, grease interceptor size and pump-out schedule, cleaning water disposal, wash and rinse water temperature, and sampling location relative to commingling of wastewater lines. Variables were not included, due

to either unreliable survey responses or being classified as not a restaurant management practice. Some or all of these unreported variables may also influence the effluent grease interceptor TSS, BOD_5, FOG and average flow values. Consequently, inappropriate conclusions may be drawn from the importance of certain parameters on the effluent grease interceptor values due to other non-evaluated parameters.

1.4　Research Scope and Objectives

This study had two specific research objectives:

1) Determine the optimal design, sizing, and operations and maintenance criteria for grease interceptors. Researchers employed experimental and numerical techniques to understand and quantify the performance of grease interceptors. They developed alternative designs using numerical models followed by physical models of the most promising alternative designs, which were tested on a laboratory scale grease interceptor. Researchers examined different theoretical residence times to quantify the increase in FOG removal performance with reactor size. In addition, they investigated the impact of temperature and detergents to determine how food service establishments' operational conditions influence the FOG removal process within grease interceptors. The research team conducted field measurements of grease interceptors to understand the dynamics of FOG separation when food solids are also discharged into the grease interceptor.

2) Develop a grease interceptor design methodology that can be submitted to the International Association of Plumbing & Mechanical Officials (IAPMO) for consideration for inclusion into the Uniform Plumbing Code (UPC). (See FOG Interceptor Design and Operation (FOGIDO) Guidance Manual, 03-CTS-16TB).

CHAPTER 2.0

MATERIAL AND METHODS

During the course of this research several field grease interceptors were observed for real-world data collection. A wide variety of tests were performed to characterize these interceptors. Below is a discussion of the experiments performed, the equipment utilized, and some of the terminology referred to with regards to field grease interceptors.

2.1   Field Measurements of Grease Interceptors

The research team made a series of flow measurements at several food service establishments (FSEs) during this project. In order to make theses measurements, a 4-6" coupling adapter was connected to an inlet pipe and a V-notch ISCO/Teledyne Flow-Poke flow measuring insert was attached to the expanded inlet and stabilized with a steel wire (Figure 2-1). The flow rates were then measured with a bubbler attached to flow meter.

Figure 2-1. V-notch ISCO/Teledyne Flow-Poke Flow Measurement Device in GI.

2.2   Assessment of FOG and Solids Profile in Field Grease Interceptors

The research team utilized a sludge judge (Figure 2-2a) to assess the rates of accumulation of both food particles and separated grease in a grease interceptor (referred to in this document as the maturation of a grease interceptor). The sludge judge is a clear acrylic pipe of approximately 1 inch diameter and approximately 6 feet long. The device is lowered into a grease interceptor until contact is made with the interceptor floor. As a result of a check valve at the bottom of the device, when the sludge judge is pulled out of the interceptor, a visualization of the grease interceptor profile at that given location is possible. The magnitude of FOG thickness was then measured from the top while food solids accumulation was measured at the bottom of

the device. Spatial variation in sample location allows for an understanding of the basic FOG and solids profile within the grease interceptor (Figure 2-2b).

The research team observed the maturation of a given interceptor by taking several sludge judge measurements throughout the interceptor volume over a period of time between, and following, scheduled grease interceptor clean outs. Researchers compared the size of the FOG and solids layers for different grease interceptor configurations and sizes, and under conditions when the food service establishment discharged waste from a food grinder.

In addition to measuring the flow and FOG thickness in field interceptors, researchers quantified FOG concentrations, pH, and dissolved oxygen (DO) at some field sites. Samples of the influent and effluent at field grease interceptors were sent to commercial laboratories for analysis with U.S. EPA Method 1664. Researchers used an Accumet[©] AP85 Portable pH meter. Samples from the sludge judge were injected into sample jars for pH measurement. The pH was measured quickly to minimize the effect of atmospheric CO_2 on pH. DO was measured in the field with a YSI 55 attached to a long rod placed at varying elevations in the field grease interceptor to obtain a DO profile.
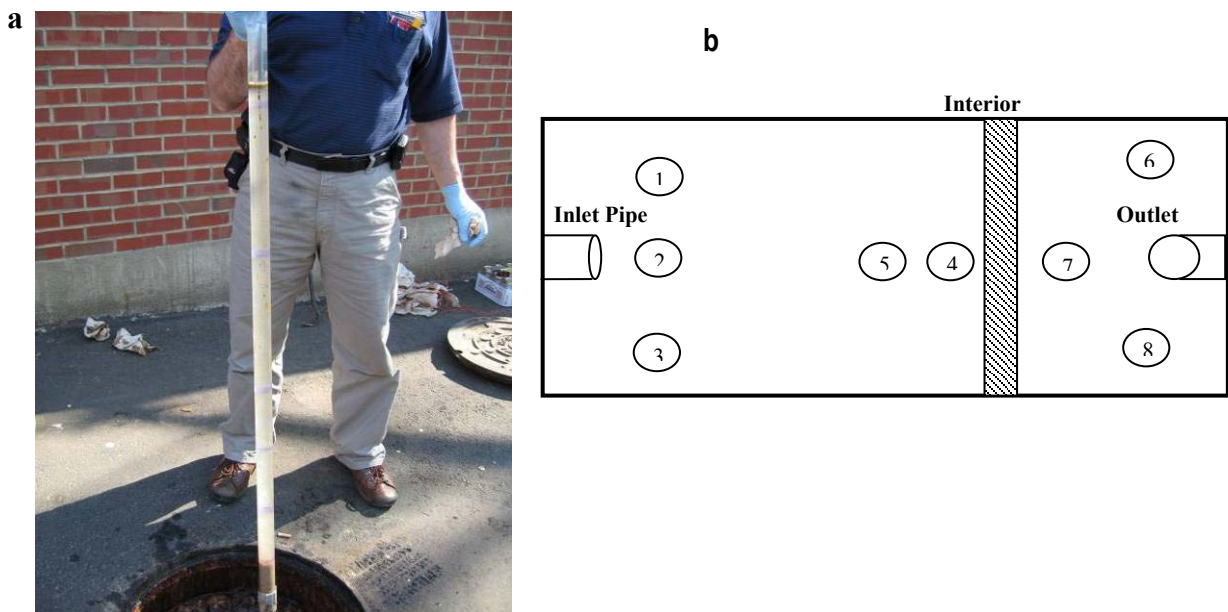
Figure 2-2. Picture of Sludge Judge Sample Locations and Sludge Judge.

2.3 Pilot Scale Grease Interceptor

The pilot scale grease interceptor is a 300-gallon fiberglass tank (Figure 2-3). The grease interceptor is configured in the lab to allow variation in influent temperature, oil concentration, and flow rate (Figure 2-4). In this research, two residence times were investigated: 20 minutes and one hour. The 20 minute residence time corresponds to a 15 gpm volumetric flow rate into the pilot reactor, while a one hour residence time corresponds to a 5 gpm flow rate. Performance

of any given grease interceptor was determined by its percent removal of the influent oil following Equation 2.1:

$$\% \, \text{Removal} = 100 \times \left(1 - \frac{C_{out}}{C_{in}} \right) \tag{2.1}$$

where C_{in} denoted the influent oil concentration and C_{out} denotes the concentration in the effluent stream at a given residence time.

An oil/water emulsion (Figure 2-5) was achieved through the continuous mixing of precise volumes of oil and water in a 55-gallon drum. A Lightnin EV1P50 was utilized with an A200 impellor type at 1380 RPMs for the duration of the experiment. The emulsion was mixed for at least 20 minutes prior to the initiation of the experiment to ensure a stable droplet size for the duration of the experiment (Sis et al., 2005). After thorough mixing, the emulsion was pumped into the main flow line. Variation of the oil/water flow rate then allowed for the desired target oil concentration.

Figure 2-3. Pilot Scale Grease Interceptor.
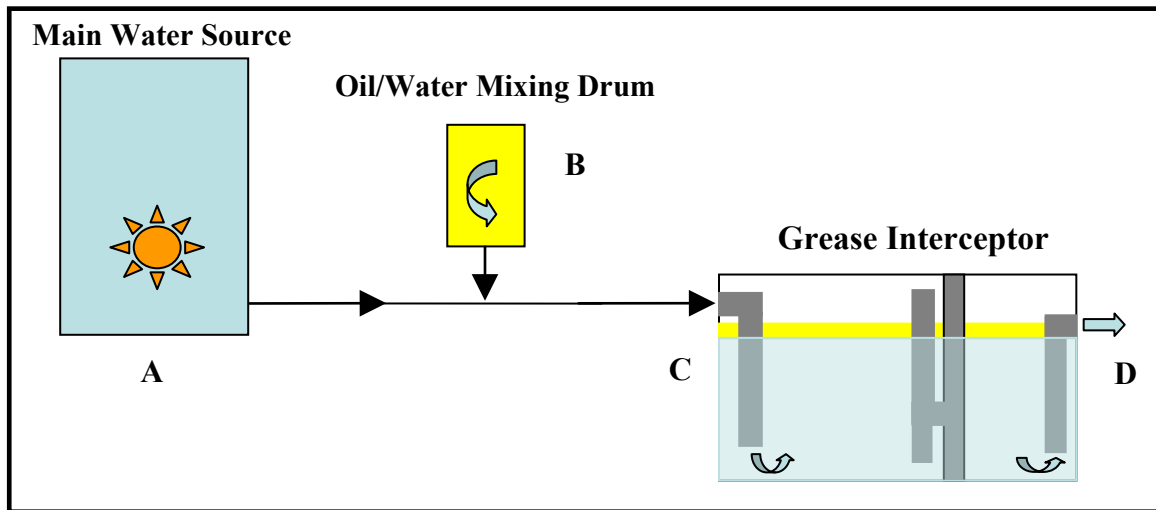
Figure 2-4. Conceptual Schematic for Lab Grease Interceptor: a) How Water Source, b) Oil/Water Mixing Tank, c) Influent Sample Location of GI, d) Effluent Sample Location of GI.

Experiments began with an initially empty grease interceptor. The reactor was then allowed to mature for 3 residence times past filling. Researchers collected grab samples from the influent and effluent sample locations (Figure 2-6) for concentration analysis described later. In discussing the internal geometry of grease interceptors, several terms denote configuration features or sample locations. Figure 2-7 defines several of the key locations. Two oil types were utilized in this study: Mazola brand corn oil and Executive Choice peanut oil (Figure 2-8).

Figure 2-5. Oil/Water Mixing Drum.

WERF
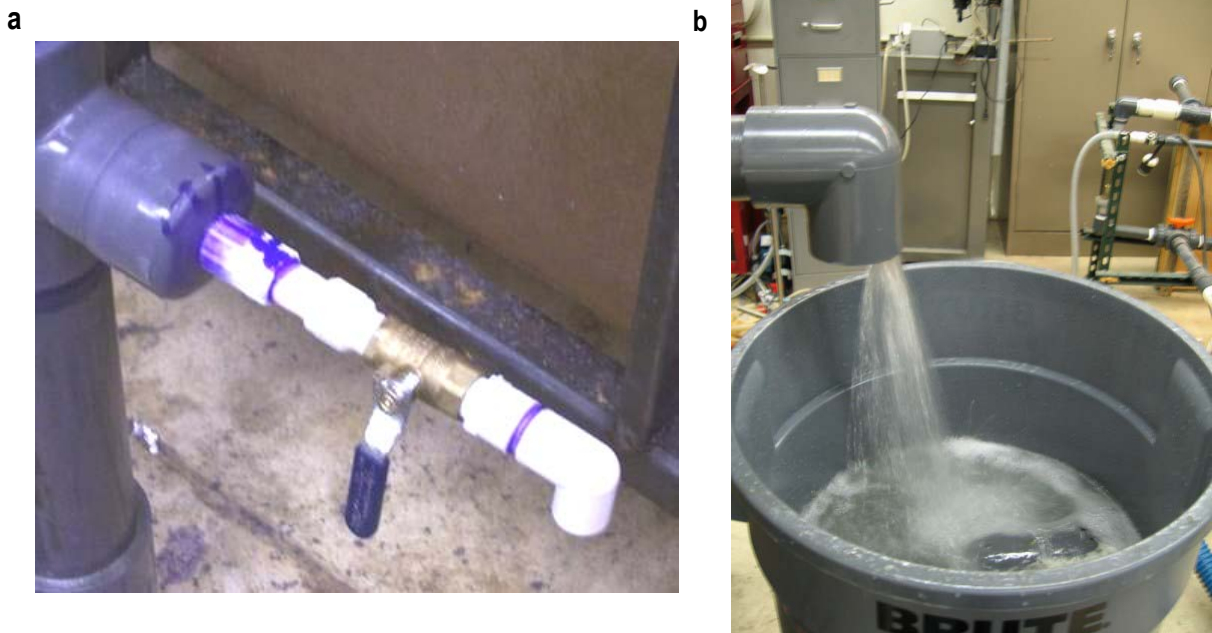
Figure 2-6. Inlet and Outlet Sample Location.

Standard Grease Interceptor Configuration
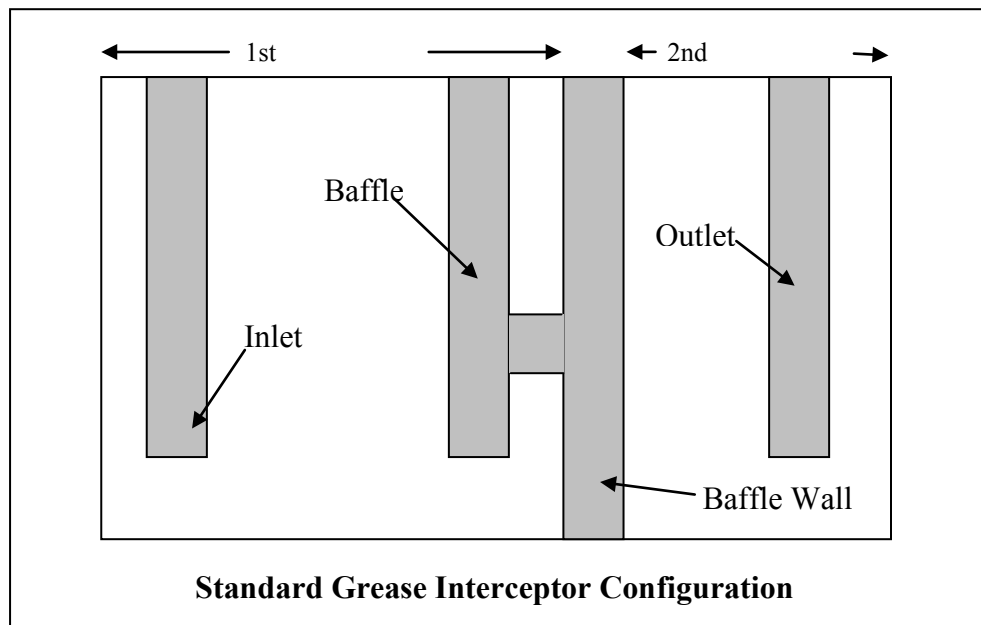
Figure 2-7. Definition of Grease Interceptor Terms.

Figure 2-8. Corn and Peanut Oil Used in Bench and Pilot Experimentation.

2.4 Bench Scale Grease Interceptor

The bench scale grease interceptor is a 10-gallon interceptor constructed of clear acrylic and PVC piping (Figure 2-9). Configuration with smaller pumps and mixers has enabled the same flexibility present with the pilot grease interceptor (flow, temperature, and oil concentration). In addition to the equal experimental flexibility, the maintenance time between experiments for the bench scale reactor is observably less than its larger pilot counterpart.

Little is known regarding the performance of a scaled down reactor with regards to oil removal efficiency. At present, the most influential variables to the performance of a grease interceptor have been the residence time, the internal geometry, and the inlet droplet size. The first two variables are easily modified at the bench scale. The third, though shown to be important to the overall performance of a grease interceptor from CFD simulations, is extremely difficult to quantify. The research team attempted to maintain a constant droplet distribution by adjusting the mixer energy within the feed tank. The trends observed on the bench scale, through the modification of geometry and residence times, should translate to the pilot scale and CFD work. Researchers performed standard bench scale experiments in an identical fashion to the pilot scale experiments described above, where influent at a constant concentration was pumped into a reactor, which was initially empty. The reactor was allowed to mature for three residence times after filling and then sampled for FOG concentration.

2.5 Experimental Tests on Impact of Influent Temperature

In addition to the experimental tests discussed above, researchers performed several experiments to test the effect of influent temperature on the performance of various configurations. In these temperature experiments, the reactors were filled with oil-free water at a temperature cooler than the influent. A corn oil layer was created by slowly pouring oil into the first compartment (so it would readily separate to the surface). The experiment began with an

WERF

initially cooled tank (approximately 70ºF) with an influent of approximately 110ºF at a 1000 mg/L corn oil concentration.

Researchers designed the temperature experiments to observe the effect of a buoyant plume of warmer influent on the separation performance of the grease interceptor. Samples were taken on a much shorter time interval (fractions of one residence time) in order to better capture potential short term effects of temperature differences. For comparison, duplicate experiments were performed with a tank filled initially with oil-free water of the same temperature as the influent. This comparison allowed for isolation of temperature dependent behaviors.
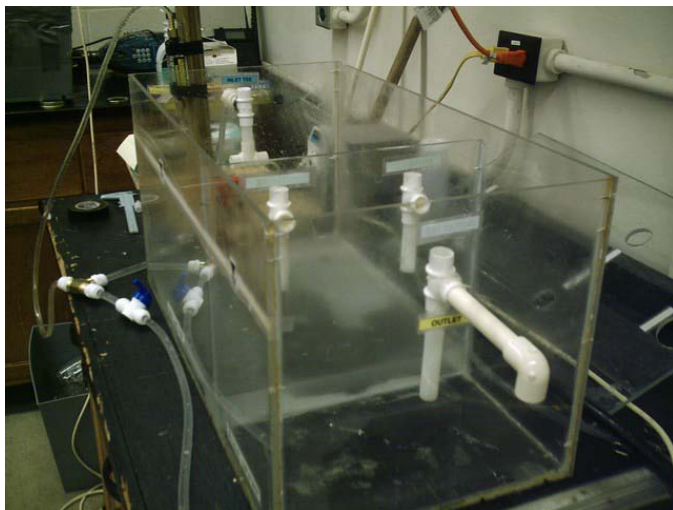
Figure 2-9. Bench Scale Reactor with Distributive Tee Configuration.

2.6   Analysis of FOG Concentration Using Infracal Device

The Infracal TOG/TPH $^®$ analyzer Model HATR-T2 (Figure 2-10), a product from Wilkes Enterprise, Inc., was one of the methods for the measurement of oil concentration in the bench and pilot scale experiments. The Infracal analyzer is designed for the purpose of measuring solvent extractable material (hydrocarbons or oil and grease) by infrared determination in water or wastewater. The device measures the infrared light reflection from a sample applied to a cubic zirconia crystal (Infracal User Manual). For this analysis, hexane was the solvent.

Samples analyzed with the Infracal unit must initially undergo an extraction process for the separation of the extractable material (oil in this study). The oil/water samples were first acidified with hydrochloric acid (HCl) until reaching a pH less than 2. The samples were transferred to a 500 mL graduated cylinder and the sample volume noted. Ten percent, by volume, of hexane was added to the sample container to remove any residual oils from the container wall. The sample and hexane were stirred in the graduated cylinder with a magnetic stirrer for approximately two minutes. After stirring, the sample was allowed to re-separate for one minute. A pipette was used to suction off the hexane layer. The separated hexane layer was passed through a filter with sodium sulfate to capture any residual water in the extraction. The sample is ready for testing with the Infracal after the filtration of the extraction component.

The Infracal® device has multiple settings. If desired, calibration data can be stored internally in the device and concentrations can be reported exactly. Alternatively, calibration curves can be constructed externally by testing samples of known concentrations, and reading absorbance values. Researchers utilized the latter calibration approach. Testing can commence after adequate warm up time for the Infracal® unit (approximately 1 hour). With the use of a syringe, 50 µL of the extract is applied to the cubic zirconia slide on top of the Infracal unit. Pressing the RUN button commences a four minute countdown, after which an absorbance value appears. Multiple replicates of these values are measured for a given sample and used to calculate the concentration of oil within the grab sample. After each run, a small amount of hexane is applied and wiped from the lens for cleaning. The Infracal® is run again to ensure an absorbance reading of no more than +/- 2 between samples.

Figure 2-10. Infracal® Device Used for FOG Concentration Measurements.

2.7   Analysis of FOG Concentration using U.S. EPA Method 1664

EPA Method 1664 is suitable for the measurement of "extractable materials that are relatively non-volatile hydrocarbons, vegetable oils, animal fats, waxes, soaps, greases, and related materials." (EPA Method 1664). For this research, samples analyzed through method 1664 contained various food grade fat, oil, and grease. Samples comprised of pure vegetable oils were utilized in the lab setting and heterogeneous solutions of various food grade FOG and other substances found in kitchen discharges were obtained with samples collected in the field. The cited documentation for Method 1664 describes two forms of analysis, a hexane extractable material analysis (HEM) and a silica-gel treated hexane extractable material method. For this study, analysis of samples was only done using the HEM approach.

Analysis of FOG using Method 1664 (HEM) essentially involves determining the mass of FOG through extraction and distillation. It can be summarized in a few general steps:

1. acidification of sample with HCL or H_2SO_4 to pH < 2
2. mixing of hexane with sample in separatory funnel
3. removal of water from extract

4. evaporation of hexane
5. determine the mass of residual hexane extracted materials (FOG)
6. calculate concentration through residual mass and sample volume

A detailed discussion of the method can be found at:
http://www.epa.gov/waterscience/methods/method/oil/1664.pdf

      For this research, Method 1664 testing was performed at two local commercial laboratories, certified to perform Method 1664. The laboratories provided samples jars and instructions regarding sample collection, storage, and delivery.

CHAPTER 3.0

NUMERICAL METHODS

This study involves the development of a computational fluid dynamics (CFD) model that integrates the reactor hydraulics (flow field and turbulence modeling) and FOG transport (Algebraic Slip Model). CFD is the science of determining a solution to fluid flow through space and time. CFD models include a description of the flow geometry, a set of coupled differential equations describing the physics and chemistry of the flow, boundary and initial conditions, and a structured mesh of points at which these equations are solved (Warsi, 1993). The equations of motion (Reynolds averaged mass and momentum conservation equations) are solved by a finite difference, finite element, or finite volume technique (Fletcher, 1991).

3.1   Flow Field and Turbulence Modeling

The simulation of a turbulent flow field requires the solution of the Reynolds averaged conservation of mass (Equation 3.1) and momentum (Equation 3.2) equations.

Continuity:

$$\frac{\partial \overline{U}_i}{\partial x_i} = 0$$

(3.1)

Navier Stokes:

$$\frac{\partial \overline{U}_i}{\partial t} + \frac{\partial (\overline{U_i U_j})}{\partial x_j} = -\frac{1}{\rho}\frac{\partial P}{\partial x_i} + \frac{\partial}{\partial x_j}\left[\nu(\frac{\partial \overline{U}_i}{\partial x_j} + \frac{\partial \overline{U}_j}{\partial x_i}) - \overline{u_i u_j} \right]$$

(3.2)

Equations (3.1) and (3.2) are not sufficient to solve all the variables due to the existence of turbulence stress term, $-\overline{u_i u_j}$. The sections below describe the different closure relationships for the Reynolds stresses.

3.1.1 Two-Equation Turbulence Model

Launder and Spalding (1974) developed standard two equation k-ε model to solve turbulence stress closure problem using the following equations:

Kinematic eddy viscosity:
$\nu_t = C_\mu k^2/\varepsilon$

(3.3)

Turbulence kinetic energy:

$$\frac{\partial k}{\partial t} + \overline{U}_j \frac{\partial k}{\partial x_j} = v_t \left(\frac{\partial \overline{U}_i}{\partial x_j} + \frac{\partial \overline{U}_j}{\partial x_i} \right) \frac{\partial \overline{U}_i}{\partial x_j} + \frac{\partial}{\partial x_j} \left[(v + \frac{v_t}{\sigma_k}) \frac{\partial k}{\partial x_j} \right] - \varepsilon \qquad (3.4)$$

Dissipation rate:

$$\frac{\partial \varepsilon}{\partial t} + \overline{U}_j \frac{\partial \varepsilon}{\partial x_j} = C_{\varepsilon 1} \frac{\varepsilon}{k} v_t \left(\frac{\partial \overline{U}_i}{\partial x_j} + \frac{\partial \overline{U}_j}{\partial x_i} \right) \frac{\partial \overline{U}_i}{\partial x_j} - C_{\varepsilon 2} \frac{\varepsilon^2}{k} + \frac{\partial}{\partial x_j} \left[(v + v_t / \sigma_\varepsilon) \frac{\partial \varepsilon}{\partial x_j} \right] \qquad (3.5)$$

Reynolds stresses:

$$-\overline{u_i u_j} = v_t \left(\frac{\partial \overline{U}_i}{\partial x_j} + \frac{\partial \overline{U}_j}{\partial x_i} \right) - \frac{2}{3} k \delta_{ij} \qquad (3.6)$$

The empirical constants used in this model are shown below:
$C_{\varepsilon 1}$ = 1.44, $C_{\varepsilon 2}$ = 1.92, C_μ = 0.09 σ_k = 1.0, σ_ε = 1.3

For the wall boundary conditions, the no slip condition (i.e., velocities equal to zero) was applied to all solid surfaces. At very small distances near the solid wall, a viscous sub-layer exists followed by an intermediate layer and turbulent core. In the viscous sub-layer, the flow is influenced by viscous forces and does not depend on free stream turbulent parameters. Typically, the viscous sub-layer is too thin to discretize and is therefore not included as a significant region in turbulence models in grease interceptors. However, the intermediate region, which includes the effects of both the viscous sub-layer and the turbulent core, is more significant in size and requires more care in predicting the velocity and turbulence in this region. The intermediate sub-layer is bridged by utilizing empirical wall functions to provide near-wall boundary conditions for the mean-flow and turbulence transport equations. In this study, the equilibrium log-law wall functions were used. The velocity, turbulent kinetic energy, and energy dissipation rate in the equilibrium wall functions are as follows:

$$u^+ / u_\tau = Ln(Ey^+) / \kappa \qquad (3.7)$$

$$k = u_\tau^2 / \sqrt{C_\mu} \qquad (3.8)$$

$$\varepsilon = C_\mu^{0.75} k^{1.5} / (\kappa Y) \qquad (3.9)$$

where u^+ is the absolute value of the resultant velocity parallel to the wall at the first grid node, u_τ is the resultant friction velocity ($u_\tau = \sqrt{\tau_w / \rho}$), Y is the normal distance of the first grid point from the wall, y^+ is the dimensionless wall distance ($y^+ = u_\tau Y / \upsilon$), C_μ is a constant based on the two-equation turbulence model selection, κ is the von Karman constant and E is a roughness parameter. κ = 0.41 and E = 8.6, which is appropriate for smooth walls. Equation 3.7 is known as the wall logarithmic law and should only be used when the y^+ value range between 30 and 500, which was maintained in this study.

WERF

3.2   Numerical Simulation Setup

For inlet conditions, the average mean velocity normal to the inlet plane was specified. All tangential velocities were set to zero. The turbulent kinetic energy and energy dissipation rate inlet conditions were defined as: $k_{inlet} = (I\ U)^2$, $\varepsilon_{inlet} = k_{inlet}^{1.5}/(0.1\ D)$ where $I = 0.05$, U is the normal average velocity at the inlet, and D is the pipe diameter. For the outlet conditions, the gradients of all variables were zero in the flow direction with the exception of the pressure. The pressure was set to zero gauge.

A finite volume commercial CFD code PHOENICS (CHAM, England) was used to perform the simulation. PHOENICS utilizes the Semi Implicit Method for Pressure Link Equation (SIMPLE) numerical scheme to take care of the pressure velocity couple. A sharp monotonic algorithm for realistic transport (SMART) scheme (Gaskell and Lau, 1988) was used to discretize the convection portion of the transport equations. Convergence of the numerical solution was based on: a) the sum of the absolute residual sources over the whole solution domain must be less than 0.01% of the total inflow quantity and b) the values of the monitored dependent variables at several locations must not change by more than 0.01% between successive iterations. Irregular boundaries were handled using a cut-in cell method (Yang et al., 1997). The grid size was determined through successive refinement in the grid until changes in the turbulence and mean velocity profiles were less than 1% between successive refinements. The fluid velocities and turbulence determined during this portion of the modeling was used as initial conditions for the algebraic slip model (ASM) described in the next section to improve the convergence requirements for the ASM model. The ASM model was found to take 50% to twice the simulation time without these initial conditions.

3.3   Algebraic Slip Model

The two phase (oil and water) numerical grease interceptor simulation was based on the ASM approach (Pericleous and Rhodes, 1986; Pericleous, 1987). ASM simulates the phases as multiple interpenetrating continua. The probability of each phase's existence is based on the phase's volume fraction at a point in space. In the ASM approach, a single differential equation is solved for continuity of the mixture, a single differential equation is solved for the momentum of the mixture, and a single differential equation is solved for each phase. The equations for the continuity, mixture momentum, and volume fraction for the dispersed phase equations are shown below:

$$\frac{\partial}{\partial t}\left(\rho_m\right) + \frac{\partial}{\partial x_i}\left(\rho_m u_{m,i}\right) = 0 \tag{3.10}$$

$$\frac{\partial}{\partial t}\left(\rho_m u_{m,j}\right) + \frac{\partial}{\partial x_i}\left(\rho_m u_{m,i} u_{m,j}\right) = -\frac{\partial p}{\partial x_j} + \frac{\partial}{\partial x_i}\left[\mu_m\left(\frac{\partial u_{m,i}}{\partial x_j} + \frac{\partial u_{m,j}}{\partial x_i}\right)\right] + \rho_m g_j$$

$$+\frac{\partial}{\partial x_i}\sum_{k=1}^{n}\alpha_k \rho_k u_{D,k,i} u_{D,k,j} \tag{3.11}$$

$$\frac{\partial}{\partial t}(\alpha_d \rho_d) + \frac{\partial}{\partial x_i}(\alpha_d \rho_d u_{m,i}) = -\frac{\partial}{\partial x_i}(\alpha_d \rho_d u_{D,d,i}) \tag{3.12}$$

where $\rho_m = \sum_{k=1}^{n} \alpha_k \rho_k$, $\mu_m = \sum_{k=1}^{n} \alpha_k \mu_k$, $u_m = \dfrac{\sum_{k=1}^{n} \alpha_k \rho_k u_k}{\rho_m}$

The ASM approach treats the motion of each phase relative to the center of the mixture mass. This is handled by introducing the concept of a diffusion or drift velocity ($u_{D,k}$) and is calculated as follows:

$$u_{D,k} = \frac{(\rho_m - \rho_k)d_k^2}{18\mu_c(0.018\,\text{Re})}\left[g - \frac{Du_m}{Dt}\right] - \frac{1}{\rho_m}\sum_{i=1}^{n-1}\alpha_i \rho_i \frac{(\rho_m - \rho_i)d_i^2}{18\mu_c(0.018\,\text{Re})}\left[g - \frac{Du_m}{Dt}\right] \tag{3.13}$$

In the ASM approach, turbulence is included in the determination of the continuous phase viscosity (μ_c) in the drift velocity computation (Equation 3.13) and in the mixture viscosity where μ_c is described by the turbulent viscosity μ_t.

3.4 Numerical Tracer Test Model

The fluid analysis described in the previous section will provide local and spatial information about grease interceptor hydraulic behavior (i.e., mesoscale mixing behavior). However, the techniques described are non-traditional and not tools that can be easily adopted by municipalities for the analysis of field grease interceptors. They are more suited for designers of grease interceptors who are interested in enhancing the removal performance of their product. Therefore, the research team performed a simulated tracer test for analyzing the reactor scale mixing behavior (i.e., macroscale mixing) to mimic experimental tracer tests that are traditionally conducted when macro-scale hydraulic characteristics need to be determined to identify any major process hydraulic inefficiencies.

The age distribution of a fluid element in a reactor or process train can be determined by injecting a known quantity of tracer mass at the reactor or process train influent and measuring the resulting tracer concentration over a period of time at the effluent. In order to model the transport of a chemical species through space and time, the turbulent convective-diffusion equation is used and is described by Equations 3.14 and 3.15:

Convective-Diffusion Equation

$$\rho\frac{\partial C}{\partial t} + \rho\sum_j \frac{\partial(U_j C)}{\partial x_j} = \rho\sum_j \frac{\partial}{\partial x_j}\left(\frac{\nu}{\Pr(C)}\frac{\partial C}{\partial x_j} - \overline{u_i c}\right) \tag{3.14}$$

Reynolds Mass Flux Equation

$$-\rho\overline{u_i c} = \frac{\nu_T}{\Pr_T(C)}\frac{\partial C}{\partial x_i} \tag{3.15}$$

where

WERF

C = mean tracer concentration
c = turbulent fluctuating tracer concentration
Pr (C) = Schmidt number = 1
Prt (C) = Turbulent Schmidt number = 1

Researchers performed the simulated tracer analysis in two parts: first a CFD simulation that characterizes the reactor fluid velocities and turbulent parameters is performed followed by a second CFD model to solve the turbulent convective-diffusion equation. As in an experimental tracer study, the CFD tracer simulation can be run as either a pulse-input test or step-input test. For the pulse-input test, tracer boundary conditions are setup to allow the tracer mass to be injected in a finite amount of time. For the step-input test, tracer boundary conditions are setup to inject the tracer continuously throughout the simulation time period. Although either method of tracer boundary condition will lead to the development of the same residence time density (RTD) curve, the step-input boundary condition is preferred since it minimizes the amount of mathematical manipulation for the creation of the RTD curve and was used in the analysis of the grease interceptor

As in the experimental tracer study, quality assurance/quality control checks were performed to validate the numerical solution. These checks include:

- ♦ Comparison between numerically computed mean hydraulic detention time and the theoretical hydraulic detention time. The computed hydraulic residence time is within 5% of the theoretical hydraulic residence time
- ♦ Effluent tracer concentration is equal to the influent tracer concentration (For step input test boundary conditions).
- ♦ Numerical solution does not change significantly with grid size or time step interval.
- ♦ Convergence limit has been reached.

Tracer simulations were redone if any of these QAQC checks were violated.

WERF

CHAPTER 4.0

FIELD ASSESSMENT OF
GREASE INTERCEPTOR PERFORMANCE

4.1   Food Waste Solids Characterization

The research team analyzed waste food solids discharged into floor drains from a commercial kitchen operations (full fare buffet style restaurant) grease interceptor (GI). The liquid stream discharged into the GI includes dishware and equipment washing, floor cleaning, food preparation, serving and production activities that generate waste food particles, in addition to inert material introduced into drains, sinks, and other openings. Waste food particles have heterogeneous dimensions, weight, specific gravity, and composition. In order to characterize these particles, researchers characterized the settling characteristics and size. Food solids were collected from the GI inlet using a vacuum suction chamber (Figure 4-1a). In addition, a sock capturing device was used to retrieve additional solids that would not be captured with the vacuum suction chamber due to its size (Figure 4-1b).

In the vacuum suction chamber, a vacuum is created via the use of an automatic, programmable peristaltic pump mechanism often employed in wastewater sampling equipment (Figure 4-1c). The suction chamber is used since the rollers in the flexible silicon tubing that creates the vacuum would destroy any soft vegetable or organic material pumped into and through the pump housing. By creating a vacuum, the solids are deposited into the chamber without any physical damage or alteration. After collection, the sample containing waste food solids and wastewater were poured into a clean container for transport to the laboratory. Waste food solids in the outlet tee sock were collected over a 24 hour period. A 25 ml beaker was inserted into the center of the food solids mass and removed. Captured solids were re-suspended into 1 L of tepid water before sizing, weighing, and subjecting to settling test.

Once the solids were captured using either the vacuum chamber or the sock device, they were placed on a stainless steel mesh table (Figure 4-1d). The mesh table consists of 12 2-inch diameter holes that each contains a stainless steel mesh, which varies in size between 0.065 and 0.437 inch. The mesh apparatus was set over a laboratory sink, under which large mouth 1000 ml beakers are placed. A 1 L sample with food solids was poured through #2 mesh. Any water/solids mixture that did not pass through the #2 mesh was collected for that size. The #2 mesh-recovered water/solids mixture was then poured through the #3 mesh with its recovered material then being captured and subsequently poured in the #4 mesh. This procedure was repeated until all recovered water/solids have been poured through each successively smaller mesh, ending with mesh #12. Waste food particles, after having been sized by various meshes, were picked from their respective mesh, photographed with a centimeter scale (Figure 4-1e), weighed while wet, kept hydrated, and ultimately dropped into the open top of a 1 meter 4" settling column filled with 90°F. water. Timed settling rates, in feet per second, were recorded for each particle measured.

Figure 4-1. Solids Capturing and Measurement: a) Suction Chamber, b) Sock Capturing Device, c) Automatic Pump and Sampling with Suction Chamber, d) Stainless Steel Mesh Table, e) Image of Particles.

WERF

4.2   Grease Interceptor Influent Solids and Particle Analysis

The results of the particle size analysis using the mesh apparatus is shown in Tables 4-1 and 4-2. In Tables 4-1 and 4-2, the results show a range of food items captured by the mesh apparatus including vegetable, meat, poultry, fish, and starch. For this grease interceptor, food items were retained by all mesh sizes, indicating that a wide range of particle sizes (2-11 mm) can be found in full-fare restaurant waste streams. In addition, the settling rates for the different food items ranged from 0.05-0.2 ft/s. These results suggest that typical food waste solids have a high settling rate and would likely settle out efficiently in a grease interceptor assuming that quiescent fluid flow patterns have been developed. Any transport of these types of solids into a second compartment of a two compartment grease interceptor suggests the following conditions:

1) quiescent fluid flow patterns have not been maintained
2) inappropriate grease interceptor clean out frequency
3) density outfall event

In the first case, quiescent fluid flow patterns are developed when there are no major instances of high velocity zones within the grease interceptor (i.e., any locations where "jet like" velocity conditions have developed). These "jet like" velocities may occur in the standard grease interceptor design with a standard single opening mid-baffle wall and a single pipe effluent. High velocity zones near the influent, mid-baffle, and effluent pipes can cause scouring of settle solids (i.e., re-suspend them) and transport them into other locations into the grease interceptor and potentially out of the grease interceptor effluent. Revised grease interceptor designs suggested in the next chapter can help maintain these quiescent fluid flow patterns and alleviate the transport of solids under case 1.

Case 2, inappropriate clean out frequency, can lead to solids accumulation in the second compartment or higher total suspended solids in the grease interceptor effluent from the re-suspension of settled solids that have accumulated from lack of pump-out maintenance. All grease interceptor designs may be prone to this type of solids transport and can be easily avoided by enacting an appropriate pump-out schedule. In addition, the solids loading rate for the specific food service establishment and allocation of the appropriate solids storage volume should be determined during the design phase to help reduce the possibility of solids transport near the grease interceptor effluent.

Finally, case 3 may occur when the food service establishment discharges a highly concentrated waste stream (i.e., sugar/syrup mixture) where the influent mixture density is greater than the bulk fluid density in the grease interceptor and flows primarily towards the bottom. This bottom flow may re-suspend the settled solids and transport them towards the grease interceptor effluent. Case 3 can be avoided with best management practices within the food service establishment.

Other types of solids may be deposited into the grease interceptor from the food service establishment waste stream depending on the type of wastewater connected to the discharge line. In addition, low frequency grease interceptor cleanout schedules may lead to the generation of biosolids that do not have high settling velocities and can be easily transported out the grease interceptor effluent. Consequently, proper scheduled maintenance of the grease interceptor may be more important to reduce any transport or generation of these types of solids into the grease interceptor effluent.

Table 4-1. Results of Particle Analysis from Full Fare Buffet Style Grease Interceptor (Part 1).

Mesh Size	Particle 1		
	Description	Wet Weight	Settle Rate
		(g)	(ft/s)
Mesh 2			
Mesh 3			
Mesh 4			
Mesh 5	lemon seed	0.13	0.202
Mesh 6	rice kernel	0.09	0.165
Mesh 7	1/2 rice	0.04	0.175
	pepper		
Mesh 8	seed	0.03	0.156
Mesh 9	cabbage	0.01	0.063
Mesh 10			
Mesh 12			

Mesh Size	Particle 2		
	Description	Wet Weight	Settle Rate
		(g)	(ft/s)
Mesh 2			
Mesh 3			
Mesh 4	fish	0.16	0.101
Mesh 5	pineapple	0.09	0.044
Mesh 6	carrot	0.03	0.061
Mesh 7	onion	0.02	0.043
Mesh 8	cuke seed	0.01	0.061
Mesh 9			
Mesh 10			
Mesh 12			

Mesh Size	Particle 3		
	Description	Wet Weight	Settle Rate
		(g)	(ft/s)
Mesh 2			
Mesh 3			
Mesh 4			
Mesh 5			
Mesh 6	crust	0.03	0.178
Mesh 7			
Mesh 8			
Mesh 9			
Mesh 10			
Mesh 12			

Source: Full Fare Buffet Style #1 – Full Fare - Wash sinks, dishwasher, pre-rinse sinks, prep sinks, can wash

Solids Collection Span: 12:00-4:00

WERF

Table 4-2. Results of Particle Analysis from Full Fare Buffet Style Grease Interceptor (Part 2).

Mesh Size	Particle 1 Description	Wet Weight (g)	Settle Rate (ft/s)
Mesh 2			
Mesh 3			
Mesh 4	potato	0.37	0.223
Mesh 5	fish	0.11	0.164
Mesh 6	potato	0.06	0.141
Mesh 7	rice, kernel	0.03	0.168
Mesh 8	meat: chicken	0.02	0.066
Mesh 9	1/4 rice	0.01	0.126
Mesh 10	1/4 rice	0.006	0.1
Mesh 12	? Particle	0.003	0.08

Mesh Size	Particle 2 Description	Wet Weight (g)	Settle Rate (ft/s)
Mesh 2			
Mesh 3			
Mesh 4	meat: beef	0.38	0.151
Mesh 5	meat: chicken	0.05	0.076
Mesh 6	rice	0.07	0.196
Mesh 7	1/2 rice	0.01	0.162
Mesh 8	seed, white	0.02	0.106
Mesh 9	seed, tomato	0.01	0.074
Mesh 10	meat: chicken	0.006	0.039
Mesh 12	? Particle	0.001	0.125

Mesh Size	Particle 3 Description	Wet Weight (g)	Settle Rate (ft/s)
Mesh 2			
Mesh 3			
Mesh 4	onion	0.17	0.068
Mesh 5	onion	0.06	0.051
Mesh 6	rice	0.05	0.186
Mesh 7	seed, brown	0.03	0.136
Mesh 8	seed, red	0.01	0.103
Mesh 9	corn	0.01	0.062
Mesh 10	? Seed	0.003	0.047
Mesh 12	? Particle	0.002	0.113

Source: Full Fare Buffet Style #2– Full Fare - Wash sinks, dishwasher, pre-rinse sinks, prep sinks, can wash

Solids Collection Span: 1100-11:00 (24hrs)

4.3   Grease Interceptor Influent Fluid Flow Analysis

The research team measured flow at several grease interceptors to provide additional data on the variability of the grease interceptor influent flow field. Analysis of the influent flow field is displayed in Table 4-3 (mean, minimum, and maximum) and Figures 4-2 (frequency and cumulative distributions). Figure 4-3 displays several time history trace of the flow data over a 24 hour period for different food service establishments. In Table 4-3, the total water usage to the grease interceptors ranged between 1,700 to 6,300 gallons. These values are consistent with those measured by Nashville Metro Water Services, where their GI water usage displayed values between 1,140 and 6,660 gallons. These total water usage were within the range found by Garza (2005) that also characterized the wastewater stream of several types of food service establishments. Grease interceptor sizes at these measurement sites ranged from 1,000 to 1,500 gallons.

In Table 4-3 as well as Figure 4-2, the flow data clearly shows that a large percentage of the flows (90-95%) falls below 10 gpm with 85-90% falling below 5 gpm. The time history data shows that the grease interceptor flow is highly intermittent with peak values that are 3-7 times the average occurring several times over the 24 hour period. The results show that, at the 90% mark in the cumulative distribution function (Figure 4-2b), most (75%) of the fluid flow from the food service establishments were 1/3 of the recorded peak flow. Clearly, the peak flows are associated with high FSE operation periods such as cleanup and preparation for major meals (i.e., breakfast, lunch, and dinner). Nashville Metro Water Services determined an average water flow over discrete 2-4 hr periods based on the water usage during that period and found values between 1 and 6.5 gpm. Although they did not perform actual flow measurements, the recorded total daily water usage performed by Garza (2005) showed that variability exists on different days of the week. However, Garza's recorded water usage values were determined from daily water meter readings and may include flow variability due to non-food service related activities.

The researchers did not find any strong correlation between the total water usage, average flow, or peak flow relative to the number of seats at the food service establishment. This lack of correlation between flow measurements and number of seats at a food service establishment suggest that another indicator for the flow of the waste stream derived from kitchen activities should be used, such as the quantity, size, and types of sinks, pipe size and configuration to the grease interceptor, and process equipment discharge flow rates (i.e., condensate, dishwasher, grinder).

The results in Table 4-3 and Figures 4-2 and 4-3 suggest long average residence times exceeding 2 hours under highly intermittent influent flow conditions exists for most food service establishment grease interceptors. While the FOG released from the interceptor effluent has not been measured, it is possible for excessive release of FOG in the grease interceptor effluent during peak operation under three conditions: a) when the influent water temperature is significantly higher than the GI water temperature; b) when excessive use of detergents/emulsifying agents are used; and/or c) when excessive amount of solids or a liquid stream containing a highly concentrated substance is discharged. In case (a), high temperature influent water could displace already separated FOG at the surface of the GI. However, laboratory tests of high temperature influent into a colder bulk temperature GI has shown little impact on the effluent FOG concentration with existing GI designs. As will be discussed in the next chapter, the low impact of temperature-driven density flows on grease interceptor performance is likely due to the deep location of the effluent pipe.

In case (b), the detergent/emulsifying agent may not allow time for or prevent adequate coalescing for proper separation of the influent FOG. Finally, in case (c), the high solids concentration may also cause short circuiting due to a density outfall. This may lead to an increase in the effluent FOG concentration due to the shorter path taken by the influent water through the GI. All these scenarios, however, will strongly depend on the geometric configuration of the GI (i.e., inlet/outlet piping, internal baffles, unit shape).
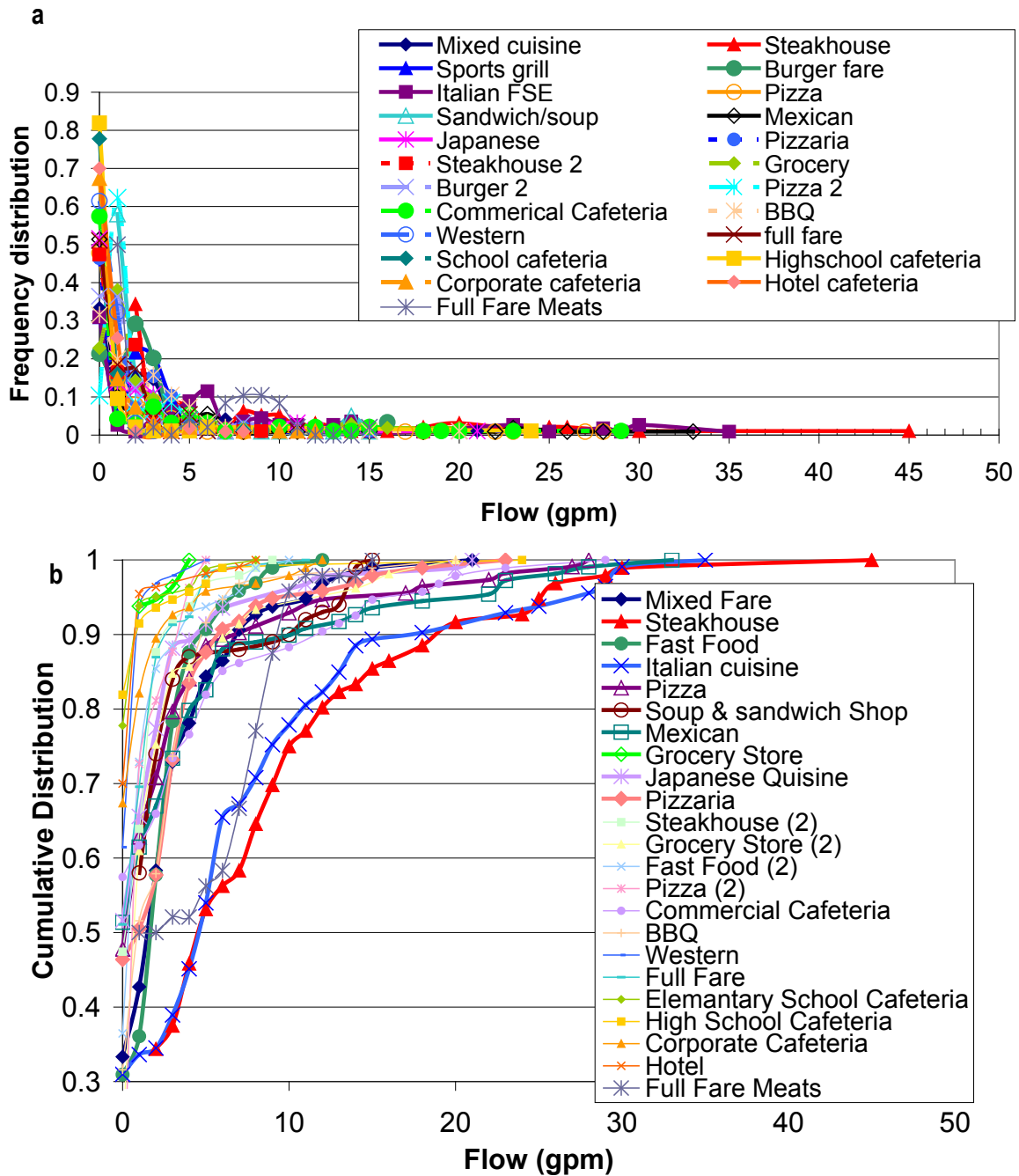
Figure 4-2. Distribution of Flow Data from Sampled Grease Interceptor Influent: a) Frequency, b) Cumulative.

Table 4-3. Flow Data from Grease Interceptor Influent from Different Restaurant Types.

FSE NAME	Total Flow to GI gpd	Max Flow gpm	Avg Flow gpm	Std. Dev gpm	GI Size market	Min HRT minute	Avg HRT hr	Seating #
full fare steakhouse	2,512	9	1.2	1.8	1000	111	14	250
grocery store	2,078	20	2.6	4.1	1200	60	7.8	5
fast food - burgers	1,421	10	1.4	2.0	1000	100	11.9	85
full service pizza	1,599	5	1.5	1.3	1000	200	11.1	90
full service - mixed cuisine	1,650	21	3.8	4.0	1000	48	4.4	320
full service steak house	6,326	45	9.8	8.4	1500	33	2.5	365
full service - mixed cuisine	1,643	12	3.0	2.3	1000	83	5.6	345
fast food - burgers	951	16	3.2	3.8	1000	63	5.2	84
full fare - Italian	4,310	35	9.4	8.0	1500	43	2.7	300
full service cafeteria	2,944	29	3.2	5.8	2000	69	10.4	300
full service pizzeria	1,235	28	4.2	6.3	1500	54	5.9	156
Single service - sandwiches	995	15	3.0	3.7	1000	67	5.6	140
full service - Mexican	1,810	33	5.0	7.4	1000	30	3.3	200
full service - meats featured	2,657	20	2.3	3.1	1000	50	7.2	172
grocery store	389	4	1.2	0.8	1000	250	13.6	1
Single service - Japanese	654	21	2.6	4.2	1000	48	6.5	44
Single service - mixed cuisine	629	5	0.5	0.9	1000	200	32	117
full service pizzeria	1,423	23	3.9	4.3	1000	44	4.3	82
full service - mixed cuisine	1,213	11	1.1	1.8	1000	91	14.7	142
elementary school cafeteria	339	8	0.5	1.3	1500	188	55.6	300
high school cafeteria	677	24	0.6	2.7	1500	63	39	450
cafeteria, corporate office	1,113	12	1.0	2.2	1500	125	26	530
full service restaurant, hotel	1,244	8	0.5	1.2	1500	188	50	101
full service meats	2,769	15	2.8	3.8	1500	100	8.9	276

WERF
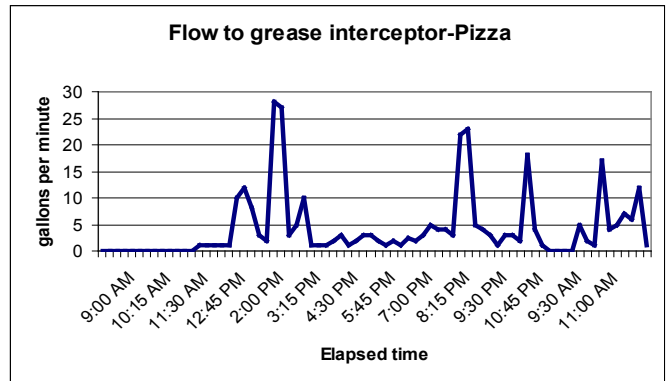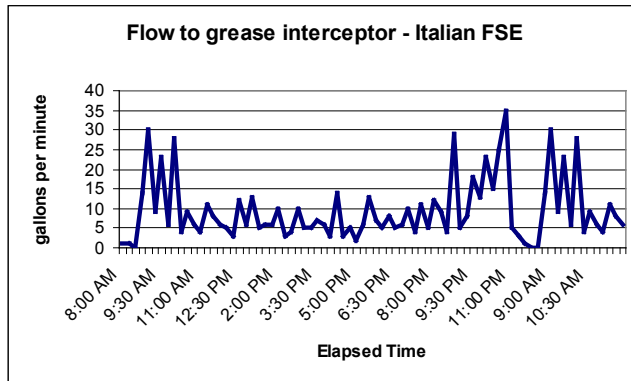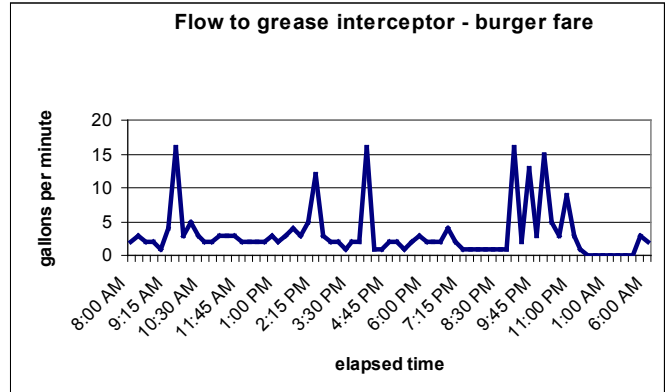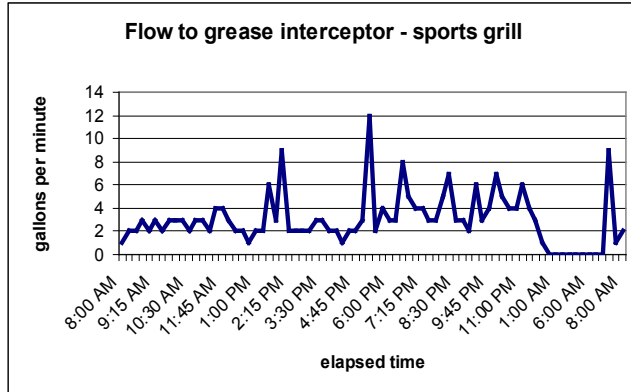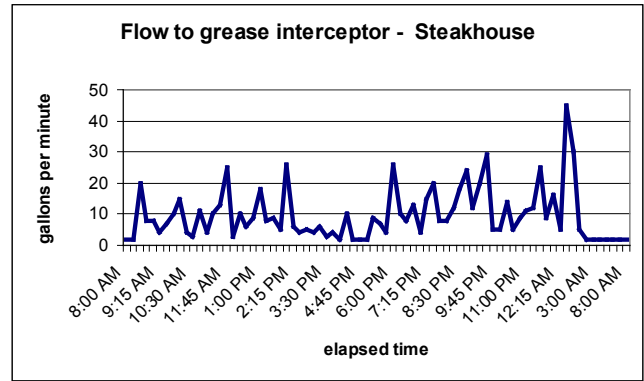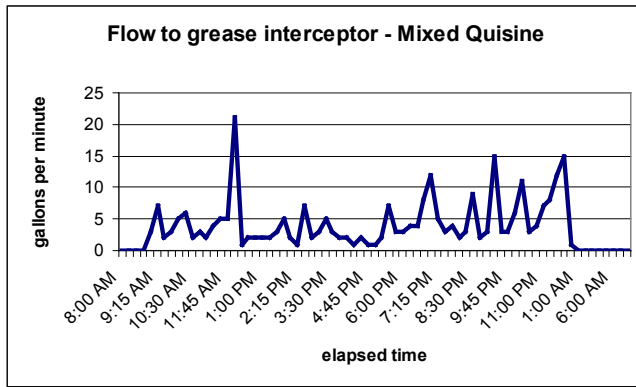
Figure 4-3a. Analysis of Flow Data from Sampled Grease Interceptor Influent from Several Restaurants.
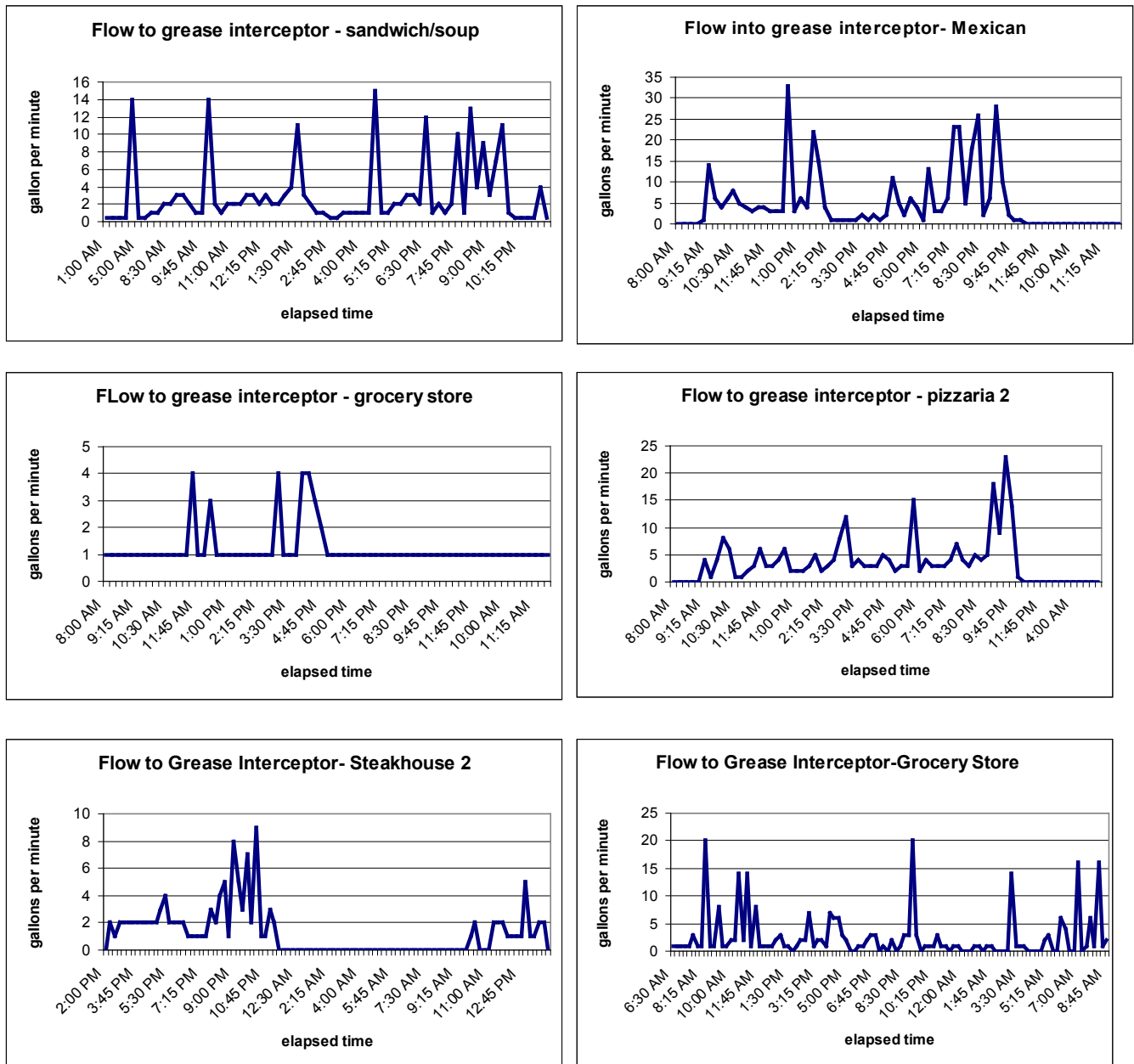
Figure 4-3b. Analysis of Flow Data from Sampled Grease Interceptor Influent from Several Restaurants.

WERF
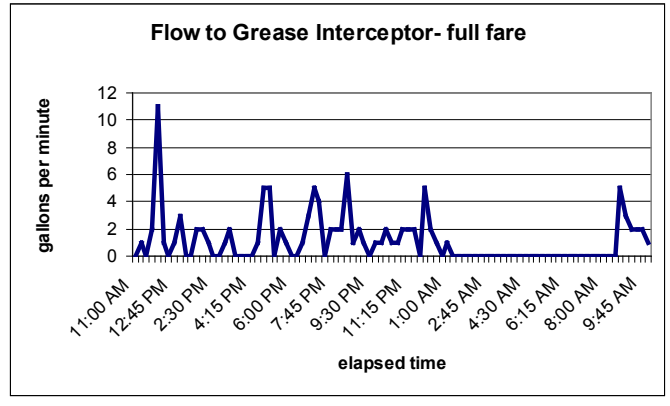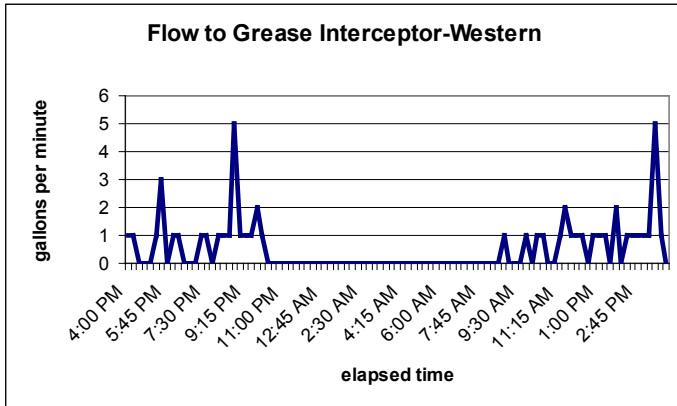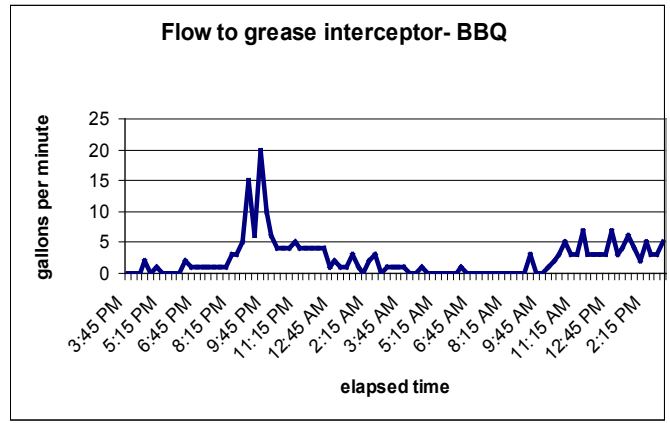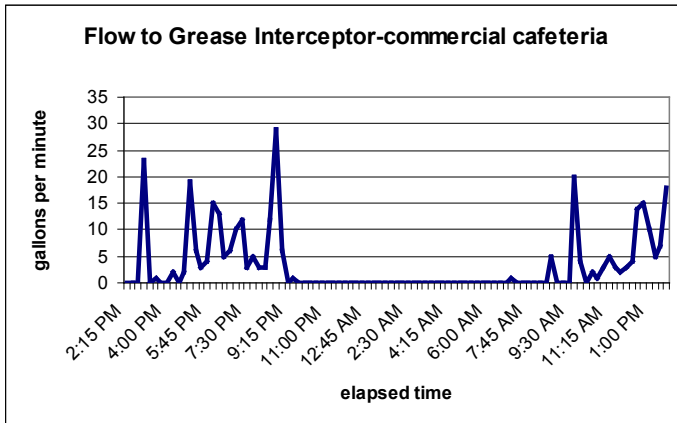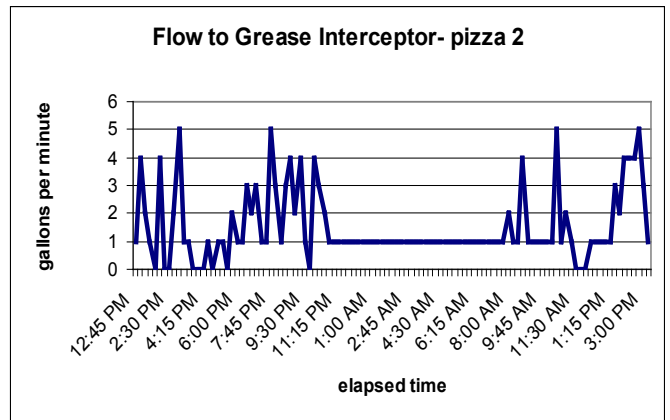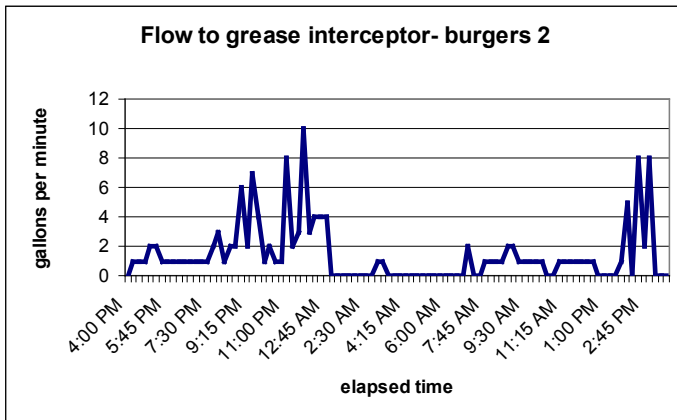
Figure 4-3c. Analysis of Flow Data from Sampled Grease Interceptor Influent from Several Restaurants.
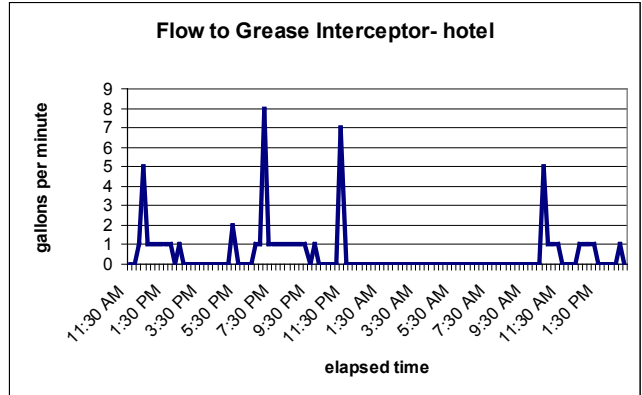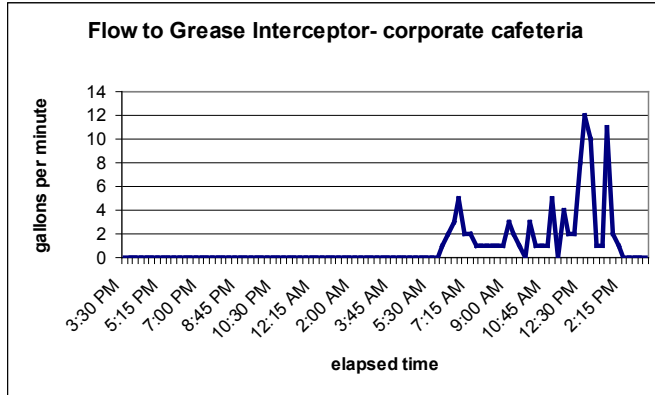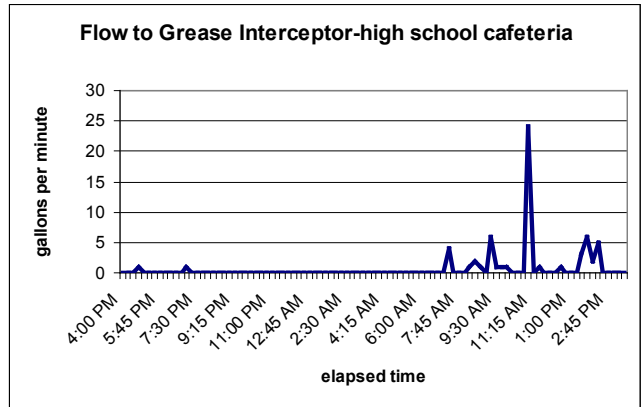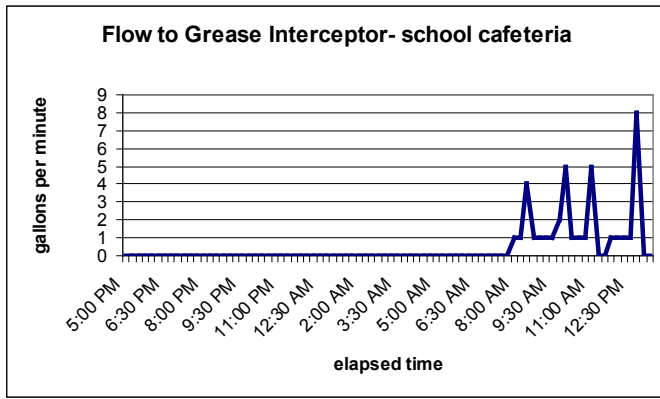
Figure 4-3d. Analysis of Flow Data from Sampled Grease Interceptor Influent from Several Restaurants.
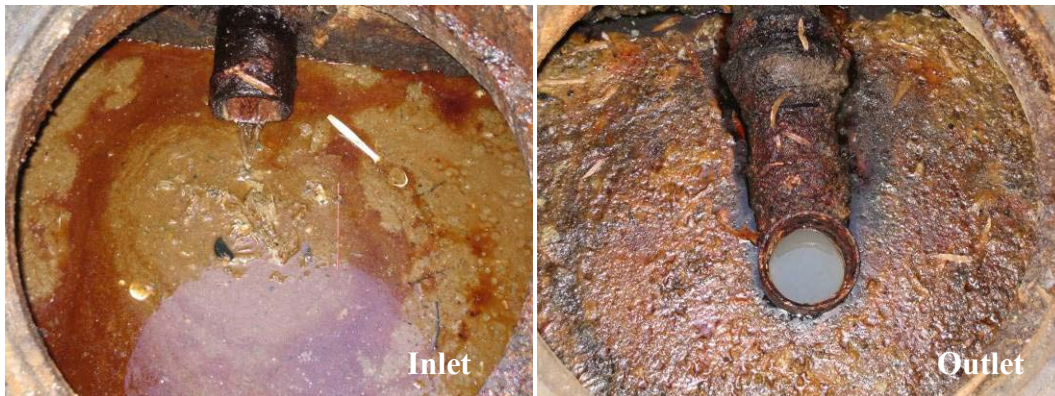
Figure 4-4. Inlet and Outlet of On-Campus Dining Facility GI.

4.4   FOG Concentration Assessment from Field Grease Interceptor

Researchers spent two separate days observing an on-campus grease interceptor shown in Figure 4-4. During periods of observably high or turbid flow, influent and effluent samples were collected for total oil and grease (TOG) analysis (Tables 4-4 and 4-5). The data clearly displays variability in the TOG over a 6 hour period and ranged between less than 5-1300 mg/L in the influent and 70-24,000 mg/L in the effluent. The high 24,000 mg/L (Table 4-5) effluent value was likely caused by excessive vibration at the outlet tee, which dislodged a chunk of hardened grease into the effluent.

Table 4-4. Total Oil and Grease Measurements at Clark Dining Hall, Day 1 (1/11/06).

Clark Dinning Hall NCSU			
Samples obtained 01/11/06			
oil and grease (mg/L)	Influent/effluent	Time	Sample #
55.9	Influent	9:00am	1
1260	Influent	10:00am	2
407	Influent	11:00am	3
<5.1	Influent	12:00pm	4
18.4	Influent	12:30pm	5
107	Influent	1:00pm	6
1240	Influent	2:00pm	7
97.2	Influent	3:00pm	8
1130	**Effluent**	**9:00am**	**1**
188	**Effluent**	**11:00am**	**3**
166	**Effluent**	**12:30pm**	**5**
99.3	**Effluent**	**2:00pm**	**7**

Table 4-5. Total Oil and Grease Measurements at Clark Dining Hall, Day 2 (1/19/06).

Clark Dinning Hall NCSU			
Samples obtained 01/19/06			
oil and grease (mg/L)	Influent/effluent	Time	Sample #
5.9	Influent	10:30am	1
49.7	Influent	11:15am	2
106	Influent	12:30pm	3
51.6	Influent	1:15pm	4
158	Influent	1:40pm	5
56.1	Influent	2:50pm	6
794	Influent	3:30pm	7
1210	Influent	4:00pm	8
1380	**Effluent**	**10:30am**	**1**
66.3	**Effluent**	**12:30pm**	**3**
24400	**Effluent**	**1:40pm**	**5**

In Table 4-4 and 4-5, the results suggest that there is no discernable trend between the influent or effluent FOG concentration. Although this may be as a result of sampling complications, as in the case in the 1:40 pm effluent (Table 4-5), it is most likely attributable to the large variability in the flow rate and kitchen practices observed on a day to day basis. Other field studies (Garza, 2005) showed similar trends in variable effluent concentrations although no influent grease interceptor measurements were taken.

Present inaccuracies experienced with the EPA Method 1664 for quantification of total oil and grease suggest that future research is needed to better develop a method suitable to measure total oil and grease of food service establishment waste streams.

4.5   Analysis of pH and Dissolved Oxygen in Field Grease Interceptor

A variety of samples were taken at a college dining hall facility's grease interceptor on NC State University campus. The dining hall grease interceptor utilizes a standard configuration. Researchers measured pH and dissolved oxygen content (DO) at six locations in the grease interceptor: the grease interceptor inlet, two samples in the first compartment, two samples from the second compartment, and the effluent (Figure 4-5a). The samples collected in the first and second compartment were taken using a sludge judge apparatus (Figure 4-5b) to collect samples at various depths of the grease interceptor. The measured values are reported in Tables 4-6 through 4-8.
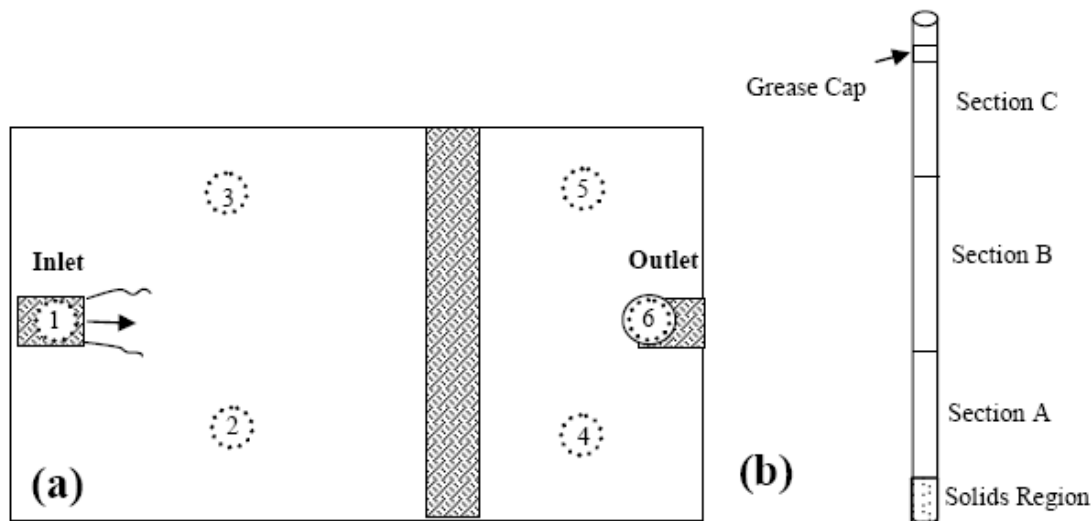
Figure 4-5. a) Sample Locations for pH Measurements, b) Sludge Judge.

Table 4-6. Influent and Effluent pH Values at Various Times.

Influent	pH	time
1	10.4	12:30pm
2	9.9	12:40pm
3	8.3	1:30pm
Effluent		
1	6.2	12:30pm
2	6.1	12:40pm
3	5.5	1:30pm

Table 4-7. pH Values at Various Location in Field GI.

Sample/Section	pH
1 (Inlet)	9.5
2A	6.4
2B	6.5
2C	6.5
3A	5.9
3B	6.1
3C	6.7
4A	4.8
4B	4.8
4C	4.8
5A	4.3
5B	4.3
5C	4.4
6 (Outlet)	5.9

In Table 4-7, the data show that the influent pH is generally more basic while the effluent more acidic. This higher influent pH is likely due to the basic nature of many cleaning products, as these chemicals are generally powerful degreasers. The effluent pH, on the other hand, is more acidic and consistent with the lower pH profile found in the GI. However, the higher pH value at the effluent (pH 5.9 at position 6) compared to positions 4 and 5 (pH between 4 and 5) in the second compartment suggest that incomplete mixing occurred in the second compartment and that there may have been a plume of fluid from compartment 1 where the pH was around 6. The pH data confirms some of the short circuiting problems identified with the standard GI configuration that will be described later.

Table 4-8. Dissolved Oxygen and Temperature Data from 1st and 2nd Compartment.

	DO (mg/L O_2)	Temperature (^oC)
Influent	3.8	45
Compartment 1		
A	0.5	43
B	0.4	43
C	0.5	43
Compartment 2		
A	0.4	41
B	0.4	40
C	0.5	37
Effluent	0.6	42

Table 4-8 displays the dissolved oxygen (DO) and temperature values taken in the center of the first and second compartments of the field GI. Temperature values shown in Table 4-8 are within values measured by others in field GIs (Garza, 2005). However, a majority of the temperature values measured by Garza were much cooler than those measured in this study and may have been caused by unknown waste streams that commingled with the food service establishment kitchen waste streams. Garza also performed DO measurements in the GI effluent and found much higher values than was measured in this study as shown in Table 4-8. Again, a major contributor to the difference between Garza's (2005) study and the present study is the location of measurement (GI effluent versus internal GI measurements in this study) and unknown commingling of grey and blackwater waste streams as discussed in Garza as a potential source of error.

The low pH and DO within the grease interceptor suggests the occurrence of anaerobic microbial activity. Though investigation into microbial activity is beyond the scope of the current research, this factor may play a significant role in the maintenance and operation of these devices. The acidic nature of the interceptor may lead to increased deterioration of the concrete walls. Additionally, there may be the production of free fatty acids along with the production of volatile organic acids (i.e., acetic, propionic, etc.) due to the metabolism of the microorganisms on waste stream constituents. Microorganisms in a GI system may metabolize the lipids through cleaving the glycerol head of triglycerides (Wakelin, Forster, 1997).

Microorganisms are known to breakdown fatty acids via beta-oxidation (Madigan et al. 2000; Vaccari et al., 2006). Matsui et al. (2005) noted that unsaturated fatty acids following initial triglyceride hydrolysis by lipase maybe preferentially broken down through beta-oxidation by microorganisms in wastewater leaving behind saturated fatty acids which can react with calcium in the wastewater to form solid tacky substances. If similar conditions occurred in sanitary sewer systems or in grease interceptors, then FOG deposits containing high levels of saturated fatty acids and calcium with lower concentrations of unsaturated fatty acids would be found in these systems. The results from characterization of FOG deposits reported previously suggest that microbial activity, if not properly managed, could contribute to the formation of these FOG deposits. However, more research is needed to confirm this hypothesis.

WWERF

4.6 FOG and Solids Accumulation Analysis

The research team observed several field interceptors around the Town of Cary, North Carolina. Comparisons were made regarding the inlet and outlet configurations and the grease cap and solids layer thickness for those interceptors. Three inlet configuration: a standard straight-pipe inlet-tee, a specially designed inlet distribution tee, and no inlet were observed in this study. Figure 4-6 depicts these configurations. The present assessment of field GI performance has been broken into three categories: A general analysis of GI performance from a large database, observation of GI maturation at a FSE without a food grinder, and observation of GI maturation at a FSE with a food grinder.
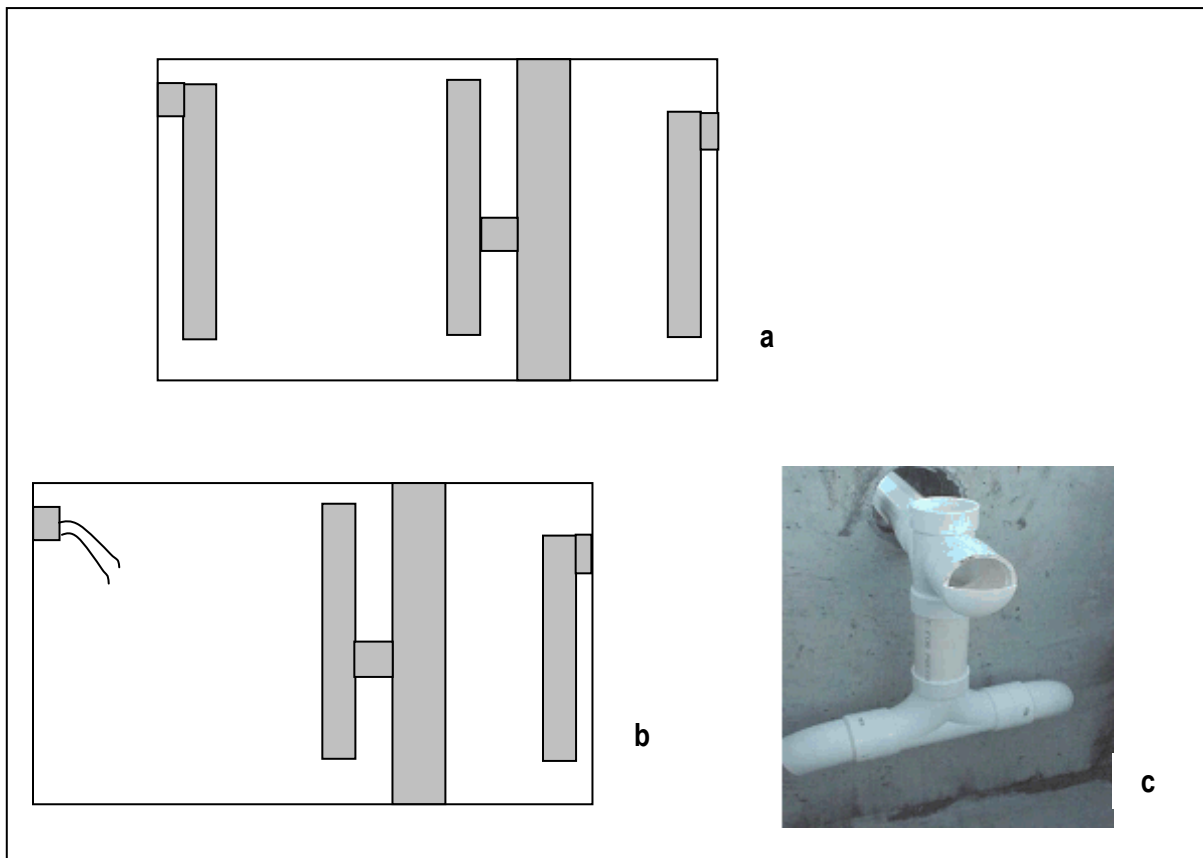
Figure 4-6. Field Grease Interceptors Observed: a) Standard Inlet Tee, b) No Inlet Tee, c) Distributive Inlet Tee.

4.6.1 Assessment of Alternative Influent Piping Configuration

The field data collected was organized based on several parameters: basic interceptor design, interceptor size, inlet, outlet configuration, FOG layer and solids layer thickness in the first and second compartments. For the present report, data was grouped to compare the results from each compartment for various inlet configurations, and 1000, 1500, and 2000 gallon grease interceptors were compared for inlet data available. Data variability was likely due to a lack of pumping history and restaurant practices. Tables 4-9 to 4-11 (and correspondingly Figures 4-7 to 4-9) show the layer thicknesses for the first and second compartments of similar volume GIs with various inlet configurations.

Table 4-9. Summary Table for Layer Thickness in 1000 Gal. GI.

1000 Gallon GI Data

	FOG Comp. 1 (in)	FOG Comp. 2 (in)	Solids Comp. 1 (in)	Solids Comp. 2 (in)
No Inlet	1.34	1.53	4.57	3.74
Standard Tee	0.98	0.50	2.00	1.18
Distributive Tee	1.82	0.83	5.35	3.37

Table 4-10. Summary Table for Layer Thickness in 1500 Gal. GI.

1500 Gallon GI Data

	FOG Comp. 1 (in)	FOG Comp. 2 (in)	Solids Comp. 1 (in)	Solids Comp. 2 (in)
No Inlet	0.90	0.70	5.60	4.03
Standard Tee	1.80	1.76	6.00	3.71
Distributive Tee	2.48	1.76	6.20	2.38

Table 4-11 Summary Table for Layer Thickness in 2000 Gal. GI.

2000 Gallon GI Data

	FOG Comp. 1 (in)	FOG Comp. 2 (in)	Solids Comp. 1 (in)	Solids Comp. 2 (in)
No Inlet	1.61	1.75	3.43	1.36
Distributive Tee	2.55	1.86	6.89	2.46

The data in Tables 4-9 through 4-11 clearly show thicker FOG and solids layers in the first compartment compared to the second compartment. In addition, there is clear evidence that solids and FOG will accumulate in the second compartment to some extent. Based on the GIs shown above, the distributive tee layout resulted in the largest thickness of oil and solids in the interceptors.

One possible way to evaluate the effectiveness of a grease interceptor layout would be to evaluate the quantity of trapped material in the interceptor. Under this assumption, in the cases shown above, the distributive tee would be the most effective at separating FOG and solids from FSE waste stream. One explanation for the higher accumulation of oil and solids is the slower inlet velocity with the distributed tees. The slower inlet velocity, which is caused by an increase in the cross-sectional flow area, allows more effective separation by permitting the upward migration of the oil droplets or downward particle settling. This analysis will be demonstrated with GI simulations described in the next chapter.

Comparison of FOG and Solids Layer Thickness in 1st and 2nd Compartment for 1000 Gal. GIs
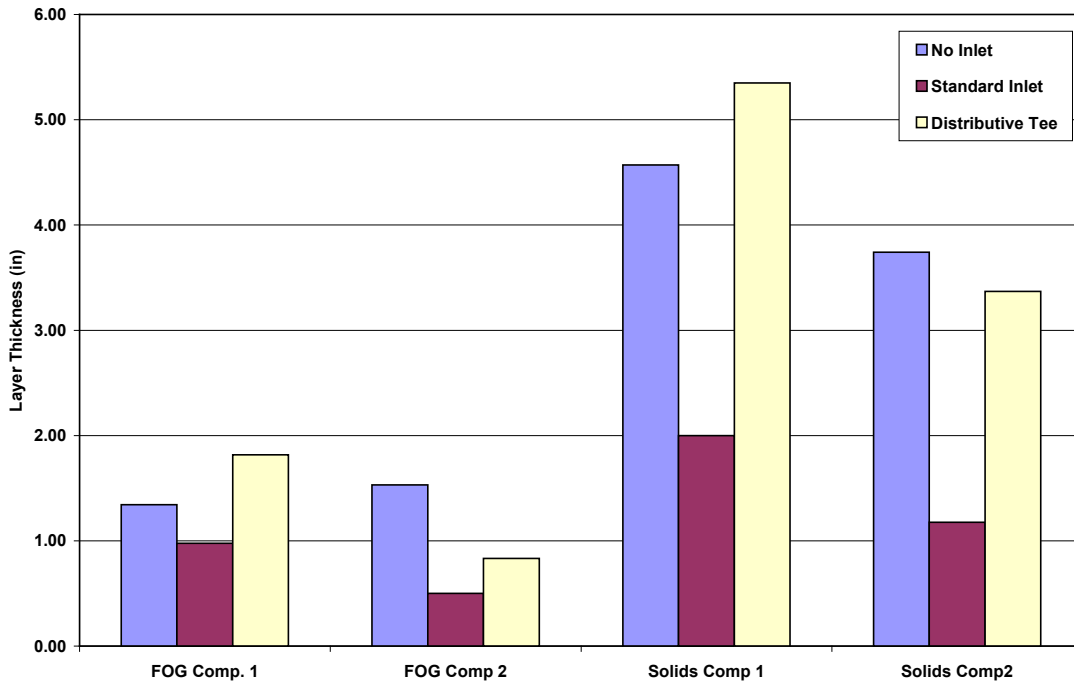
Figure 4-7. Graphical Representation of Table 4-9.

Comparison of FOG and Solids Layer Thickness in 1st and 2nd Compartment for 1500 Gal. GI's
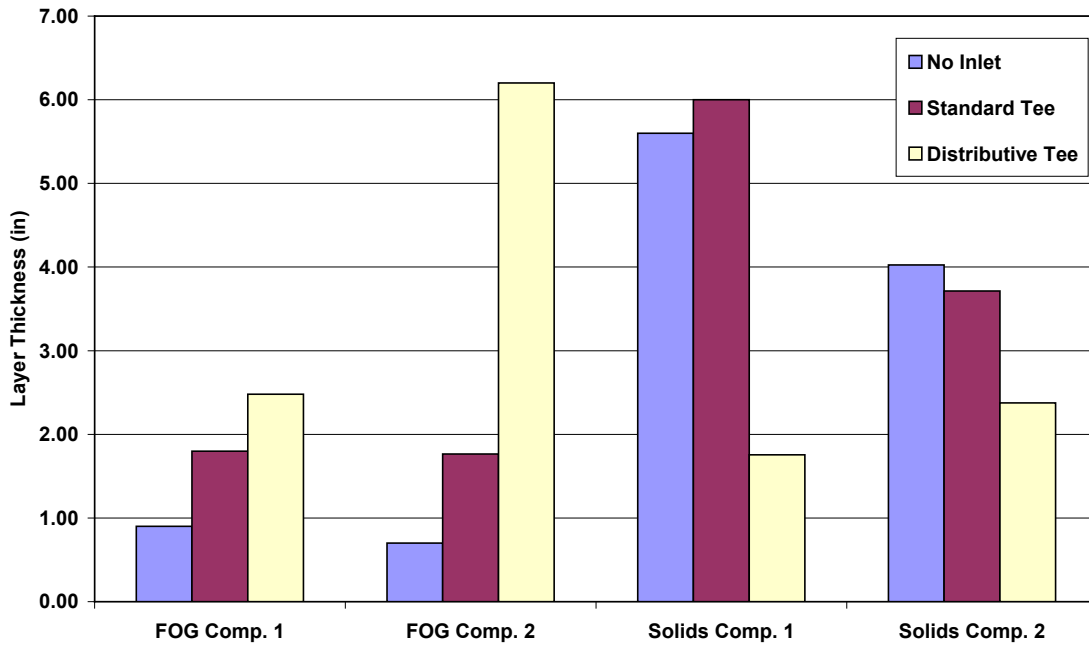
Figure 4-8. Graphical Representation of Table 4-10.

Comparison of FOG and Solids Layer Thickness in 1st and 2nd Compartment for 2000 Gal. GI's
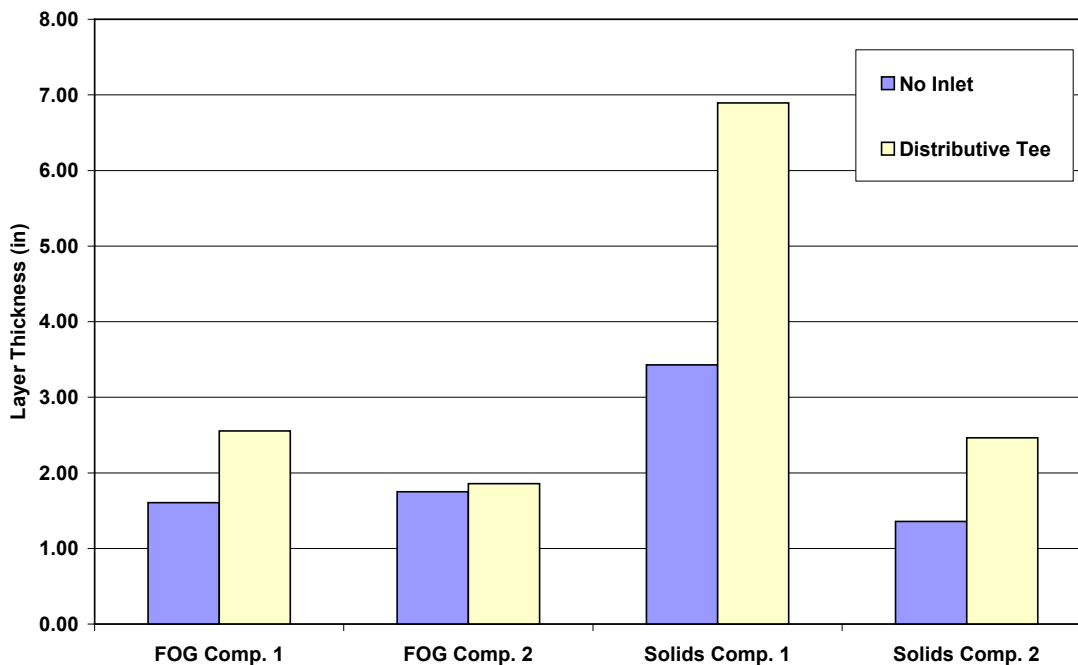
Figure 4-9. Graphical Representation of Table 4-11.

4.7 Assessment of Food Service Establishment Grease Interceptor Without Food Grinder

The thickness of the FOG and food solids layers was measured from a FSE that did not use a food grinder in the Town of Cary. The grease interceptor had a distributive style inlet configuration with a standard, straight pipe baffle and outlet. The GI was cleaned on a monthly basis. Data was collected weekly over a two month period with three measurements from both the first and second compartment of the grease interceptor. Figure 4-10 displays the sample collection points while Table 4-12 presents the results from field sampling. Figure 4-11 represents the FOG thickness over the duration measured while Figure 4-12 represents the evolution of the solids thickness during the same period. Figure 4-11d and Figure 4-12d depict the thicknesses immediately following a GI pump-out.

WERF
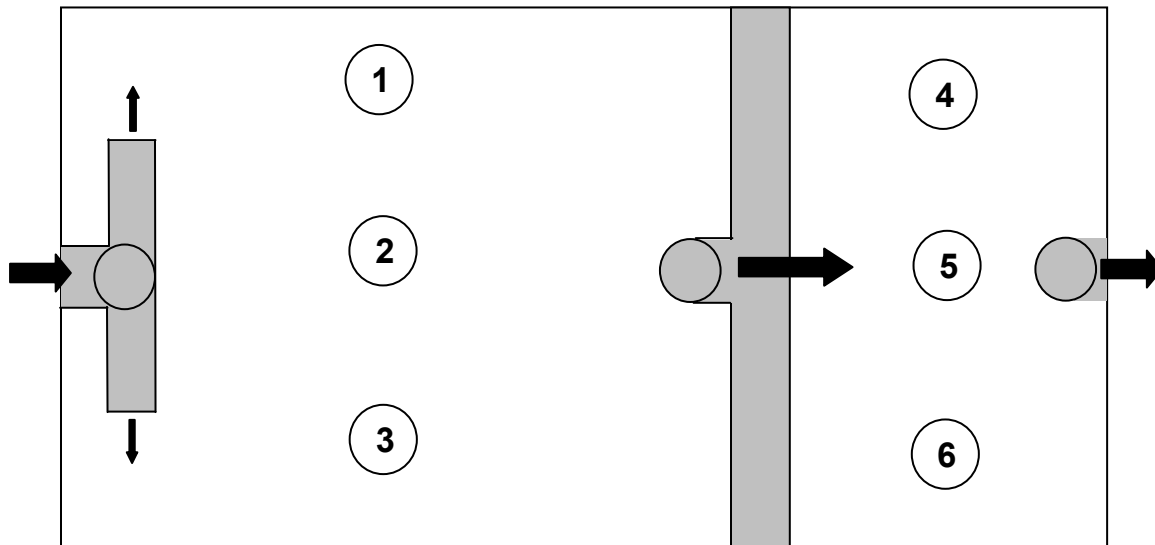
Figure 4-10. Configuration for Field GI Sample Collection.

Table 4-12. Samples from Field GI with no Food Grinder and Distributive Inlet Configuration (in).

Date	Material	1	2	3	4	5	6	Time Since Cleaning (days)
13-Aug	FOG	0.5	0.5	1	0.5	0.5	0.75	17
13-Aug	Solids	11.5	11.5	11.5	7	5	6	
20-Aug	FOG	0.25	0.25	0.5	1	1	1	24
20-Aug	Solids	11	12	13	9	7	5	
27-Aug	FOG	0	0	0	2	2.25	2	31
27-Aug	Solids	9	5.5	9	9	8.5	9	
4-Sep	FOG	0.25	0.5	0.5	0.25	0.25	0.25	7
4-Sep	Solids	5	0	0	5	0	0	
10-Sep	FOG	0.25	0.25	0.25	0.25	0.25	0.25	14
10-Sep	Solids	9	8	6	7.5	0	0	
17-Sep	FOG	0.25	0.25	0.5	0.5	0.5	0.25	21
17-Sep	Solids	12	10	9	7	0	0	

a

FOG Thickness - 17 Days Old

b

FOG Thickness - 24 Days Old

c

FOG Thickness - 31 Days Old

d

FOG Thickness - 7 Days Old

e

FOG Thickness - 14 Days Old

f

FOG Thickness - 21 Days Old
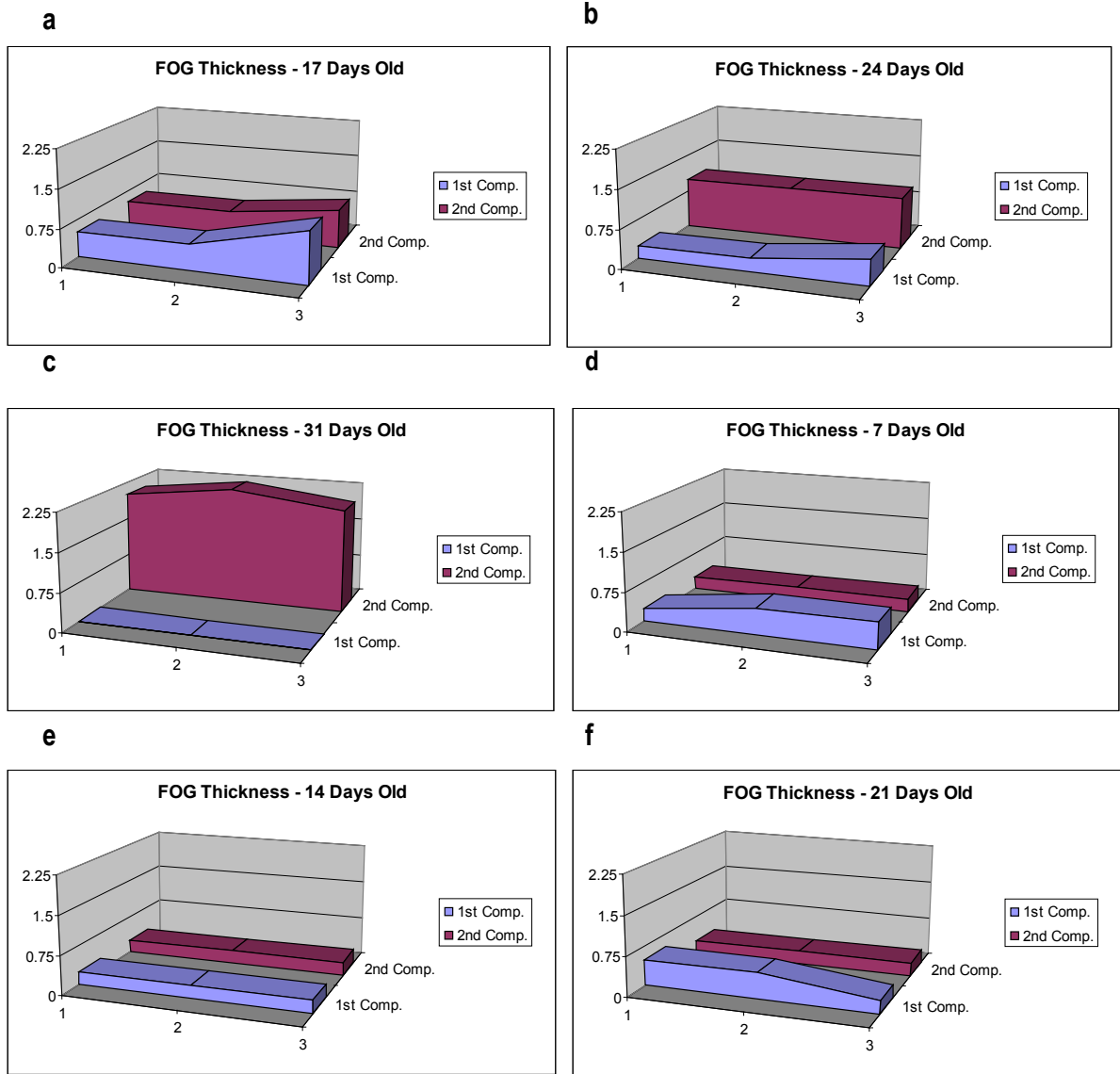
Figure 4-11. FOG Thickness in First and Second Compartment for GI with No Food Grinder.

WERF

a

Solids Thickness - 17 Days Old

b

Solids Thickness - 17 Days Old

c

Solids Thickness - 31 Days Old

d

Solids Thickness - 7 Days Old

e

Solids Thickness - 14 Days Old

f

Solids Thickness - 21 Days Old
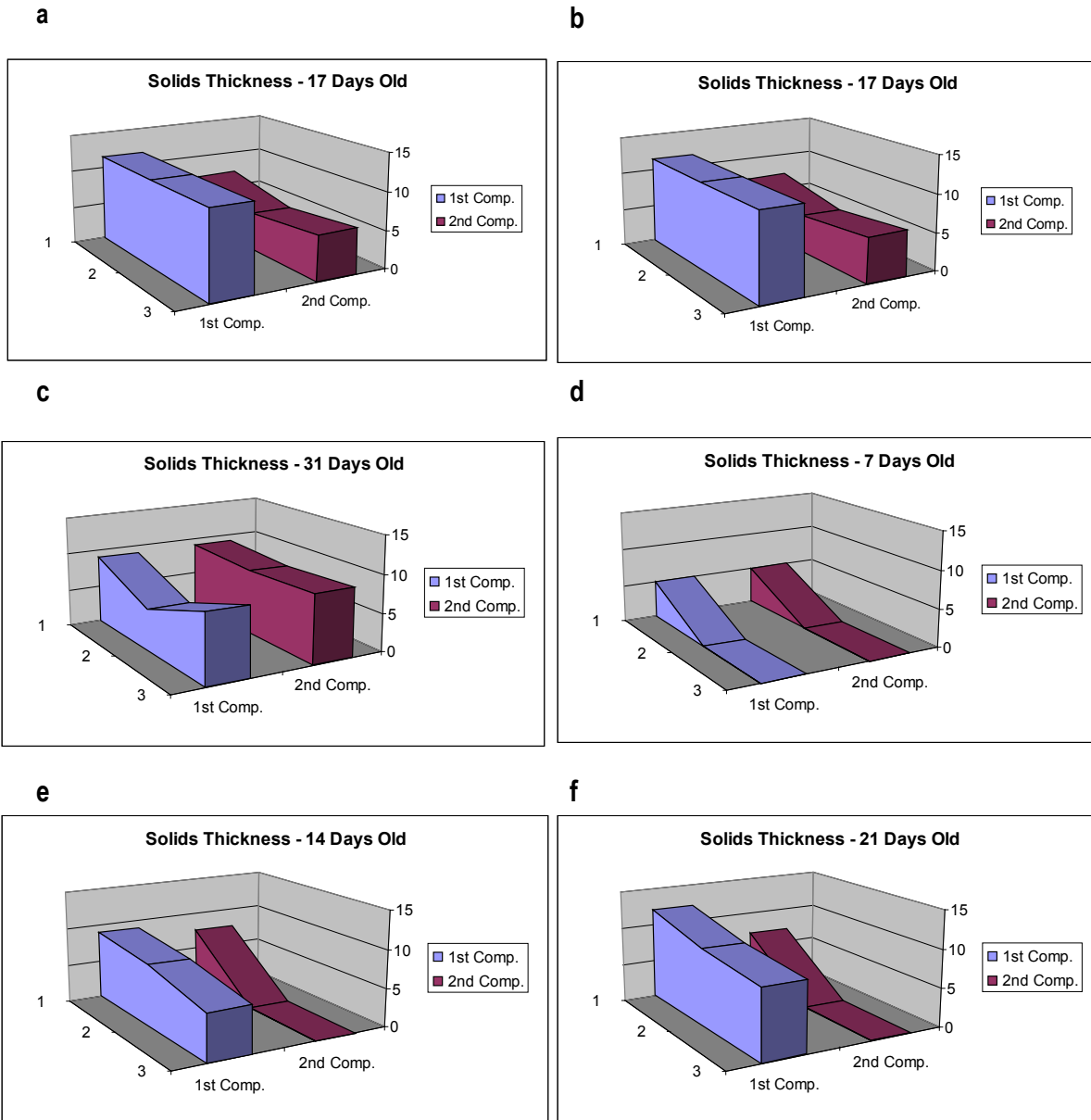
Figure 4-12. Solid Thicknesses in First and Second Compartment for GI without Food Grinder.

The observed GI displayed some variability as time progressed in the FOG thickness between the 1st and 2nd compartment. In Figures 4-11a and 4-11b (17 and 24 day GI age, respectively), the results showed that the FOG layer in the first compartment decreased slightly while the second compartment increased. By the 31st day (Figure 4-11c), the FOG layer in the first compartment was non-existent while the second compartment displayed a significantly thick FOG layer. After cleaning, however, this trend changed, with the first compartment exhibiting a decrease in FOG thickness between the 7th and the 14th day (Figure 4-11d and Figure 4-11e) while the second compartment remained constant at approximately 0.25 inches throughout. On

the 21st day (Figure 4-11f) the first compartment again increased in thickness while the second compartment remained constant.

These results suggest that some kind of gradual washout event occurred in the first compartment from the 17th to the 31st day prior to cleanout of the GI. This event did not occur during the period after cleaning as the FOG layer seemed more stable in the second compartment with some slight fluctuations in the first compartment FOG layer. No explanation was provided by the FSE as to what changed over the course of this period. It is unlikely that the washout event was due to a high flow rate as the solids layer (discussion in the next section) did not display a gradual movement of solids from compartment 1 to 2. Consequently, this change in profile is likely due to a temperature driven flow event that slowly eroded the FOG layer in the first compartment and shifted its contents to the second compartment. Moreover, the results suggest that the placement of a mid-baffle wall does not reduce the chance of significant FOG reaching regions near the effluent pipe. However, due to the deep location of the effluent pipe, it is possible that a transient event that causes erosion in the FOG layer may not result in an increase the effluent FOG concentration.

As can be seen in Figure 4-12, despite the fact that no food grinder was utilized by the FSE, significant food solids still accumulated at the bottom of the interceptor during the observed time period. Figure 4-12a indicates that at 17 days after the last cleaning event, the 1st compartment holds the majority of food solids in the interceptor although a significant thickness is present in the 2nd compartment. A week later (Figure 4-12b), more solids have accumulated in both the first and second compartment with a majority still remaining in the 1st compartment. By the 31st day (Figure 4-12c), however, a slight reduction in solids thickness around the central region is observed in the 1st compartment, while an increase can be seen in the 2nd. One week after cleaning the interceptor (Figure 4-12d), equal solid thicknesses were observed on the left side of both the 1st and 2nd compartment. In Figure 4-12e, a more distributed accumulation was observed in the 1st compartment while the second compartment appeared to slowly accumulate only on the left side of the tank. By the final observation date, 21 days after the last cleaning event (Figure 4-12f), measurement in the GI indicates further distributed accumulation in the 1st compartment with a similar left biased solids height in the second compartment. The biased accumulation observed in Figure 4-12 is a result of a slanted outlet tee for this particular field interceptor.

With the use of the distributive style inlet, an increased accumulation of FOG and solids was expected in the first compartment. As shown in Figures 4-11 and Figure 4-12, accumulation in the first compartment was not always the case. Transport of FOG between compartments appeared to take place between 17th and 24th day (Figure 4-11a through b), and more significantly between the 24th and 31st day (Figure 4-11b through c). Food solid transport took place to some degree during the entire observed period, though most significantly between the 24th and the 31st days (Figure 4-12b through c).

The likely shift in FOG layer thickness has been explained previously as a possible temperature driven event causing a buoyant plume to occur over instances of time between the measurement periods. This buoyant plume would not significantly influence the solids layer. One could also argue that the FSE may have utilized a significantly higher FOG loading during this period. However, simulation tests showed that significant shifts in the FOG layer may not occur with higher concentrations unless there is also a change in oil droplet sizes. The significance of the shift in the solids between the 24th and the 31st day may indicate the attainment of a limiting

capacity of material in the 1st compartment and the subsequent flushing into the second compartment. These results may indicate the problems associated with allowing "excessive" accumulation in GIs prior to cleanout maintenance. Highly loaded GIs may run the risk of discharging significant quantities of FOG and solids into sewer systems. This discharge could occur by reaching a threshold of removal, a high flow burst when significant materials have already been accumulated, or a density driven flow that can also erode already separated material.

In some cases, GI capacity is discussed with regards to a weight of separable grease (PDI, 1998). Present observations suggest that interceptors are highly dynamic, transferring FOG and solids between the first and second compartment (and likely out of the system) quite frequently between cleanings. Significant effort must be made to monitor the solids and FOG loading to an interceptor as standard cleaning cycles may not be sufficient when describing GIs that do not have a grinder but still receive a significant amount of solids. In addition, any flow condition that may impact the FOG layer such as high temperature discharge from dishwashers should be cooled to the temperature of the bulk GI to reduce the potential for buoyant plumes.

4.8 Assessment of Food Service Establishment Grease Interceptor with Food Grinder

The researchers observed a full-fare food service establishment equipped with a food grinder for GI performance and maturation. Researchers hypothesized that an effective GI design would display greater FOG and Solids separation in the first compartment between cleanout periods. Figure 4-13 depicts the layout of this field grease interceptor and details the location of sample points.
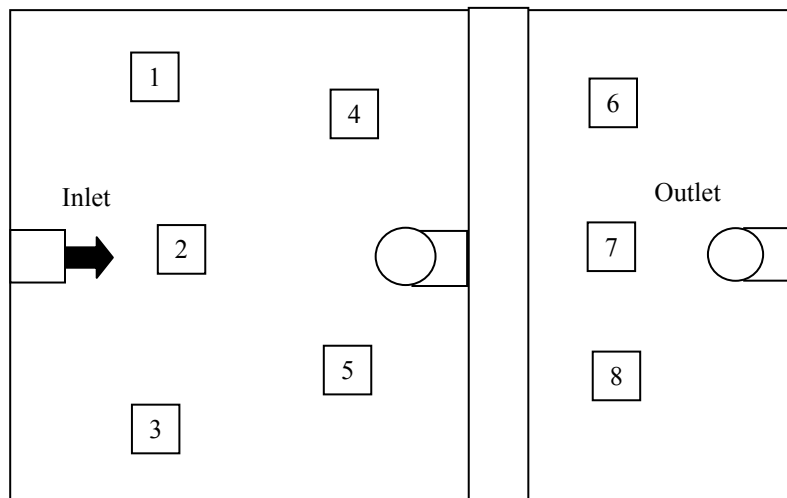

Figure 4-13. Layout of Field GI with Sludge-Judge Sample Locations.

The GI initially had no inlet tee. After multiple months of observation from that configuration, a distributive type tee (Figure 4-6c) was placed on the inlet of the interceptor followed by observations with a straight inlet tee configuration to complete analysis of key configurations of a common grease interceptor.

Researchers evaluated the performance of these field interceptors by comparing the FOG and solids thickness on the surface and tank bottom, respectively. Figures 4-14 through 4-17 and Table 4-13 display the results from the no inlet GI configuration while Figure 4-18 through 4-21 and Table 4-14 display the results from the distributive tee GI configuration. The straight inlet GI FOG maturation is then shown in Figure 4-22 through 4-25 and the data for those observations is shown in Table 4-15.

In Figure 4-14, the results show that the first compartment achieved an even distribution of FOG at 0.25 inches and the second compartment has a significantly greater accumulation of 1.75 inches by the fourth day. FOG does not appear to accumulate any further in the first compartment as shown in Figure 4-15 for day 15. The second compartment, on the other hand, continues to accumulate up to 3 inches of FOG by the 15th day. Food solids accumulation seems to occur rather differently than FOG accumulation. By day four, a significant quantity of solids can be seen in both the first and second compartment (Figure 4-16). The quantity continues to accumulate into the 13th day, at which point further solid build-up does not seem substantial (Figure 4-17). A channeling of solids in the first compartment is very clear in the GI by day 6 and this trend appears to continue until pump out. This severe channeling is most probably a result of the inlet configuration, and the higher velocity values through the baffle wall. These higher velocities through the baffle wall pipe are likely the cause of the significant solids accumulation in the second compartment.

After three days following the clean out period, the thickness of FOG in the first and second compartment has reached 0.25 inch (Figure 4-18). Unlike the no-inlet configuration, the distributive tee seems to promote FOG accumulation in the first compartment (Figure 4-19). In the seventh day, the first compartment has a uniform thickness of 0.5 inches, while the second compartment maintains its original thickness of 0.25. By day 17, the FOG layer has reached a peak of 1.5 inches in the first compartment and 0.5 inches in the second. As with the FOG accumulation, solid accumulation occurs almost entirely in the first compartment. By the 17th day, only 3 inches of food solids appear in the second chamber.

As can be seen in Figures 4-22 and 4-23, the first compartment FOG thickness remained at 0.25" for the entire observed duration. The second compartment, on the other hand developed a slightly thicker layer by day 7, however, this layer did not appear to grow for the duration of the observation. It should also be noted that the FOG valley shape generated in the second compartment suggests a scouring of the centerline FOG. This may be a result of high velocity flow coming through the baffle wall and impinging upon the outlet pipe.

Figures 4-24 and 4-25 show that the solids primarily accumulated in the first compartment, with a similar lesser thickness along the centerline (as was observed in the no-inlet configuration). This observed solids thickness in the centerline is likely the result of high velocities en route to the baffle pipe. As a result of these higher velocities, solids are prevented from settling (or scoured at high flow rates). Unlike the no-inlet configuration, however, the straight inlet only showed second compartment accumulation at day 12. It is unknown why this transient solids deposition occurred and suggests that other unforeseen dynamics may have occurred, such as different types of solids being deposited or a change in the flow pattern that allowed for deposition in the second compartment.

Short circuiting of the inlet flow can occur if the inlet velocity is too high at a specific location. With the no inlet tee, the flow enters the GI at the surface at one location. The higher velocity at this entrance point reduces the time that is necessary for proper separation within the first

compartment. Consequently, FOG accumulation and solids deposition is occurring in the second chamber. In the case of the distributed tee inlet configuration, the influent velocity is reduced since the flow is distributed over a greater pipe cross-sectional area. The lower influent velocity allows more FOG and solids to separate more effectively in the first chamber and little carry over of FOG and solids occurs in the second chamber. Further analysis of the distributed influent design using numerical modeling reveals that secondary flows seem to enhance the FOG separation process. The standard GI configuration with the influent straight pipe, mid-baffle wall and effluent pipe clearly shows the potential for re-suspending settled solids once the solids has accumulated to a certain depth. The centerline scouring was also noted for the no inlet configuration since a higher velocity down the centerline of the GI is still created with this configuration.

Table 4-13. No Inlet FOG and Solids Thickness Data.

FOG		Tank Location							
	Age	1	2	3	4	5	6	7	8
	4	0.25	0.25	0.25	0.25	0.25	1.5	1.75	1.75
	6	0.25	0.25	0.25	0.25	0.25	2	1.75	2.25
	13	0.25	0.25	0.25	0.25	0.25	3.5	2	2.25
	15	0.25	0.25	0.25	0.25	0.25	2.75	2.75	2.75
SOLIDS	Age	1	2	3	4	5	6	7	8
	4	5	7	7	4	8	6	7	6
	6	13	7	12	10	12	9	8	9
	13	15	8	17	15	17	13	12	13
	15	14	10	18.5	16	18	17	15	15

Table 4-14. Distributive Inlet FOG and Solids Thickness Data.

FOG		Tank Location							
	Age	1	2	3	4	5	6	7	8
	3	0.25	0.25	0.25	0.25	0.25	0.25	0.25	0.25
	7	0.5	0.5	0.5	0.5	0.5	0.25	0.25	0.25
	13	0.5	0.5	1.5	0.5	0.75	0.25	0.25	0.25
	17	0.75	1	1	1.5	1	0.5	0.5	0.5
SOLIDS	Age	1	2	3	4	5	6	7	8
	3	0	0	0	0	0	0	0	0
	7	6	5.5	6	9	9	0	0	0
	13	12	12.5	14	12	12.5	0	0	0
	17	11	13	15	14	14	0	3	0

Table 4-15. Straight Inlet FOG and Solids Thickness Data.

FOG		Tank Location							
	Age	1	2	3	4	5	6	7	8
	5	0.25	0.25	0.25	0.25	0.25	0.25	0.25	0.25
	7	0.25	0.25	0.25	0.25	0.25	0.5	0.25	0.5
	9	0.25	0.25	0.25	0.25	0.25	0.5	0.25	0.5
	12	0.25	0.25	0.25	0.25	0.25	0.5	0.25	0.5
SOLIDS	Age	1	2	3	4	5	6	7	8
	5	9	0.25	7	5	8	0.25	0.25	0.25
	7	8.5	0.25	6.5	5	8	0.25	0.25	0.25
	9	9	0.25	13	8	9	0.25	0.25	0.25
	12	9.5	6	12	12	12	5	5	6

4.9 Summary of Field Assessment of Grease Interceptors

Analysis of the field grease interceptors has revealed a highly dynamic, biological, separation chamber that is influenced by the type and quantity of FOG and solids that enters the GI and the internal flow pattern that is produced. The complexity of this system cannot be taken lightly and simplifying the procedure to develop a design for a specific food service establishment may result in a poor design for separating FOG and solids. The design of a GI for a specific food service establishment will have to utilize knowledge about the flow pattern produced, type and quantity of influent FOG and solids, and the maintenance schedule for the cleanout of the GI.
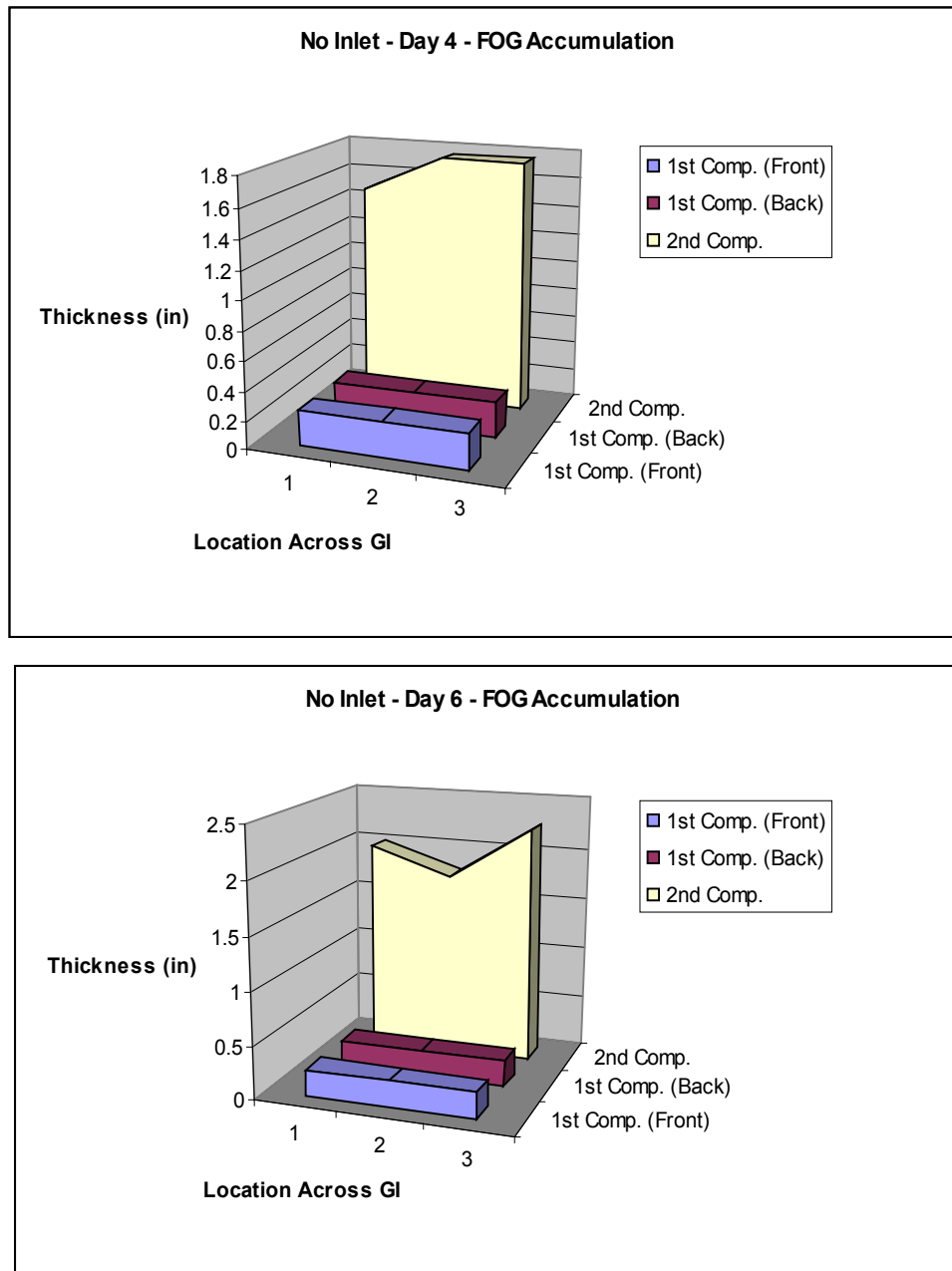
Figure 4-14. Day 4 and 6 FOG Thickness Profile in No-inlet GI.

WERF

No Inlet - Day 13 - FOG Accumulation

No Inlet - Day 15 - FOG Accumulation
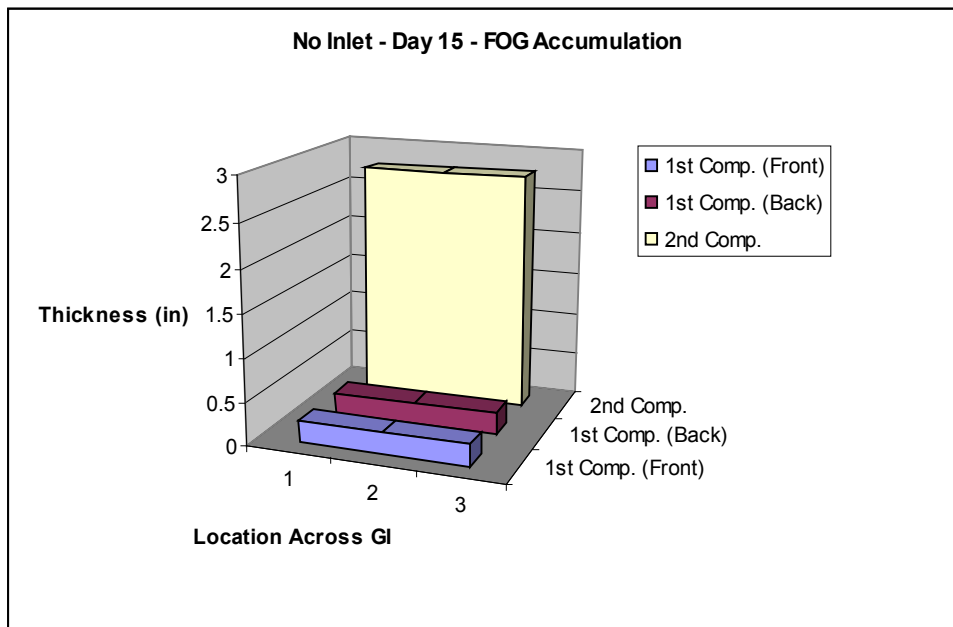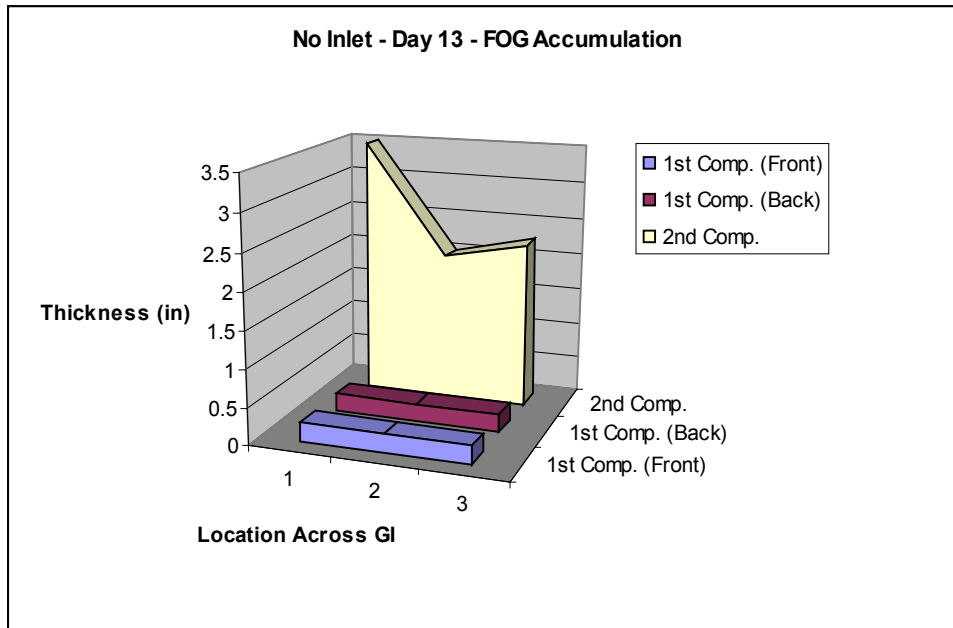
Figure 4-15. Day 13 and 15 FOG Thickness Profile in No-inlet GI.

No Inlet - Day 4 - Solids Accumulation

No Inlet - Day 6 - Solids Accumulation
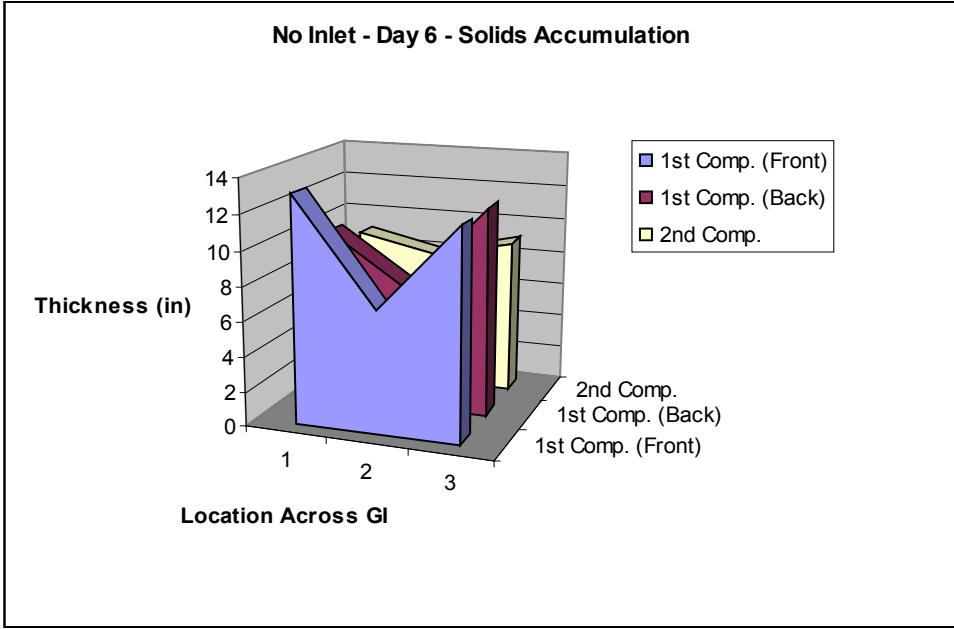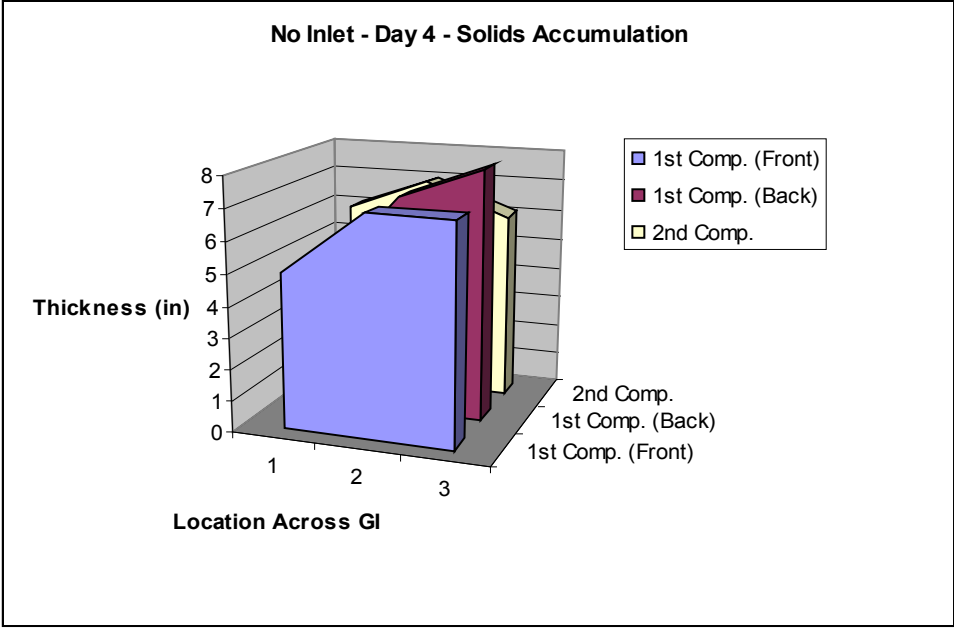
Figure 4-16. Day 4 and 6 Solids Thickness Profile in No-inlet GI.

WERF

No Inlet - Day 13 - Solids Accumulation

No Inlet - Day 15- Solids Accumulation
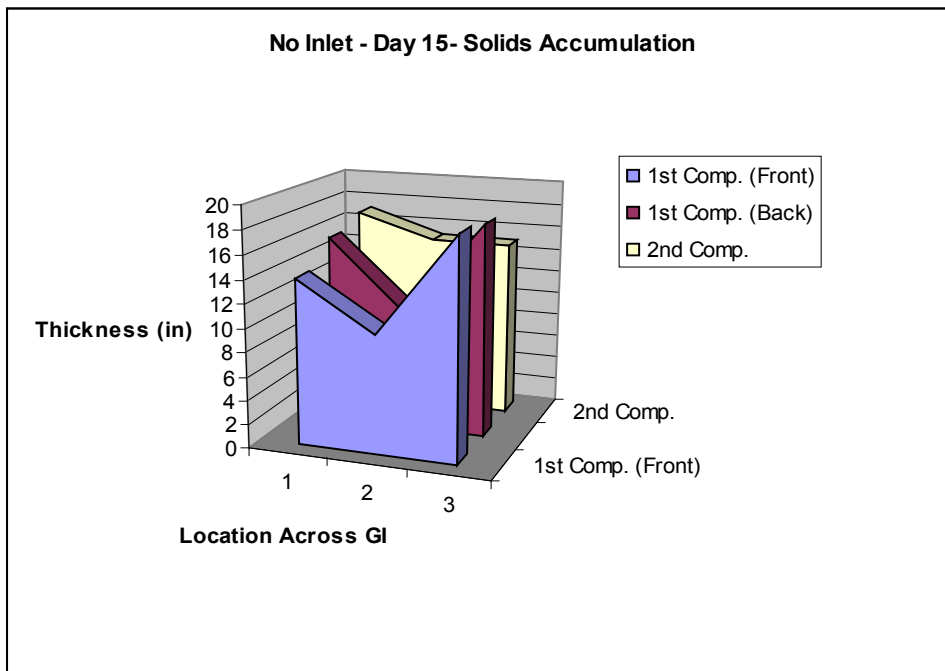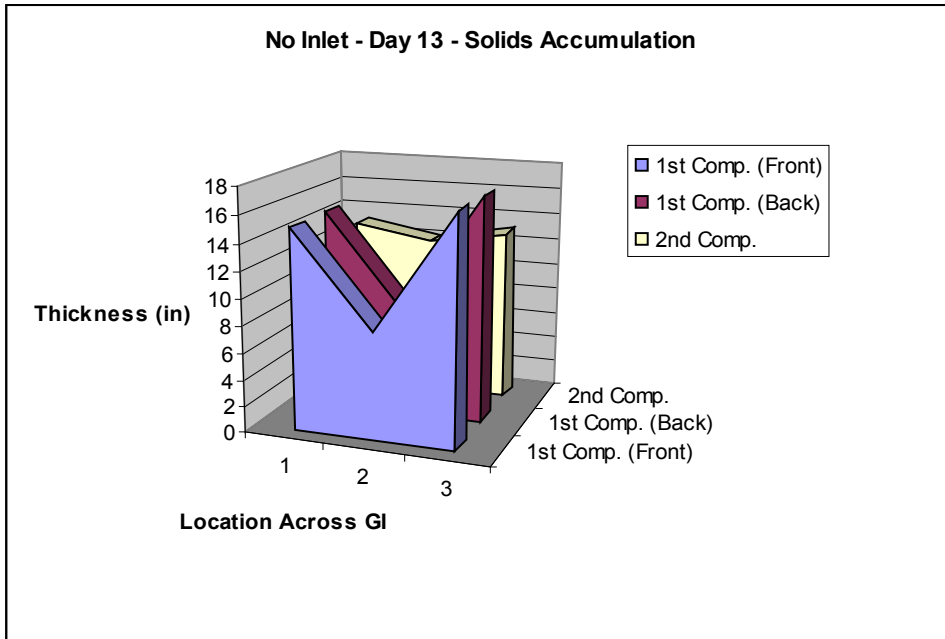
Figure 4-17. Day 13 and 15 Solids Thickness Profile in No-inlet GI.

Dist. Tee - Day 3 - FOG Accumulation

Dist. Tee - Day 7 - FOG Accumulation
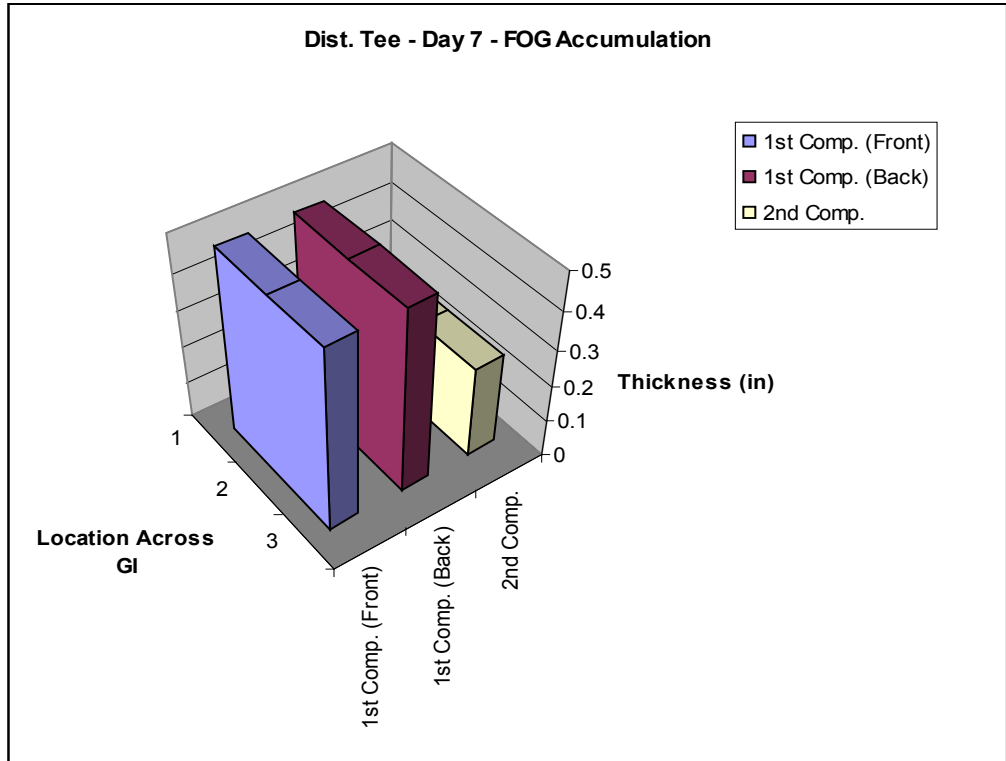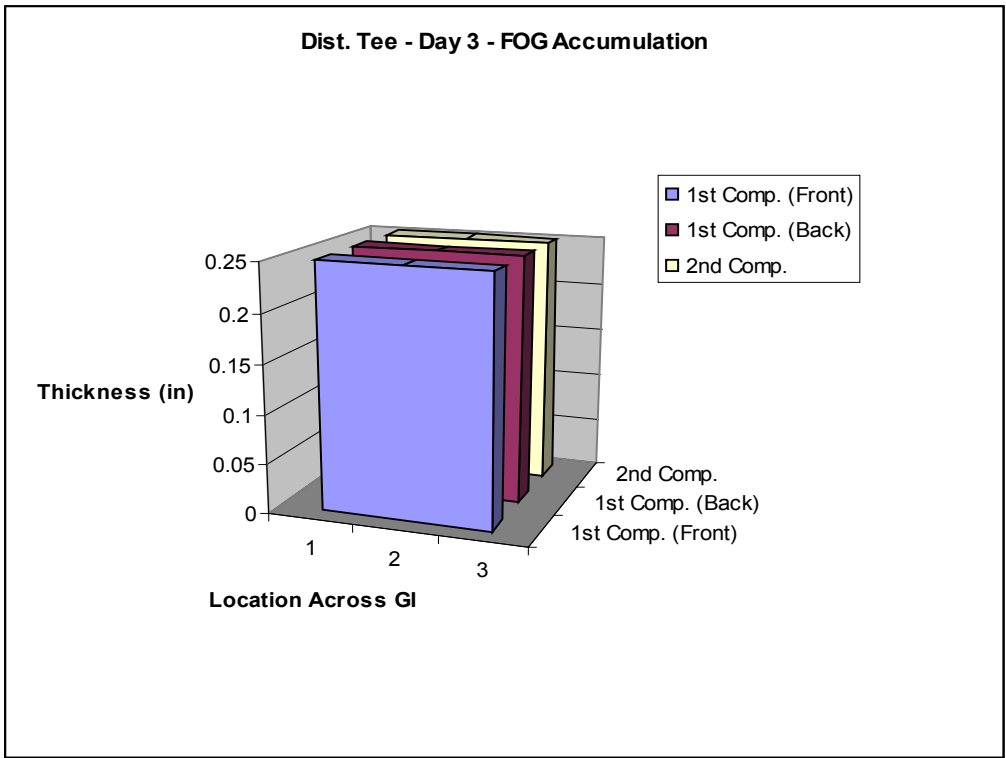
Figure 4-18. Day 3 and 7 FOG Thickness Profile in Distributive Tee-inlet GI.
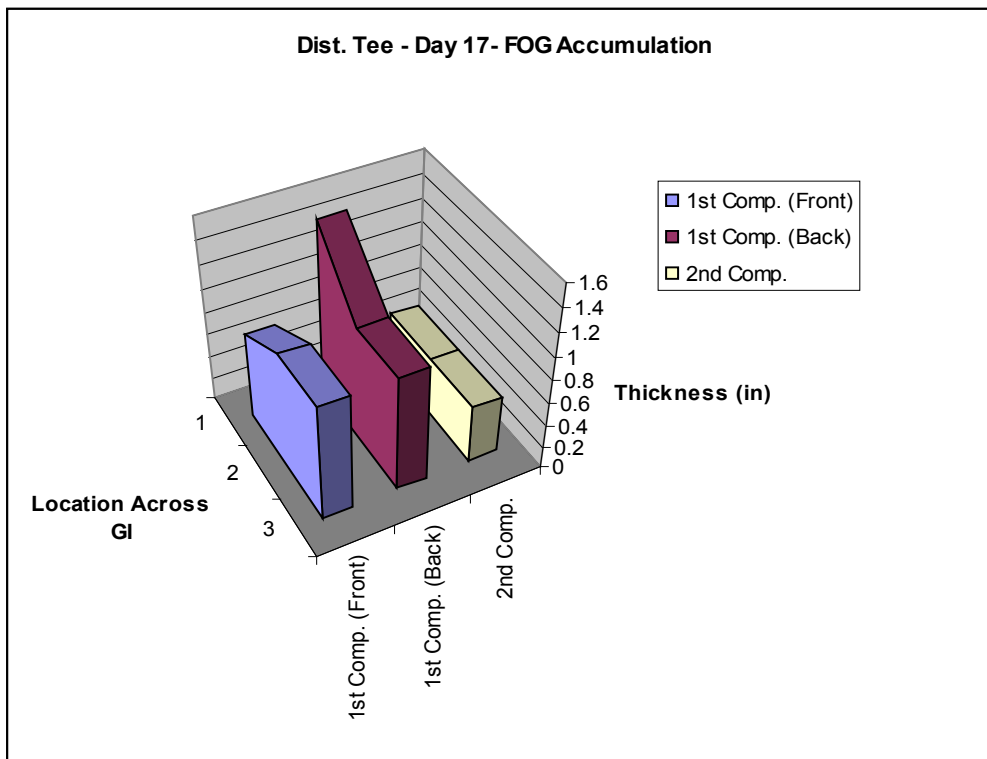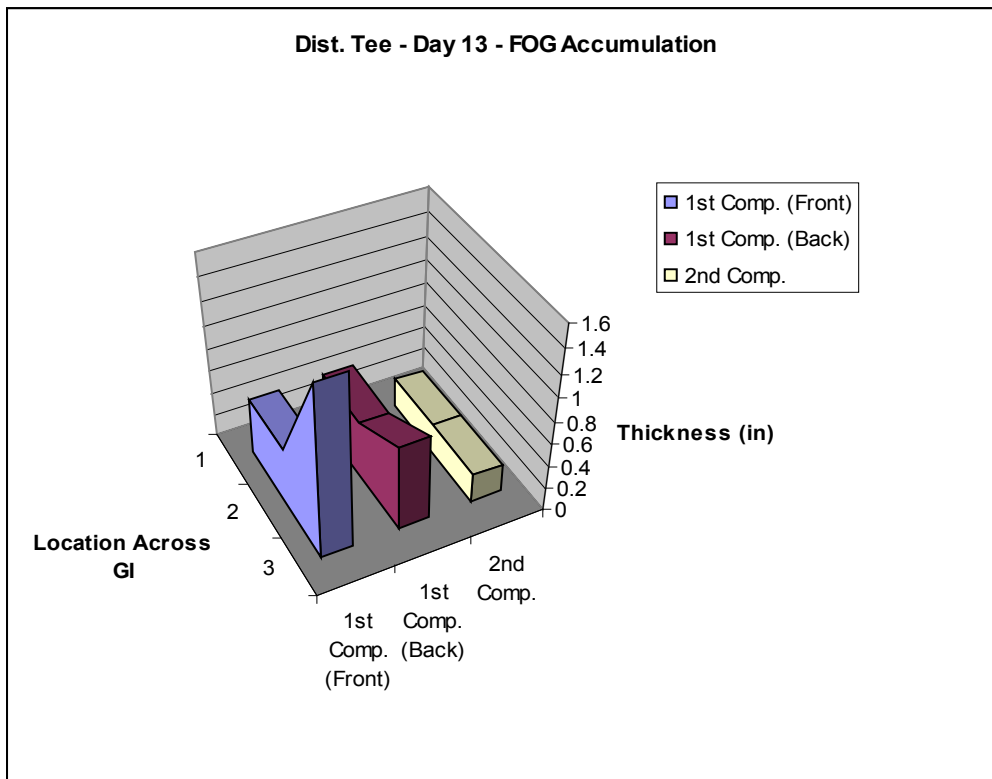
Figure 4-19. Day 13 and 17 FOG Thickness Profile in Distributive Tee-inlet GI.
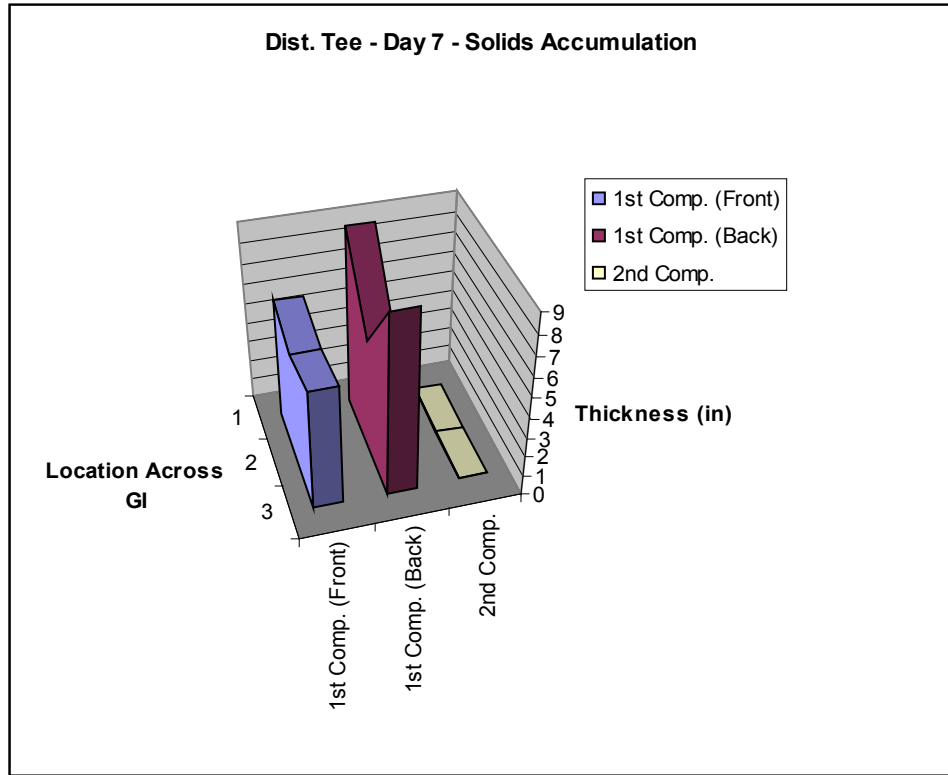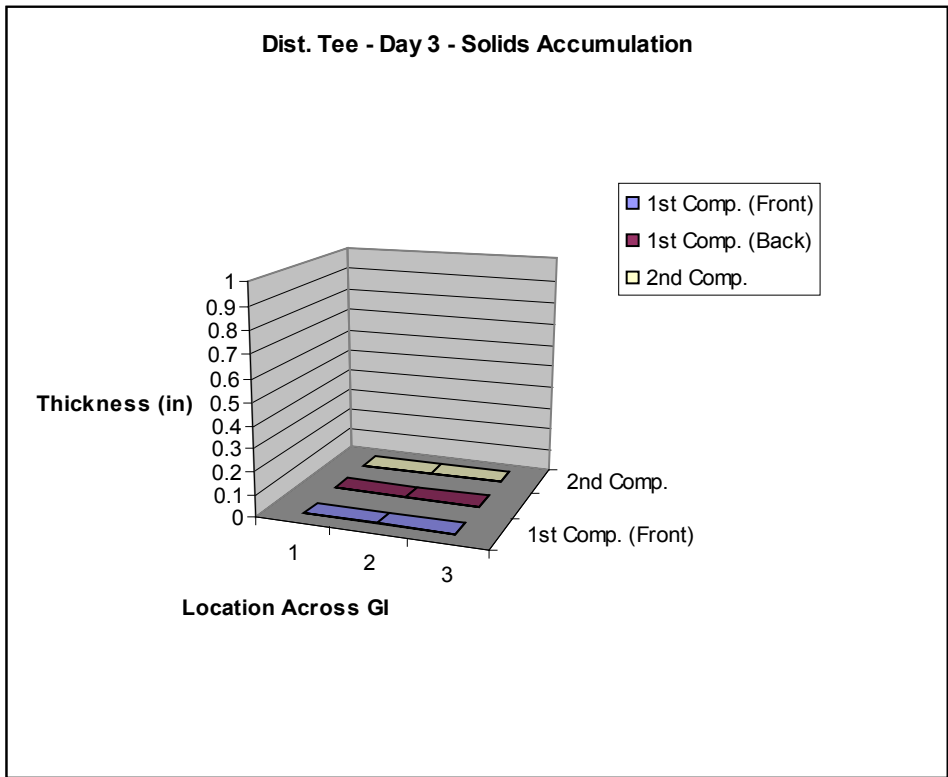
Figure 4-20. Day 3 and 7 Solids Thickness Profile in Distributive Tee-inlet GI.

WERF

Dist. Tee - Day 13 - Solids Accumulation

Dist. Tee - Day 17 - Solids Accumulation
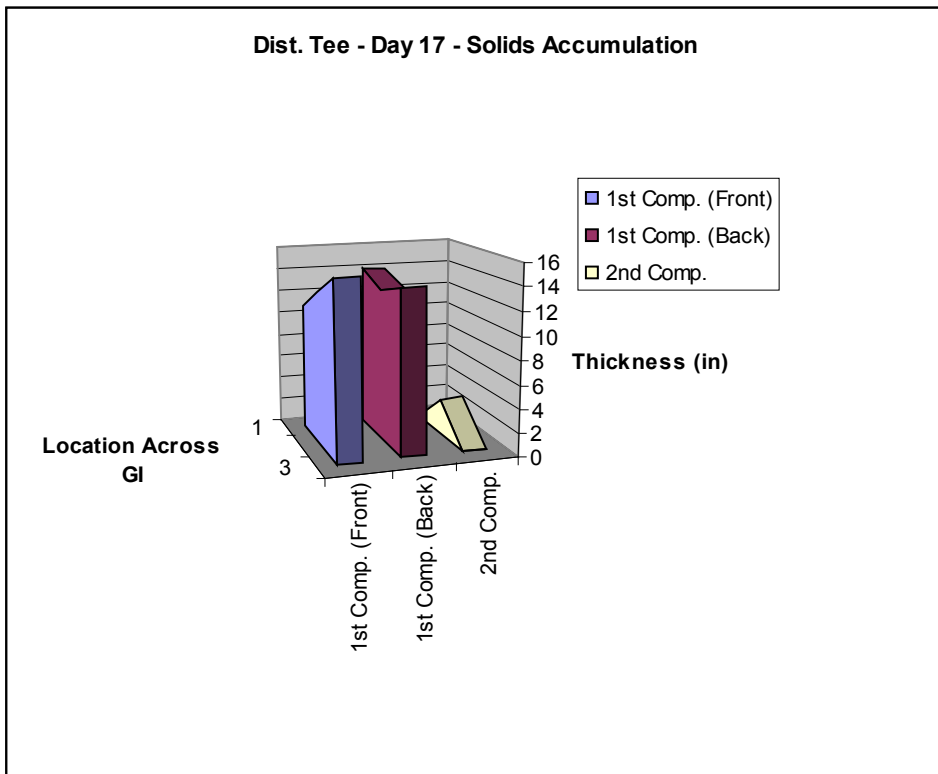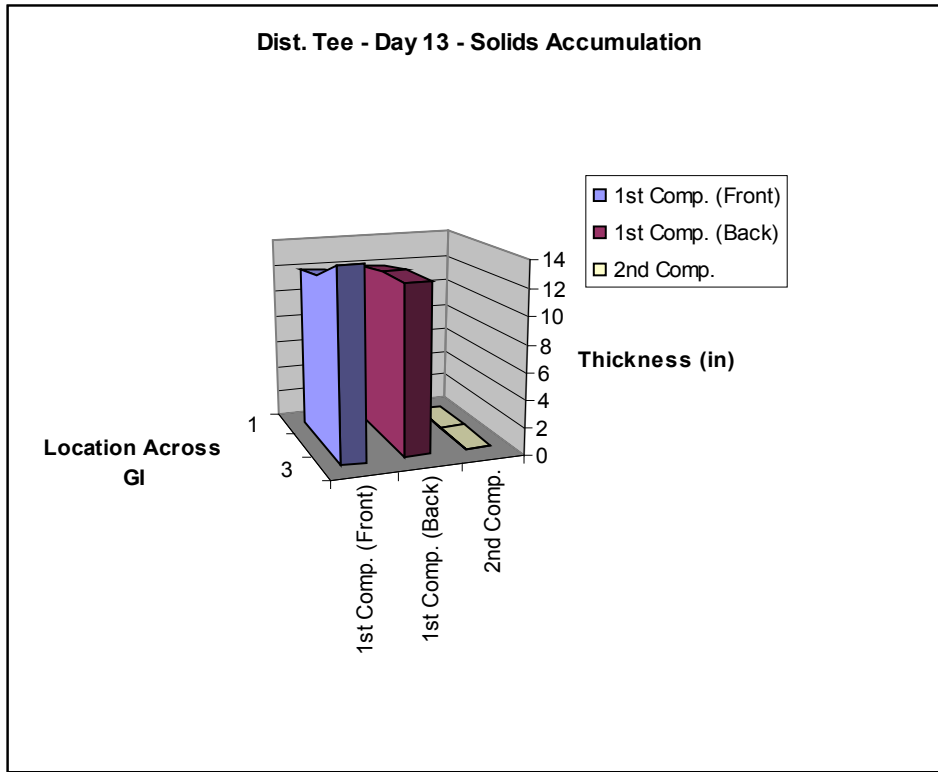
Figure 4-21. Day 13 and 17 Solids Thickness Profile in Distributive Tee-inlet GI.

Straight Inlet - 5 Day FOG Distribution

Straight Inlet - 7 Day FOG Distribution
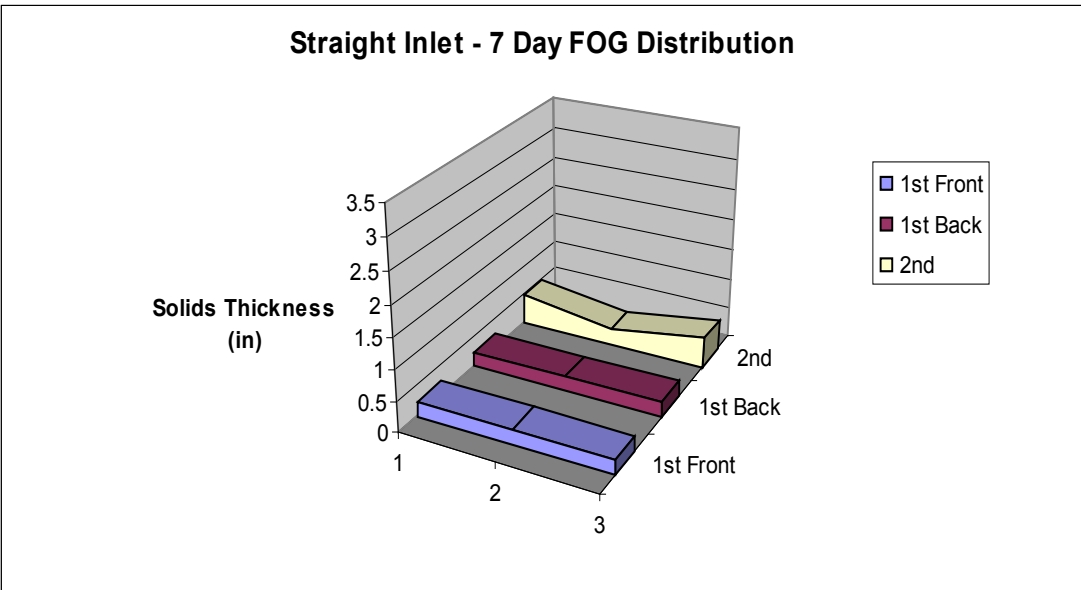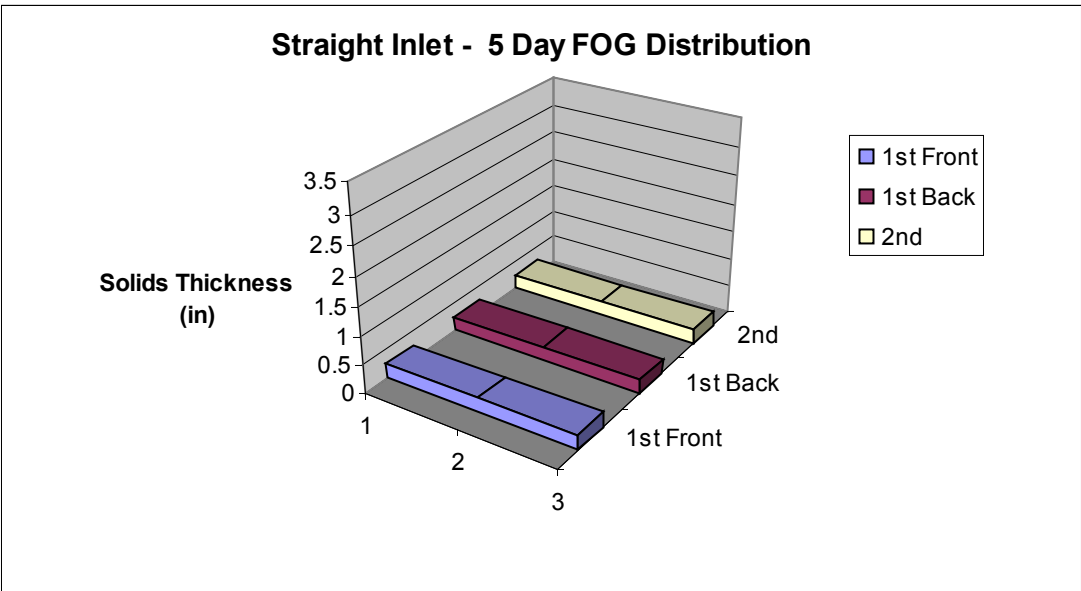
Figure 4-22. Day 5 and 7 FOG Thickness Profile in Straight Inlet GI.

WERF

Straight Inlet - 9 Day FOG Distribution

Straight Inlet - 12 Day FOG Distribution
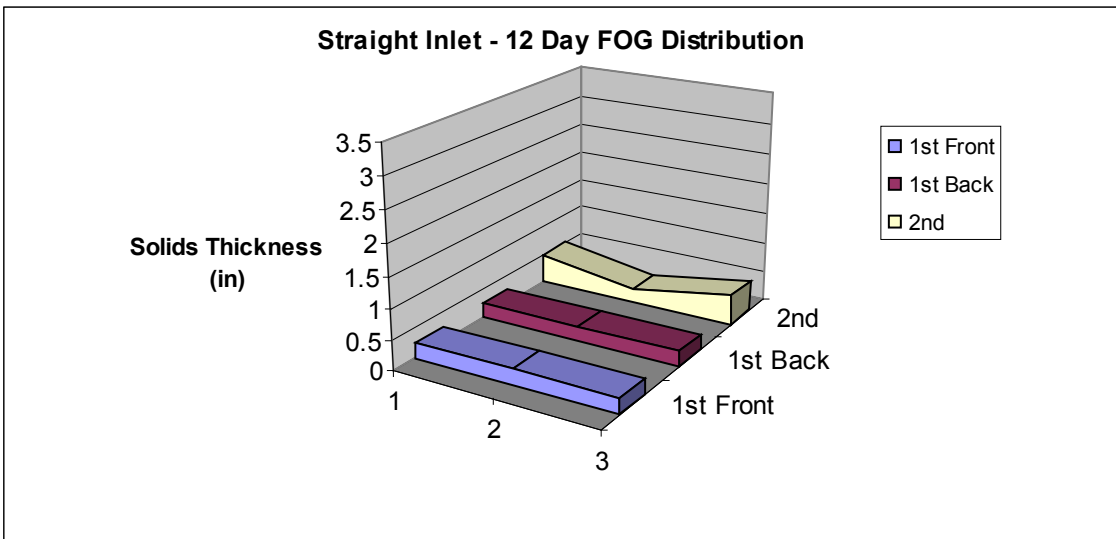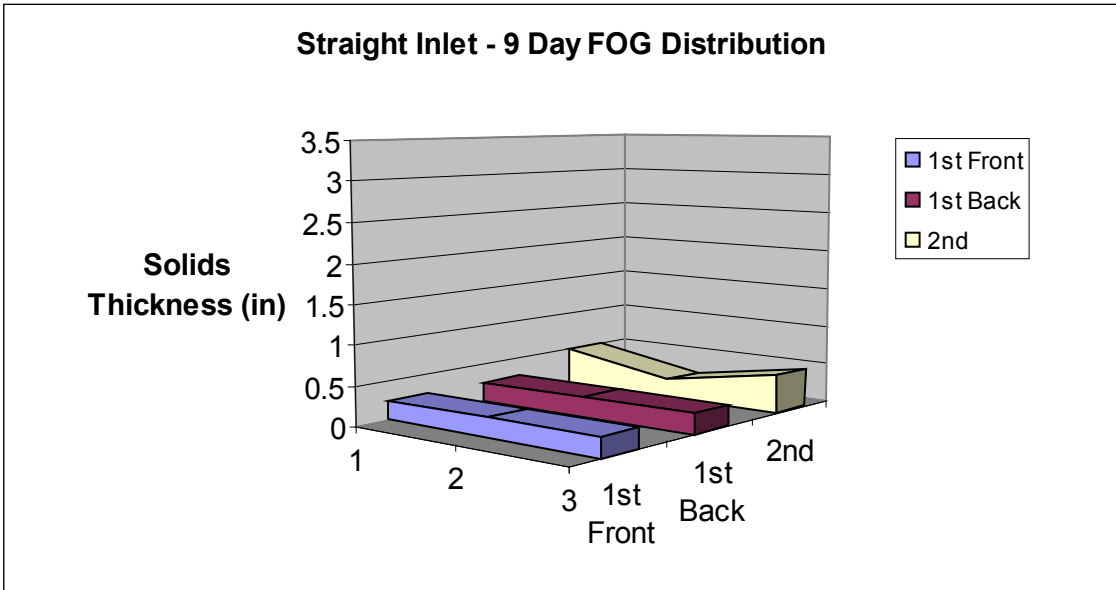
Figure 4-23. Day 9 and 12 FOG Thickness Profile in Straight Inlet GI.
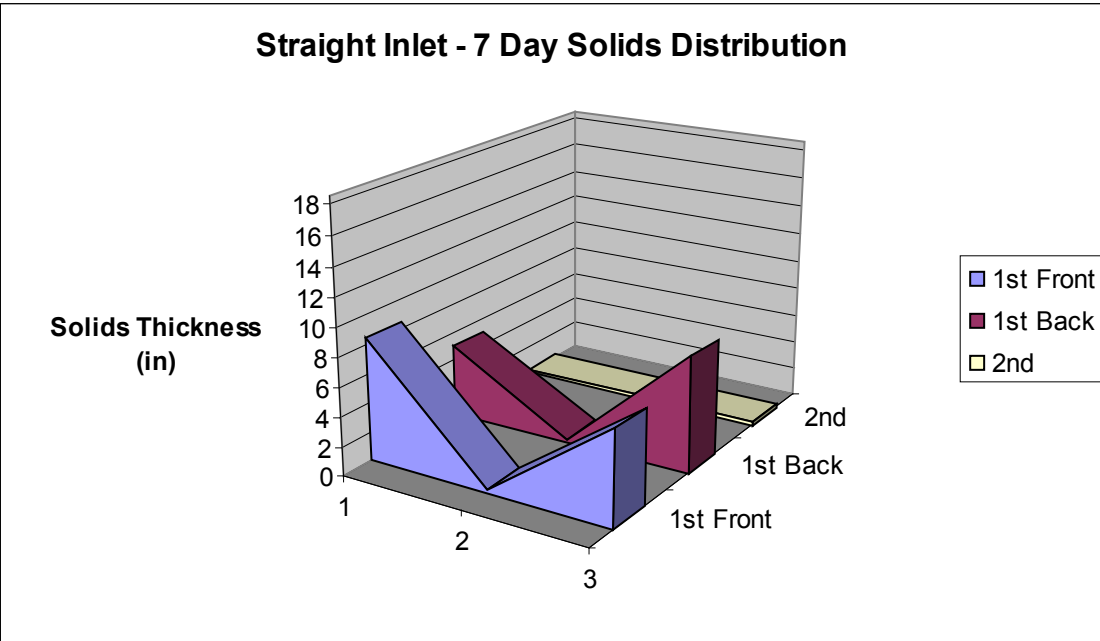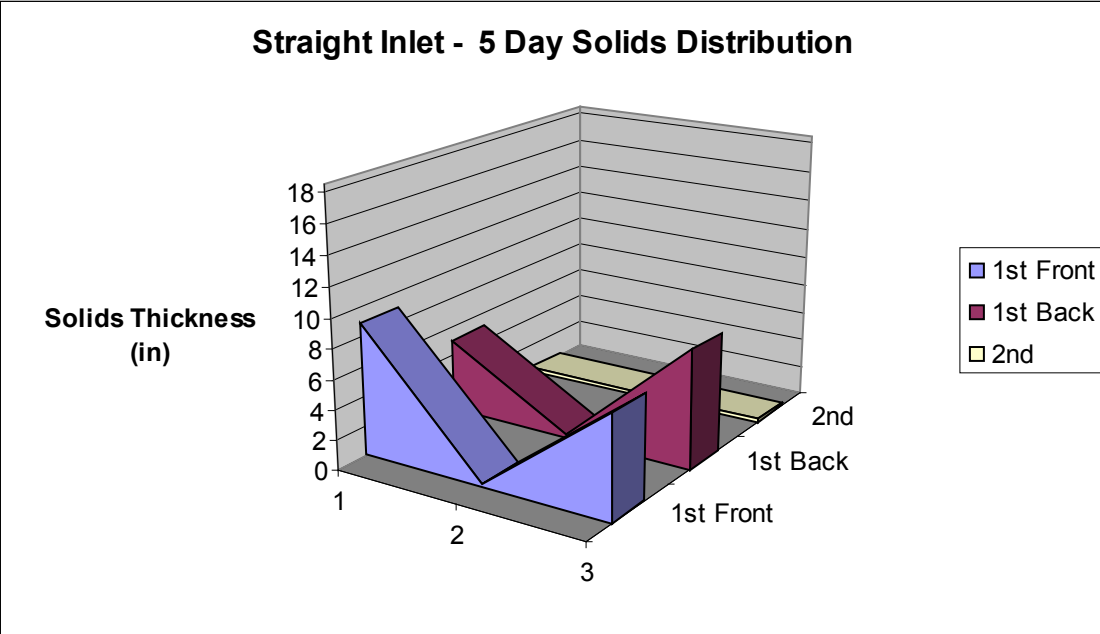
Figure 4-24. Day 5 and 7 Solids Thickness Profile in Straight Inlet GI.

WERF
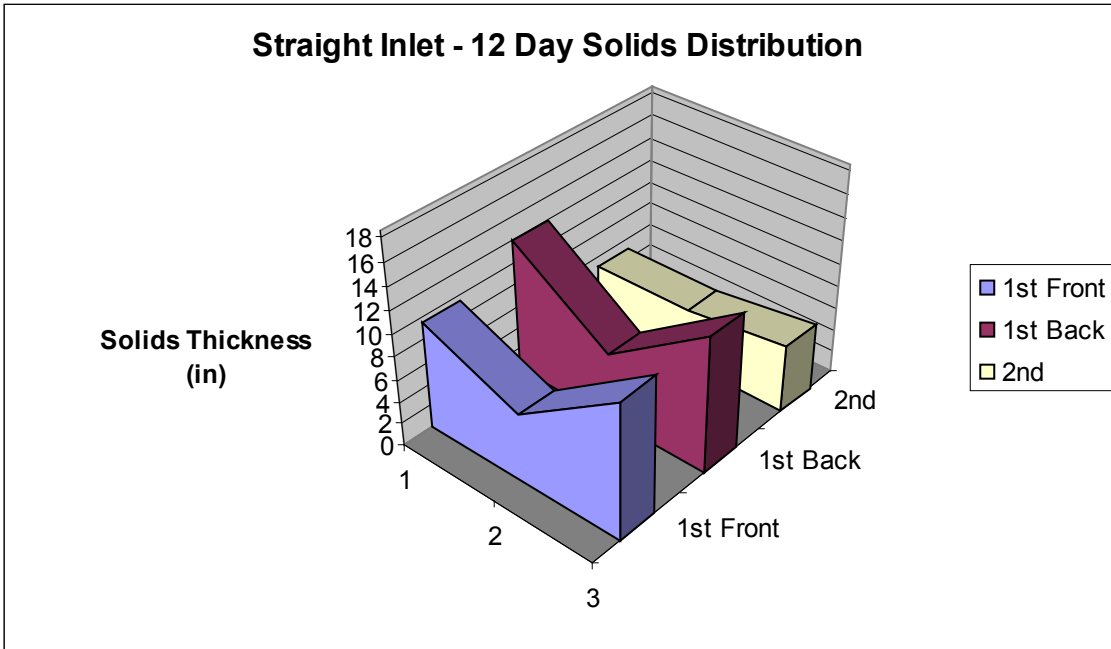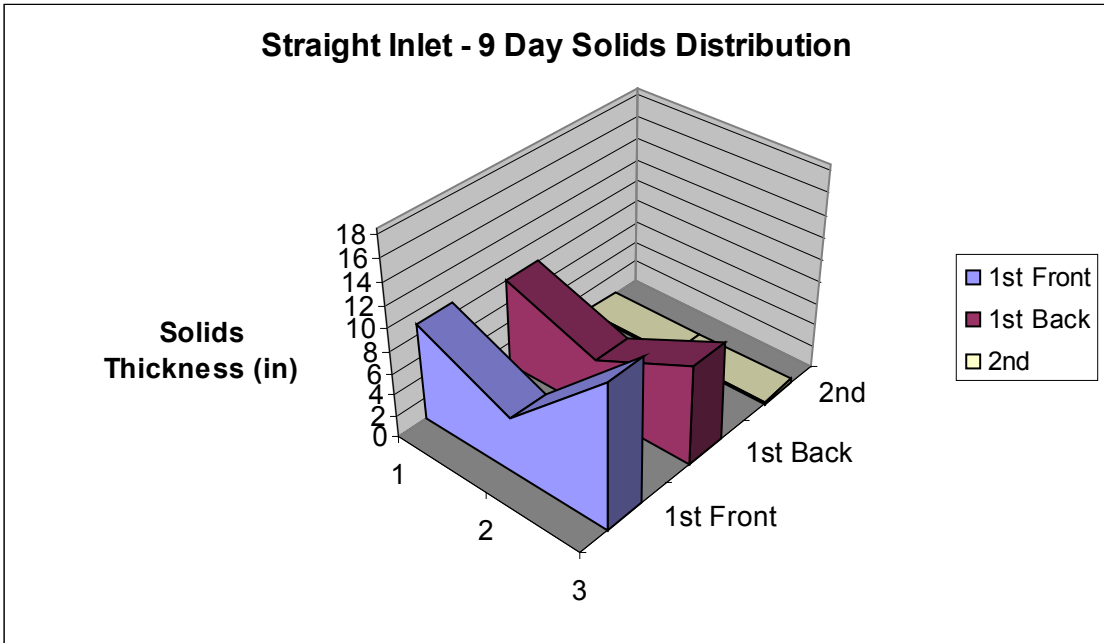
Figure 4-25. Day 9 and 12 Solids Thickness Profile in Straight Inlet GI.

WERF

CHAPTER 5.0

EXPERIMENTAL AND NUMERICAL ASSESSMENT OF GREASE INTERCEPTOR PERFORMANCE

5.1   Introduction

Initial experiments established appropriate methods for the measurement of FOG concentration from pilot and bench samples. Three different methods were utilized at various times during the course of the present research: U.S. EPA Method 1664, Evaporative Testing, and Infracal® analysis. After adequate FOG measurement methods were established, bench and pilot scale reactors were run under various operating and design configurations. As the less resource intensive of the two, the bench scale was used as a means to check the results of the computational fluid dynamics simulations. Tests were performed at the pilot scale for GI configurations that demonstrated enhanced performance.

5.2   Experimental Assessment

5.2.1   Lab Measurement of FOG Concentration

5.2.1.1   U.S. EPA Method 1664

Researchers sent several samples of known oil concentrations to two independent labs to establish the accuracy and precision of the U.S. EPA Method 1664. Each lab received four samples: three replicate samples of approximately 1137.5 mg/L and one at a lower concentration of 568.8 mg/L (Table 5-1).

Table 5-1. U.S. EPA Method 1664 Results from Two Independent Commercial Laboratories.

Actual Values (mg/L)	Lab 1		Lab 2	
	Value Measured (mg/L)	% Error (%)	Value Measured (mg/L)	% Error (%)
1137.5	800	29.67	753	33.80
1137.5	639	43.82	671	41.01
1137.5	788	30.73	678	40.40
568.8	425	25.27	405	28.79

As the results in Table 5-1 indicate, both laboratories varied significantly from the actual concentrations prepared by 25-43%. In addition, the total oil and grease measurement results using U.S. EPA Method 1664 was a function of the lab processing the sample.

Three oils of varying saturation levels were sent to one of the commercial labs to determine if the variability observed was a result of the oil type being used. The three oils included corn oil, peanut oil, and Crisco®. The oils were chosen due to their difference in fatty acid saturation level (i.e., corn oil had the lowest saturation while Crisco had the highest and

peanut fell in between these two oils). The lab received two concentrations of each oil (200 mg/L and 1000 mg/L). Results from this testing are shown in Table 5-2.

Table 5-2 suggests that the oil type utilized does not directly have an effect on the percent removal being reported with the U.S. EPA Method 1664. Such magnitudes in variability found in Table 5-2 would not allow for consistent determination of the grease interceptor removal performance under different operating conditions or changes in design configurations. Consequently, an alternate, more precise, method for assessing FOG concentration was needed.

Table 5-2. Summary of Results from U.S. EPA Method 1664 Test with Various Oil Types.

	Actual Concentration (mg/L)	USEPA 1664 (mg/L)	% Error (%)	Average (%)
Corn Oil	1000	631	36.9	34.2
	200	137	31.5	
Peanut Oil	1000	702	29.8	36.4
	200	114	43	
Crisco Shortening	1000	687	31.3	35.6
	200	120	40	

5.2.1.2 Evaporative Oven Testing

Researchers performed extensive tests with this approach at various known corn oil/water emulsions and at various sample volumes. Results showed significant variability associated with the precision scale utilized. As Figure 5-1 displays, an increase in oil mass yielded significant increases in mass recovery for known sample concentrations. This indicated an inability of the scales utilized to detect smaller oil concentration samples at a reasonable degree of certainty.
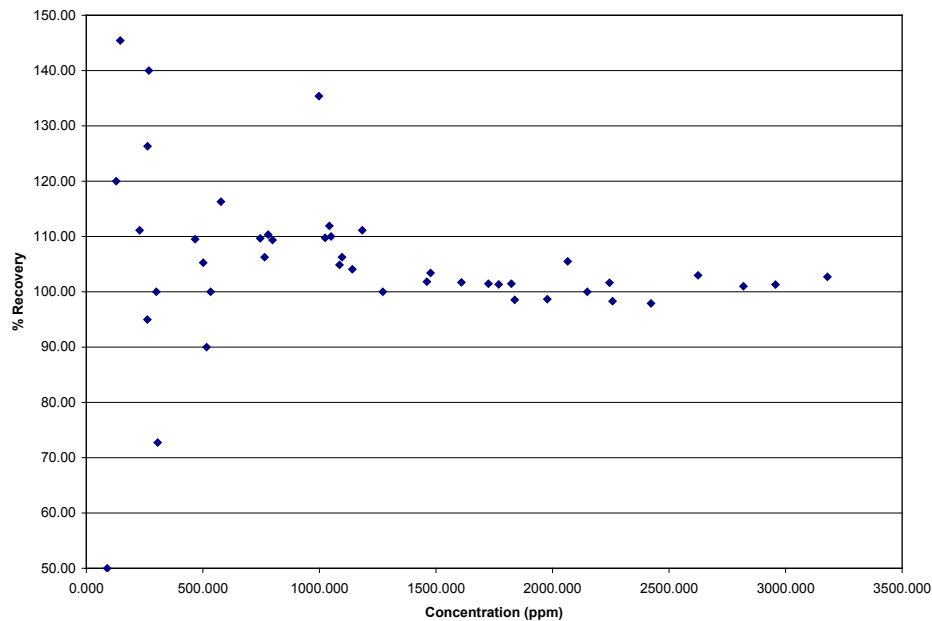
Figure 5-1. Data from Evaporative Testing at Various Concentrations.

WERF

The variability observed is most likely a result of the limitations of the electronic scales being utilized. The quantities of residual oil in the effluent testing jars (after sample evaporation) often approached the resolution of the scales being utilized. As a result, device error made the distinction between configurations often impossible. In addition to the imprecision of the device at lower concentrations, the amount of time required for the oil/water samples to dry completely was substantially longer than the Infracal® device. For those reasons the evaporative oven test was abandoned as the most feasible means for measuring oil concentration.

5.2.1.3 Infracal® Total Oil and Grease Measurements

The Infracal® unit required calibration with the specific oils utilized for use in measuring pilot and bench scale experimental samples. In order to create repeatable results, oil/water emulsions of known concentrations were made and extracted using the procedure outlined by the manufacturer (Infracal® User Manual, 2003). Using the absorbance output setting for the Infracal® unit, a calibration curve was constructed based on the range of oil concentrations that will likely be experienced in the grease interceptor influent and effluent. The Infracal® unit demonstrated sensitivity to sample temperature and sample type. Consequently, corn oil and peanut oil samples required separate calibration curves (Figure 5-2). The data for the calibration curves were then fit to a regression curve using the TableCurve 2D© software.
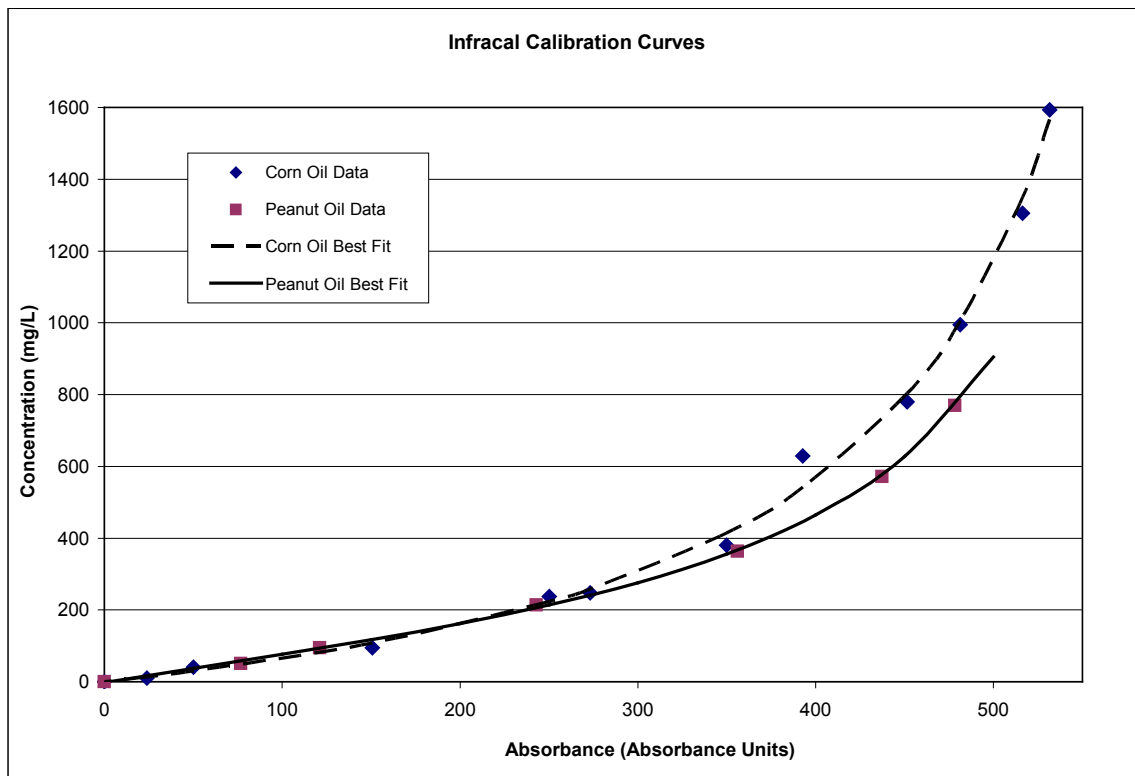
Figure 5-2. Infracal® Calibration of Corn Oil and Peanut Oil.

The variation in the calibration curve between corn oil and peanut oil is most likely due to the variations in the fatty-acid chain lengths and saturations (Table 5-3). The variation in fatty

acid content and saturation levels would result in varying levels of absorption from a given wavelength. As a result, the same calibration curve could not be developed for both oils particularly at oil concentrations above 200 mg/L, which will occur at the influent to the grease interceptor. For the FOG analysis performed with the Infracal[®®], calibration curves were made specific to the oil being utilized. The construction of the calibration curve for corn oil allowed for a wider range of concentrations. The Infracal[®] calibration curve for peanut oil, on the other hand, could not differentiate concentration values above 800 mg/L. Experimentation with peanut oil, therefore, required that the influent concentration not exceed 800 mg/L. Since corn oil was more flexible, it was utilized for more experiments in the present research.

Table 5-3. Fatty Acid Composition of Corn and Peanut Oil.
(from Physical and Chemical Characteristics of Fats, Oils, and Waxes, 2006)

Corn Oil			Peanut Oil		
FATTY ACID COMPOSITION	**% Range**		**FATTY ACID COMPOSITION**	**% Range**	
12:0	0	0.3	**12:0**	0	0.1
13:0	0	0.3	**13:0**	0	0
14:0	9.2	16.5	**14:0**	0	0.1
15:0	0	3.3	**15:0**	20	38
9c-16:1	0	0.4	**16:0**	8.3	14
18:00	0	3.3	**16:1**	0	0.2
Total 18:1	20	42.2	**9c-16:1**	0	0.2
Undefined 18:2		44.7	**18:00**	1.9	4.4
9c,12c-18:2	39.4	65.6	**Total 18:1**	36.4	67.1
Undefined 18:3	0.5	1.5	**Undefined 18:2**	14	43
20:0	0.3	0.7	**9c,12c-18:2**	14	43
Total 20:1	0	0.4	**Undefined 18:3**	0	0.1
20:2	0	0.1	**20:0**	1.1	1.7
22:0	0	0.5	**Total 20:1**	0.7	1.7
Undefined 22:1	0	0.1	**20:2**	0	0
24-0	0	0.4	**22:0**	2.1	4.4
			Undefined 22:1	0	0.3
			24-0	1.1	2.2
			15c-24:1	0	0.3

Although the Infracal[®] was established as a more precise means for quantifying FOG concentrations in the laboratory than either the U.S. EPA Method 1664 or the evaporative oven testing for the present study, some results were still sent out in duplicate for analysis with U.S. EPA 1664. Table 5-4 displays a comparison of some of these values.

WERF

Table 5-4. Comparison of U.S. EPA Method 1664 and Infracal® Tests.

Sample #	TOG Measurement Method	Influent (mg/L)	Effluent (mg/L)	% Removal (%)
1	U.S. EPA 1664	785	162	79.4
1	Infracal	1444.5	383.7	73.4
2	U.S. EPA 1664	778	266	65.8
2	Infracal*	NA	412	NA
3	U.S. EPA 1664	364	46	87.4
3	Infracal	1021	98	90.4
4	U.S. EPA 1664	165	51.6	68.7
4	Infracal	582.1	94.6	83.8

* Influent Value Calculated beyond calibration curve (Peanut Oil)

The variations observed between the two experiments is sometimes quite significant, approximately 50%. This variation does not seem to have a significant effect on the evaluation of the percentage removal from the system. When the data in Table 5-4 is combined with the clear variation in identical 1664 samples shown in Table 5-1, it appears that Method 1664 may be unreliable for the evaluation of grease interceptor performance. In addition, the consistent under-prediction of FOG concentrations with Method 1664 raises questions as to the accuracy of this approach for TOG analysis in field grease interceptors.

5.2.1.4 Experiments with Detergents
Testing was done to determine if there was a substantial effect on reported absorbance when samples had trace concentrations of detergents (Table 5-5). As Table 5-5 indicates, reported absorbance units were generally higher when detergents were present in the samples. Either a chemical change of the oils, with the addition of the detergents or the presence of the detergents in the extracted layer, may explain the increased absorbance shown. Further experimentation with extractants and wavelengths would need to be performed in order to determine how to exclude their presence and measure the true oil concentration.

Table 5-5. Infracal® Test Comparison for Known Samples with and without Detergents.

Concentration (mg/L)	No Detergents (Absorbance Units)	Detergents (Absorbance Units)
1000	481.3	490.5
600	392	473.5
200	235	371.7

5.3   Bench Experimental Tests

Several experiments with the bench scale grease interceptor were performed to evaluate the effect of geometry and residence time changes on FOG removal efficiency. Table 5-6 displays the results of these experiments, while Figures 5-3 through 5-5 displays visual images of the experiments being performed.

Table 5-6. Results from Bench Scale Analysis of Grease Interceptors.

| | Infracal | | | | |
| | Influent (mg/L) | | Effluent (mg/L) | | Result |
Experiment	Conc.	95% CL Range	Conc.	95% CL Range	% Removal
1. Standard Configuration	950.2	932 - 967	208.9	198 - 219	78
2. Standard Inlet/Outlet - No Baffle	626.5	598 - 655	98.6	96-101	86
3. Standard Configuration 1 hr. RT	1028.3	930 - 1131	98.5	98-99	90
4. Distributive Configuration	898.6	889 - 907	112.9	106 - 119	87
5. Distributive Configuration - No Baffle	890.0	874 - 905	279.8	262 - 297	69
6. Flared Inlet/Outlet - Hanging Baffle	629.3	603 - 656	109.9	107 - 112	83
7. Short Inlet, Standard Outlet - No Baffle	801.7	748 - 857	117.8	113 - 122	85
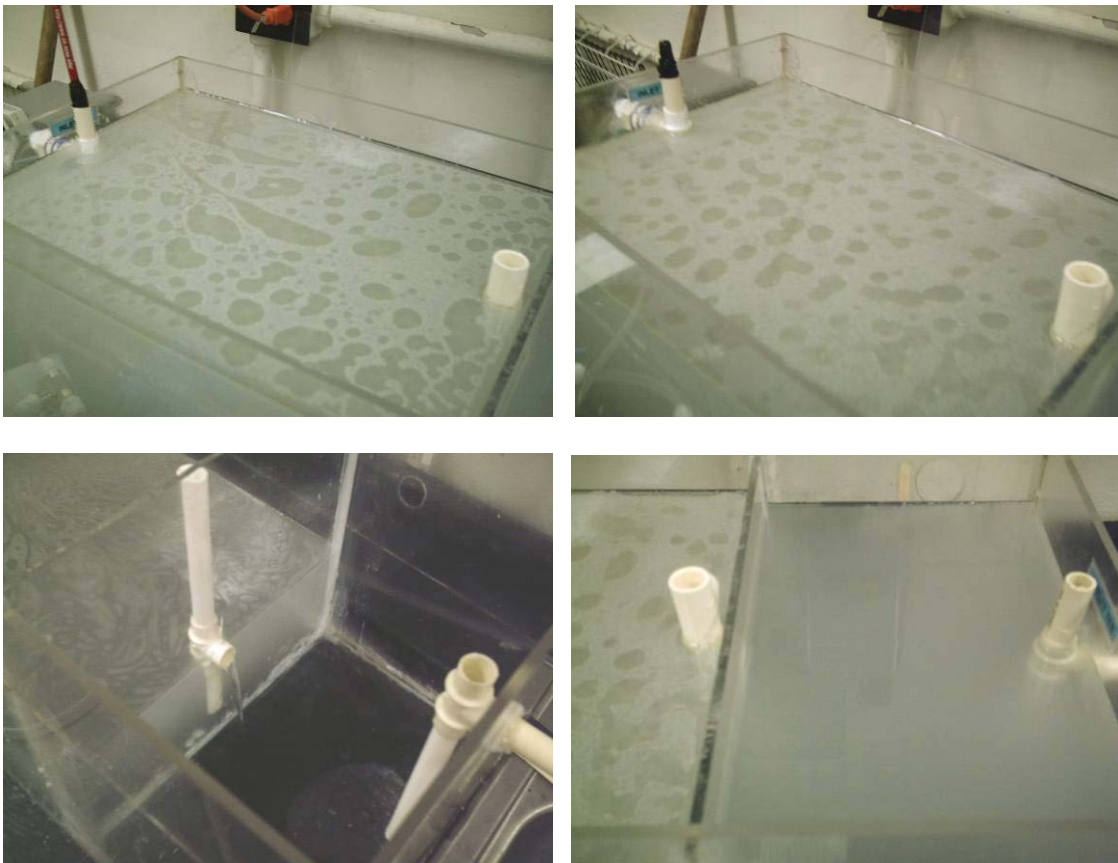
Figure 5-3. Images from Standard Configuration Bench Scale Experiment.

WERF
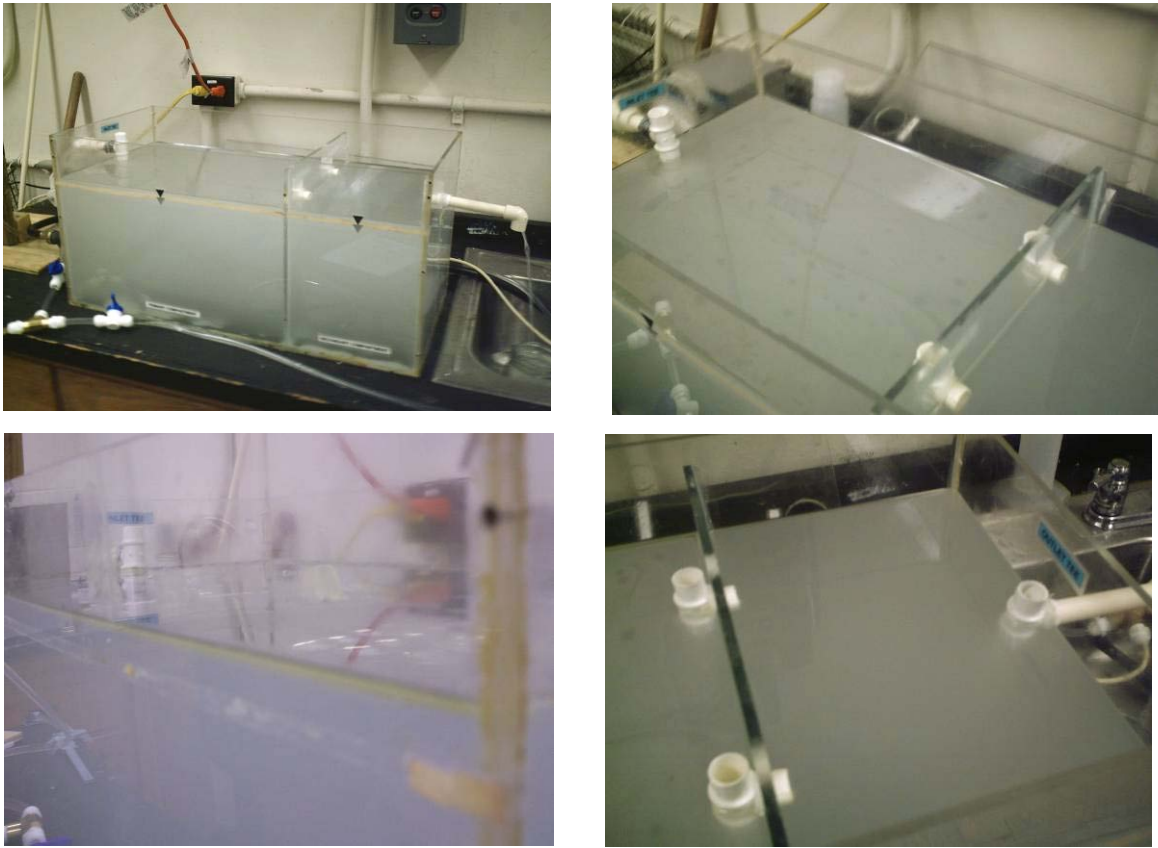
Figure 5-4. Images from Distributive Tee Bench Scale Experiment.
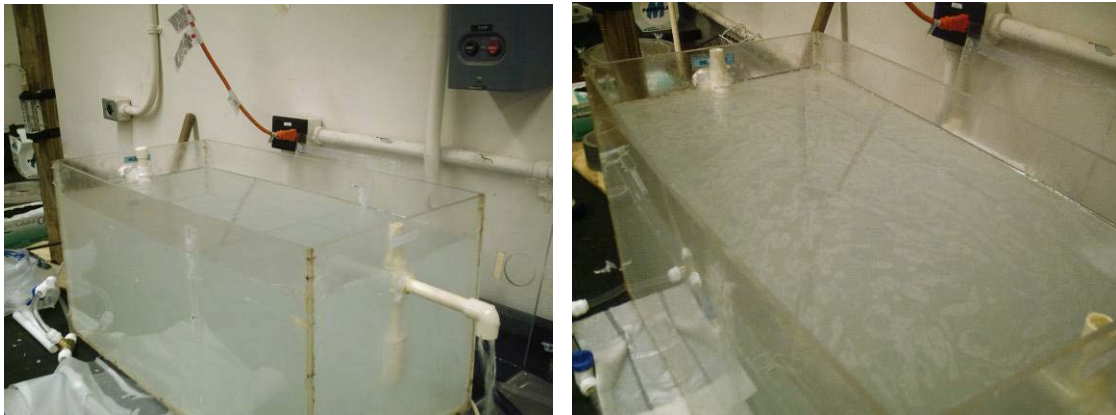
Figure 5-5. Images from Non-Standard Configurations and 1hr Residence Time Standard Configurations.

In Table 5-6, the removal of the baffle wall from the standard configuration resulted in an increase of performance of 6%. Currently, design guidelines for grease interceptors (IAMPO, 2004; NPCA, 2007) suggest the use of at least one baffle wall configuration, citing improved grease separation. As these results suggest, however, not only is this not consistently observed,

but in the no-baffle straight-pipe configurations (Experiments 2, 8), an improvement is observed when the baffle walls are removed. On the other hand, Experiment 5—the distributive inlet configuration with no baffle —displayed a significant decrease in performance (68% removal). Shifts in the flow pattern as a result of the distributive style inlet apparently resulted in poorer separation performance with this configuration. Further investigation in CFD and the pilot reactor will help confirm this hypothesis, which is discussed in a subsequent section. Inclusion of the hanging baffle (Experiment 7) did not increase the performance beyond the standard no baffle (Experiment 2), or short pipe no baffle configuration (Experiment 8). The hanging baffle experimental results suggest that even the minor constriction resulting from the hanging baffle opening may still have a negative effect on the overall GI performance compared to the no baffle configuration.

Experiments 2 and 8 compare tests performed with different inlet configurations and no mid-baffle wall. The results of experiments 2 and 8 indicate that little difference is observed with the utilization of different lengths for the straight inlet pipe. Experiment 5 investigates the distributive inlet and outlet configuration without a mid-baffle wall. The results in Table 5-6 show that the distributed configuration is significantly impacted by the absence of the mid-baffle. When the distributed mid-baffle was used with distributed inlet/outlet configuration, comparable removal results were found with the standard configuration or short inlet configuration without a mid-baffle wall. These results run contrary to the simulations and observed pilot experiments discussed later in this chapter and may largely be the result of a simplified shape of the distributive inlet being utilized (Figure 5-6).

Figure 5-6. a) Bench Scale Distributive Inlet, b) Pilot/Field/CFD Distributive Inlet Configuration.

The standard configuration was tested for two residence times: 20 minutes and 1 hour (Experiment 1 and 3). The results of this study suggest that tripling the residence time leads to only a (10%) increase in the removal of oil from the system. Previous discussion in oil-water separators from refinery wastes suggests that beyond a certain point, increases in the systems residence time provided no significant improvement in performance (Ree et al., 2006). The residence time threshold to achieve peak removal for a given interceptor is undoubtedly related to the influent droplet size distribution and whether these drops are able to coalesce or be removed by simple gravity separation. Typically, gravity separation can only remove free oil globules 150 microns or larger. Oil globules between 40 and 149 microns will require additional physical mechanisms such as dissolved air flotation or the addition of chemical agents to enhance coalescence. Oil globules below 40 microns will likely require adsorption or membrane

WERF

processes. An influent stream composed entirely of larger droplets would not require as long a retention time as an interceptor with smaller influent droplets to achieve the same percent removal assuming that you are already in the free globule range.

The research team only explored the effects of basic modifications to conventional GI designs, which refers to the rectangular foot-print, baffled interceptor most commonly seen in the field. Previous research has indicated enhanced performance through the use of plate and tube settlers (Chu and Ng, 2000). These improvements, however, would render interceptors very difficult to maintain. Changes such as decreases in inlet pipe length, the use of inlet and outlet pipe expansions, distributive tees, and other fittings can be easily added to existing GIs that may result in significant improvements. Field observations have already revealed enhanced first compartment FOG and solids separation with such devices.

Bench scale experimentation also demonstrated a clear oil separation on the surface of both compartments (Figure 5-7). More often than not, the bench scale grease interceptor displayed more substantial accumulation in the first compartment when the baffle wall was present (Figure 5-8).
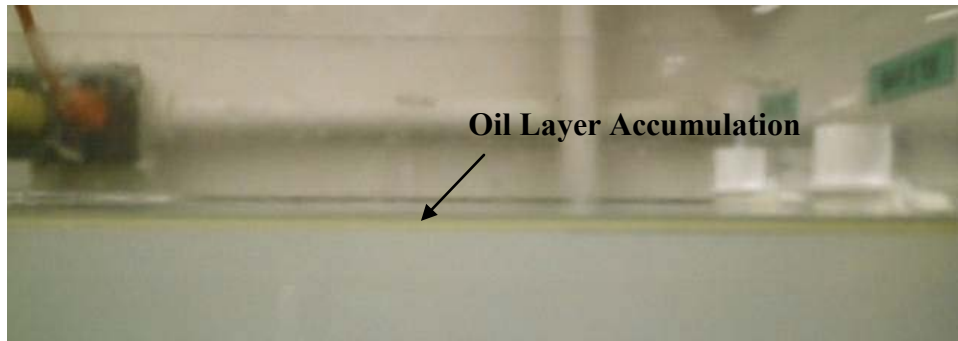

Figure 5-7. Oil Layer on the Surface of the First Compartment of the Bench Reactor during a 1hr Experiment.
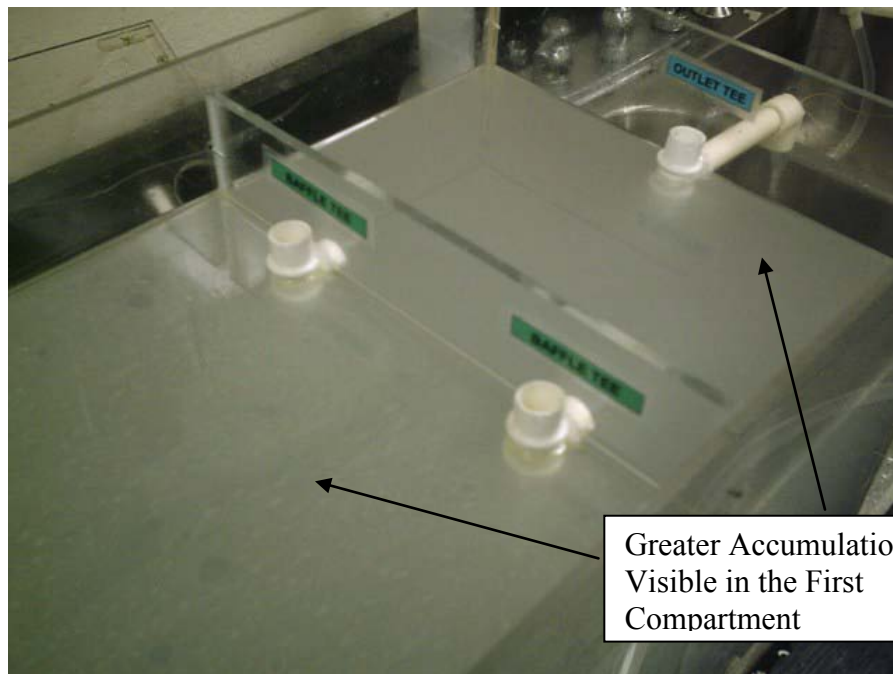

Figure 5-8. Top View of 1hr Residence Time Bench Scale Experiment.

Therefore the bench scale experimentation seems to support the observations in the field with regards to the location of greater separation and with the presence of some separation in the second compartment.

Temperature experiments performed with the standard straight pipe configuration and varying initial tank temperatures indicated some interesting trends (Figure 5-9).

Standard Config: Comparison of % Removal w/ Time
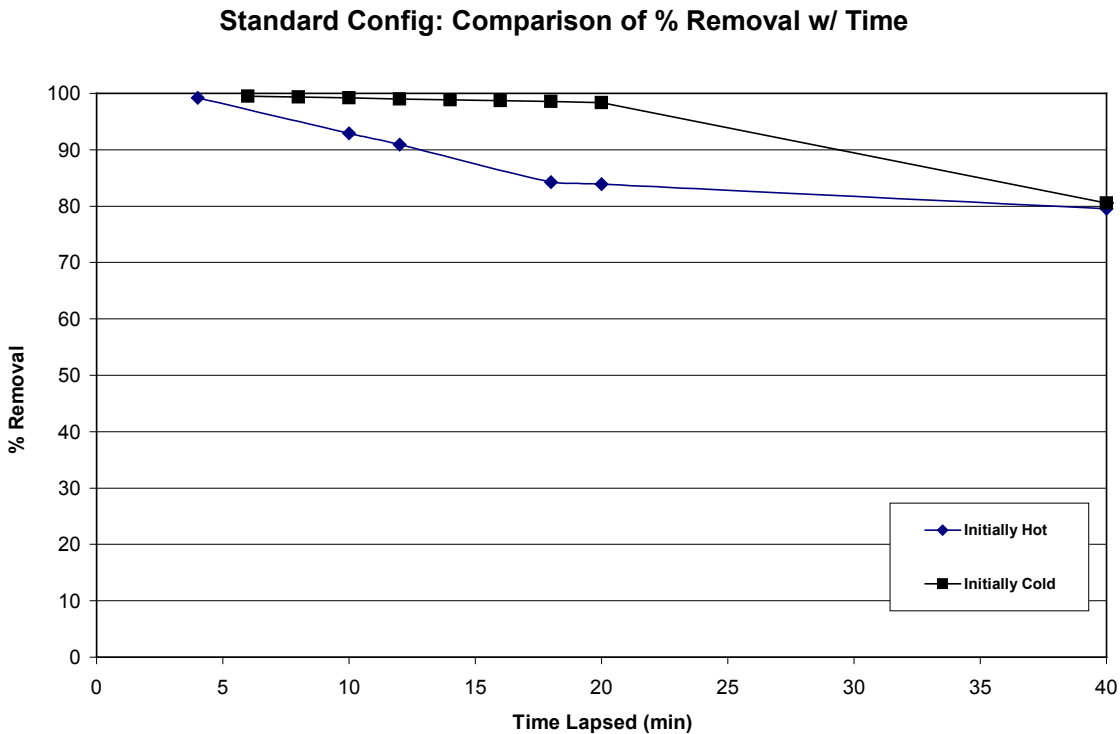
Figure 5-9. % Removal Over Time for Standard Configuration with Initially Cold or Initially Hot Water.

As samples in both the initially cold (70ºF) and initially hot (110ºF) tank were taken at fractions of one residence time, differences in the performance of the two reactors was apparent. The initially cold tank resulted in a more buoyant influent, thereby increasing the fluid element path length within the reactor. As a result, it took longer for the early influent oil droplets to reach the outlet. By 40 minutes (two residence times) this effect had disappeared. It appears that both the initially cold and the initially hot reactor will merge into the range observed in the initial bench experimentation (Experiment 1 in Table 5-6) which indicated approximately 78% removal.

As the temperature effect disappeared within two residence times, it appears that any impact due to temperature differences between the influent and bulk grease interceptor temperature (i.e., scouring of the separated FOG layer) may be negligible with the standard configuration. The temperature difference (40ºF) utilized in the lab experiments represent an exaggerated condition that will unlikely occur in field grease interceptors. Field grease interceptor analysis generally showed temperature differences of no more than (10-20ºF). These results suggest that any potential scouring that happens within the interceptor may not lead to degradation in performance if they happen over a short time period. However, more experiments

WERF

will have to be performed with thicker FOG layers to see if a higher concentration breakthrough occurs in the effluent.

5.4   Pilot Experimental Tests

Pilot-scale tests with the standard configuration and the distributed configuration (Figure 5-10) were performed since the distributed configuration was found to increase the solids and grease cap thickness in field grease interceptor observations. Results from these experiments are shown in Table 5-7.

Figure 5-10. Images of Standard Configuration and Distributive Inlet Configuration in Pilot.

Table 5-7. Results from Pilot Experiments.

Pilot Experiment	% Removal
Standard Configuration	50
Distributive Inlet/Standard Baffle	66.5

The addition of the distributive inlet resulted in a 16.5% improvement in the percent removal from the standard configuration. The enhanced performance provided by the inclusion of the distributed inlet is likely due to more favorable velocity pattern that allowed for more contact between the oil globules and the separated oil layer at the top of the grease interceptor.

The magnitudes of the percent removal for the bench scale and pilot scale are substantially different (~ 30%). One possible reason for the difference between the bench and pilot grease interceptors is the extent of mixing for the influent oil globules into the flow stream. Scaling mixing processes can be very difficult; often resulting in non-intuitive process outcomes. The bench scale system utilizes a mixing system that involved different types of impellers and reactor configuration compared to the pilot scale mixing system. As a result, the bench and pilot reactors likely experienced different droplet distributions due to the differences in spatial distribution of turbulence. As will be discussed in the modeling section, a significant drop in performance can be experienced when the droplet size falls below 150 microns (i.e. the free globule size) into the emulsified and dispersed phase globule size (i.e., 20 to 140 microns). The bench scale reactor, as the CFD results will indicate, appears to be receiving droplets generally greater than the free globule size (150 micron). Though differences were observed in the bench and pilot scale reactors, the positive impact of utilizing a distributed inlet pipe configuration was illustrated at both scales.

5.5   Numerical Assessment

Two phase computational fluid dynamics (CFD) simulations of grease interceptors were performed to better understand the fluid dynamics within these reactors. Initial simulations were performed with less computationally demanding 2D scenarios. After this initial investigation, the information obtained on configurations that provided relative enhanced separation performance was applied to the development and evaluation of 3D models. Finally, using the simulation data from 3D simulations, a numerical tracer analysis was performed to investigate what types of information can be obtained from macro-scale hydraulic tests that could be performed in field grease interceptors.

5.5.1   2D CFD Simulation of Grease Interceptor Performance

Initial 2D simulations were performed to evaluate the effect of influent droplet size on the separation efficiency. Figure 5-11 displays the influent oil percent removal as a function of droplet sizes for flow rates of 15 gpm (20 minute residence time) and 5 gpm (1hour residence time). The results in Figure 5-11 confirm information in the literature that there is a substantial increase in performance with larger droplet size.
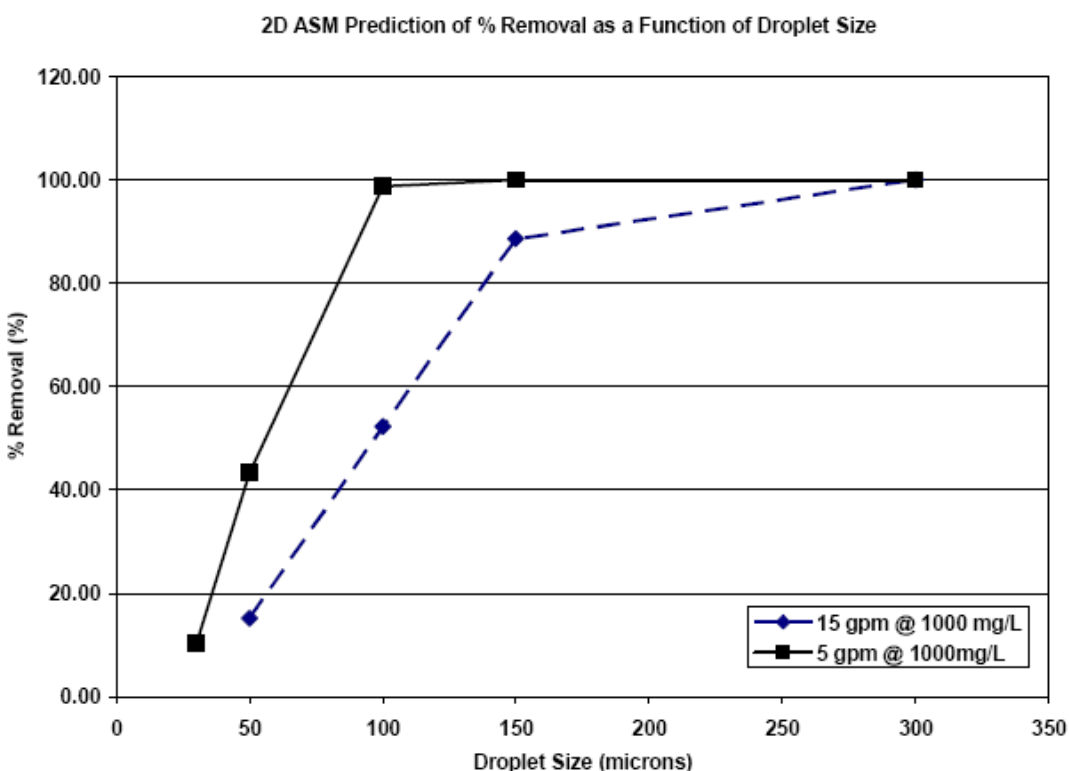
Figure 5-11. 2D Summary of Simulations Comparing % Removal w/ Droplet Size.

Figure 5-12 displays contours of the velocity flow pattern for influent oil phase with an average droplet size of 80 and 150 microns. In Figure 5-12, the numerical results display a shift in the flow pattern as a result of the change in droplet size. The larger influent droplets (Figure

5-12a) cause an immediate up flow due to a strong transfer of momentum from a larger buoyancy force. This flow pattern provides an early opportunity for the oil phase to separate. Figure 5-12b on the other hand identifies a short circuiting flow pattern. In the case of the smaller droplets, the effect of their buoyancy on the flow pattern is negligible.
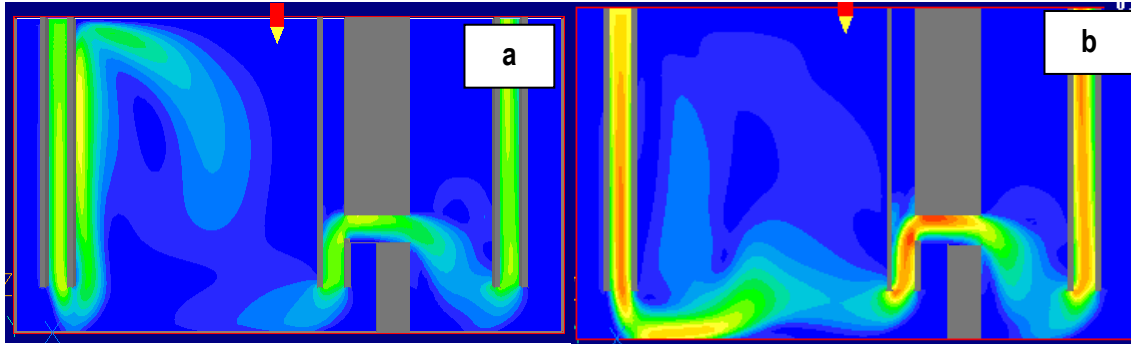
Figure 5-12. Comparison of Standard GI Simulation with 150 Micron a) and 80 Micron, b) Mean Droplet Distributions.

This shift in flow pattern can help explain the overall reduction in separation performance (Figure 5-13) with decreasing droplet size. In Figure 5-13, a drop of almost 50% in the removal efficiency occurred for the 80 micron influent oil stream compared to the 150 micron oil stream and was likely the result of significant short circuiting of a fraction of the influent flow directly towards the mid-baffle wall pipe. The 2D simulation in Figure 5-13 provided the first glimpse of how the standard grease interceptor can contribute to inefficient removal for all oil globule sizes due to poor velocity distribution of the influent flow.

As the computational run time associated with 2D simulations was far less than the 3D simulations, a parametric study was devised to investigate the various GI configurations. The parametric study of the 2D GI configurations (Figure 5-14) consists of 25 simulations varying five inlet lengths (L) and five baffle wall locations (R2/R1).
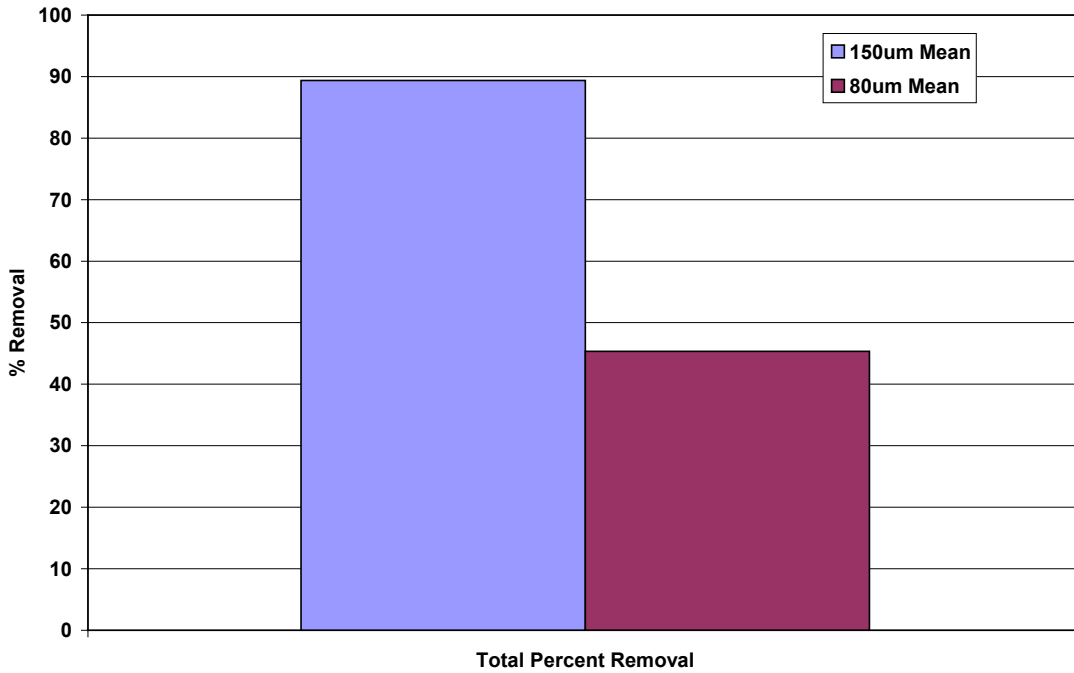
Figure 5-13. 2D Simulation Results from a Change in Droplet Size from 150 Micron to 80 Micron.
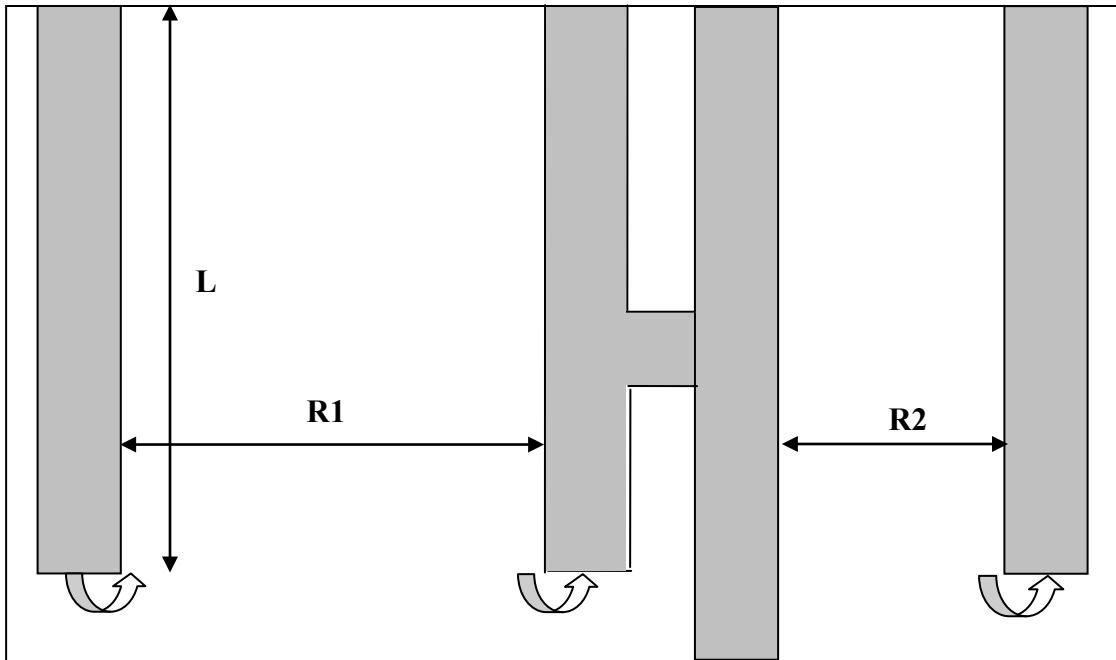
Figure 5-14. Layout of 2D GI Simulations with Variable Descriptions.

The results of this parametric study are displayed in Table 5-8. The greatest percent removal occurred with simulation number 11 (L=0.4, R2/R1 = 0), removing 57.6% of the influent oil concentration. While the worst configuration was with simulation number 5 (L=0,

WERF

R2/R1 = 0.9), removing only 28.2% of the influent oil concentration. The standard configuration (Figure 1, simulation 18, L=0.75, R2/R1 = 0.3) yielded 40.7% removal.

The 2D simulations results indicate that the presence of the baffle wall may actually hinder the performance of grease interceptors. This was observed in bench scale experimentation, where several experiments without the baffle wall showed an improvement in performance. Although the 2D parametric simulation provided some helpful insight into the impact of simple geometric GI configurations, the more descriptive 3D simulations were needed for greater assessment of the GI performance.

Table 5-8. 2D Parametric Study, Summary of Results.

Sim. #	L	R2/R1	Influent	Effluent	% Removed
1	0	0	1.10E-03	5.89E-04	46.5
2		0.2	1.10E-03	7.41E-04	32.6
3		0.3	1.10E-03	7.67E-04	30.2
4		0.6	1.10E-03	7.83E-04	28.8
5		0.9	1.10E-03	7.89E-04	28.2
6	0.2	0	1.10E-03	4.67E-04	57.5
7		0.2	1.10E-03	5.97E-04	45.7
8		0.3	1.10E-03	6.06E-04	44.9
9		0.6	1.10E-03	6.07E-04	44.8
10		0.9	1.10E-03	6.00E-04	45.4
11	0.4	0	1.10E-03	4.66E-04	57.6
12		0.2	1.10E-03	6.17E-04	43.9
13		0.3	1.10E-03	6.17E-04	43.9
14		0.6	1.10E-03	6.18E-04	43.8
15		0.9	1.10E-03	6.11E-04	44.4
16	0.75	0	1.10E-03	4.86E-04	55.9
17		0.2	1.10E-03	6.45E-04	41.4
18**		0.3	1.10E-03	6.52E-04	40.7
19		0.6	1.10E-03	6.32E-04	42.6
20		0.9	1.10E-03	6.24E-04	43.3
21	0.8	0	1.10E-03	6.28E-04	42.9
22		0.2	1.10E-03	6.38E-04	42.0
23		0.3	1.10E-03	6.35E-04	42.3
24		0.6	1.10E-03	6.37E-04	42.1
25		0.9	1.10E-03	6.34E-04	42.4

5.5.2 3D CFD Simulations of Grease Interceptor Performance

Several configurations were simulated using a 3D model (Figures 5-15 to 5-17). These variations included the short inlet, no baffle configuration (Figure 5-15b) that provided enhanced oil separation performance from the 2D simulations. The distributive type configurations investigated in bench and pilot experiments were not possible in two dimensions and were therefore of great interest in the 3D model simulations (Figure 5-16). These simulations involved the use of an inverted pipe tee, with 45° elbows pointing towards the bottom corners of the grease interceptor. The aim of the distributive configuration was to reduce short-circuiting by

better influent flow distribution. Variations of this type of configuration included the use of a dual piped baffle wall, a standard baffle configuration, and the use of no baffle wall.

Finally, as preliminary results indicated an improved GI performance with reduced influent velocity due to better flow distribution, the project team developed a configuration to further enhance influent flow distribution within the GI (Figure 5-17a). This configuration featured the expansion of the standard 3" pipe diameter to a flared rectangular fitting. Within the fitting, flow splitters act to distribute the flow along the rectangular area (Figure 5-17b). The reduced height of the inlet coupled with the absence of a baffle wall was designed to enhance droplet separation through greater quiescent flow conditions. This setup is known as the distributive plane jet (DPJ) configuration.

(A) **Standard GI Configuration** – Straight inlet and outlet pipes w/ standard baffle wall and single baffle tee.

(B) **Short Inlet** – Shortened inlet pipe, standard outlet pipe w/ no baffle wall.

(C) **Flared Standard GI** – Standard configuration with pipe diameter flared from 3" to 6"
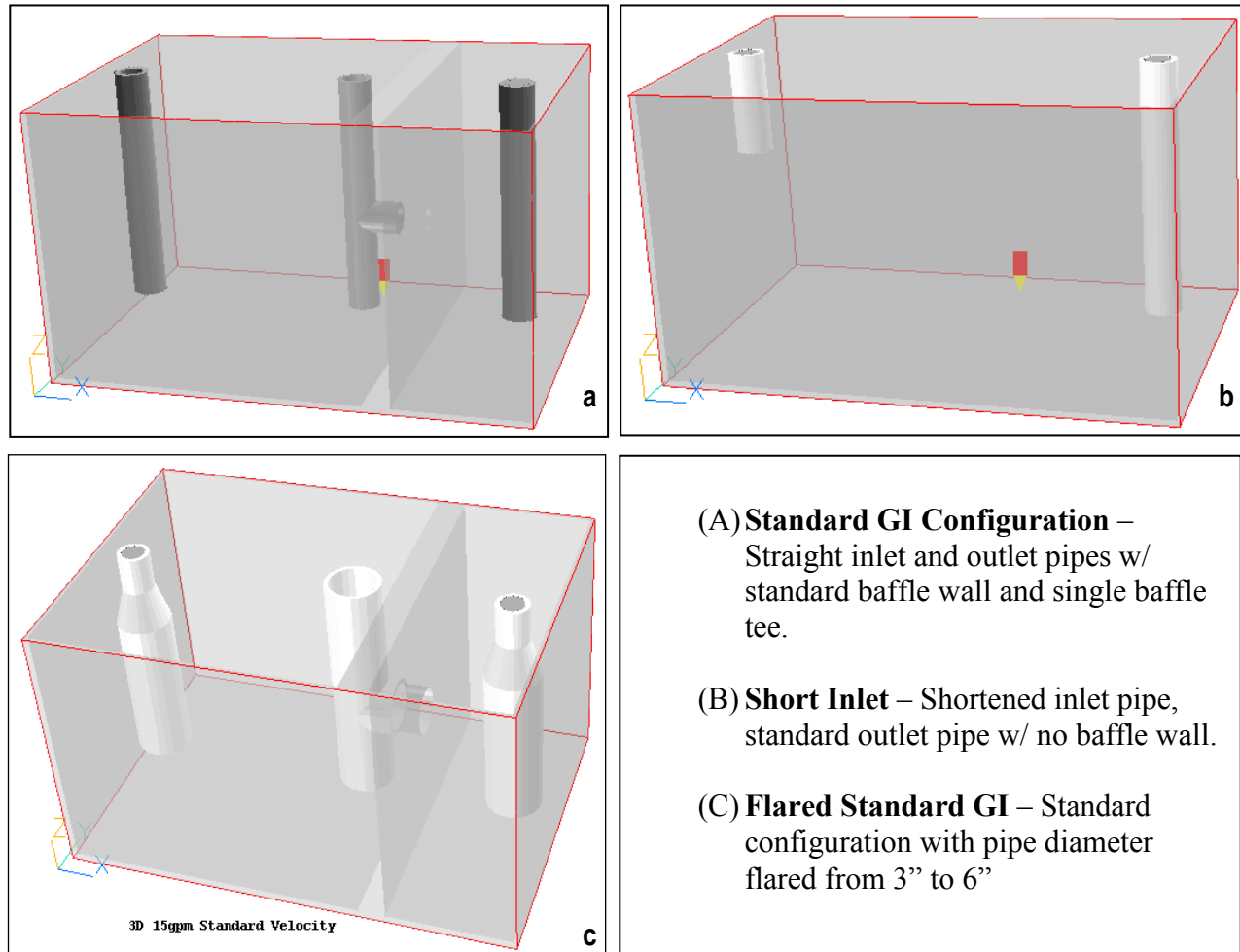
Figure 5-15. Simulated 3D GI Configurations (Straight Pipe Configurations).

(A) **Distributive Configuration** – Distributive inlet and baffle wall w/ dual baffle pipes and standard straight outlet pipe.

(B) **Distributive Inlet Standard Baffle** – Distributive inlet pipe w/ standard straight pipe baffle and standard outlet pipe.

(C) **Distributive Inlet No Baffle** – Distributive inlet w/ no baffle and a straight outlet pipe
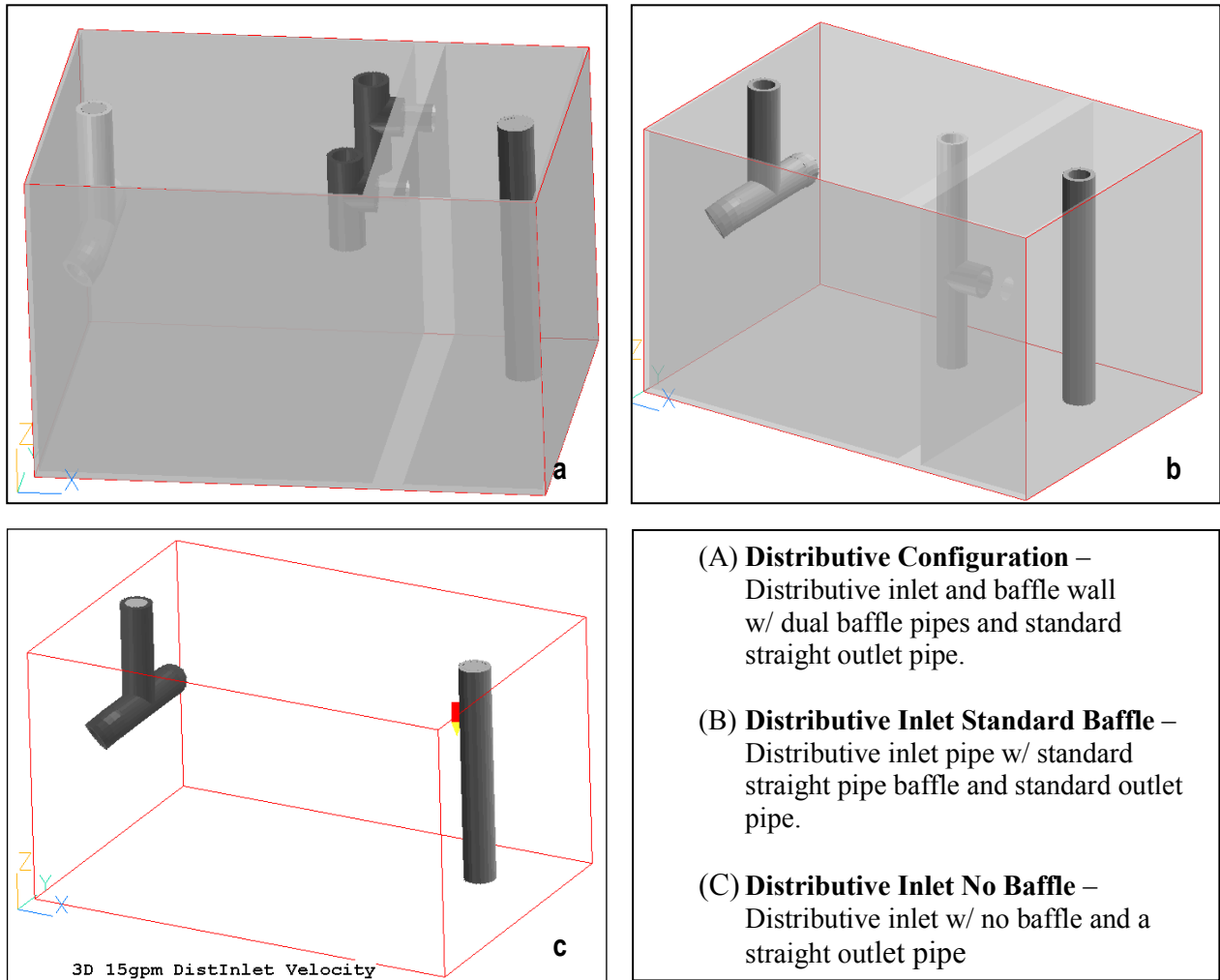
Figure 5-16. Simulated 3D GI Configurations (Distributive Configurations).
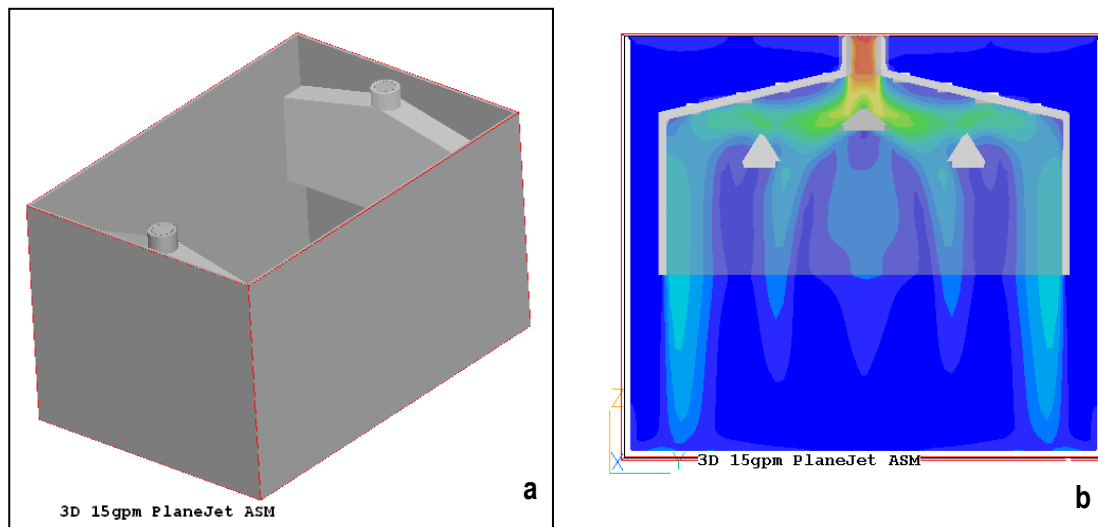

Figure 5-17. a) Simulated 3D GI Configurations (Distributive Plane Jet Configuration), b) Velocity Contours Depicting the Flow Distribution in the Inlet.

The 3D simulations, like their 2D counterparts, ran for three residence times after filling. Along with the 20 minute residence time simulation, the standard configuration was simulated with a 1hr residence time. The simulations utilized the two-phase ASM simulations with influent droplet size of 150 microns. The performance of the interceptors was determined by computing the average effluent volume fractions. Table 5-9 details the performance of each of these interceptors.

Table 5-9. Summary of 3D CFD Results.

3D Simulations	% Removal
Standard Configuration	56.7
Standard Configuration (1hr)	97.5
Short Inlet	89.3
Flared Pipe	81.6
Distributive Inlet - Standard Baffle	74.0
Distributive Inlet - No Baffle	95.8
Distributive Inlet - Distributive Baffle	75.7
Distributive Plane Jet Inlet	92.2

The highest performing simulation was observed with the Standard configuration run with a 1hour residence time (97.5%). This was not surprising since the experimental results also demonstrated better removal performance given more residence time. However, both the distributive inlet – no baffle (95.8%) and the distributive plane jet inlet (92.2%) predicted high percent removal at the 20 minute residence time. The short inlet configuration (as the best performer in 2D) also displayed a reasonable percent removal at the 20 minute residence time (89.3%).

The standard configuration displayed substantially poorer performance than any of the other simulations (56.7%). Close observation of the velocity contours (Figure 5-18) of the cross-section within the reactor suggests that the cause for this reduced performance may be due to higher local velocities near the inlet, baffle, and outlet pipes, all contributing non-quiescent flow conditions, which enhances the vertical separation of droplets. Further examination of the velocity contours in the direction of flow (Figure 5-19) suggests several regions of high velocity along the bottom of the tank and along the side walls.
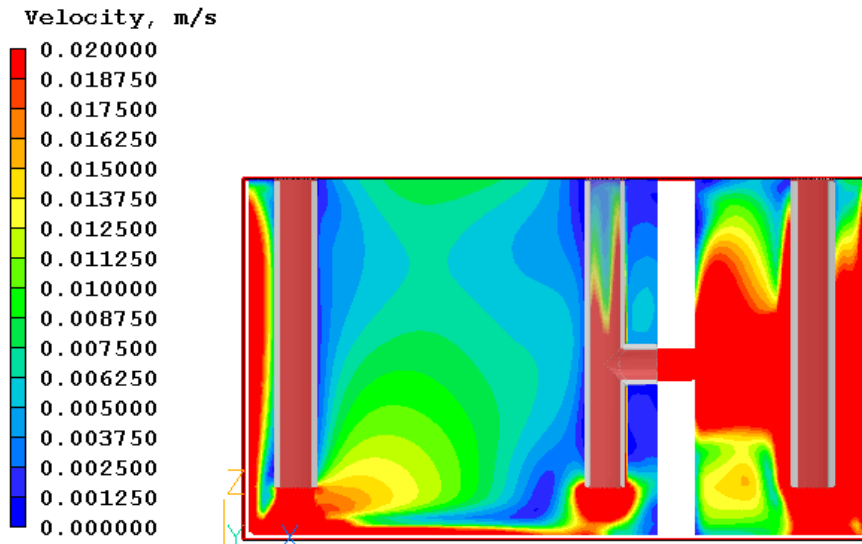
Figure 5-18. Velocity Contours Along the Center of the Standard 15gpm Simulation.

3D 15gpm Standard ASM
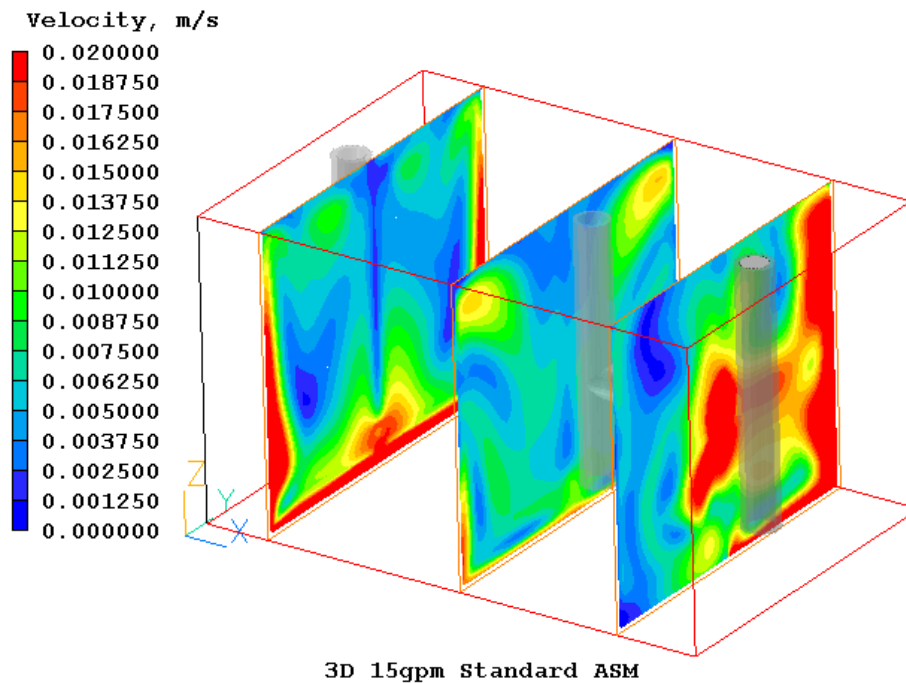
Figure 5-19. Velocity Contours in the Flow Direction for Standard Configuration.

Observation of the distributive plane jet (DPJ) inlet's cross section and flow direction contours suggests a more favorable flow pattern (Figures 5-20 and 5-21). The DPJ configuration significantly reduces the high velocities observed in the standard configuration and provides greater opportunity for the oil droplets to experience quiescent flow conditions. The DPJ design seems to generate these secondary gentle upward-velocity patterns (Figure 5-22), which may act to increase the FOG separation in the reactor.

As with the DPJ design, similar secondary gentle upward velocity patterns can be observed with the distributive inlet/no baffle configuration (Figure 5-23), which had 95.8% removal efficiency. However, the magnitude of the velocity in this upward motion was slightly larger than those produced in the DPJ design (Figure 5-24), and may explain the higher percent removal observed with the distributive-no inlet configuration. While the results in Figures 5-23 and 5-24 may lead to a conclusion that increasing the upward velocity motion results in higher percent removal, it is important to recognize that the flow conditions created still allowed for quiescent conditions, which is still a very important component to achieve higher percent removal. Consequently, any design modifications must work to balance velocity distribution and quiescent conditions.

Another, perhaps more intuitive way to observe the performance of the configurations described in Table 5-9, is by observing the oil volume fractions in the various simulations. The locations of high and low concentrations can then be used to better explain the behavior of the GI separation performances.

Figures 5-25 to 5-32 depict the oil volume fraction for the configuration of Table 5-9. The standard, straight pipe configuration (Figure 5-25) clearly demonstrates the unfavorable regions of high oil concentration. The result of the high velocity in the direction of the outlet tee lead to the increased transport of oil droplets into the second compartment and out of the grease interceptor, resulting in the lower separation performance (56.7%). Both the short inlet/no baffle configuration (Figure 5-26) and the flared configuration (Figure 5-27) eventually allowed for more quiescent flow (by reducing the flow velocity in the tank). This is particularly clear with the short inlet configuration, as there is a region of low concentration near the outlet region. The increase in residence time to 1 hour (Figure 5-28) also performed favorably be reducing the velocity to the outlet and thereby allowing for greater separation in the system.

The distributive configurations achieved increased performance by better distributing the flow along the cross-section of the GIs. In the case of the distributive configuration with the dual baffle wall (Figure 5-29), this better flow distribution appears to be successful until the dual baffle wall is reached. The dual baffle wall, with higher baffle pipes, however, pulls from the region of higher concentration and transports FOG into the second compartment. From there the system behaves more like a standard configuration (as the outlet is a standard straight pipe), and greater mixing takes place. The distributive inlet/standard baffle configuration (Figure 5-30) appears to have initial use of the cross-section but then reverts again to a standard type configuration as a result of the higher velocity in the single baffle pipe region. When the baffle pipe is completely removed from distributive configuration (Figure 5-31) the oil phase concentration clearly demonstrates why this configuration out performed other GI configurations.

The distributive inlet allows for the upward migration of the higher influent concentration (Figure 5-24), unhindered by the constrictions of a baffle wall. As the flow approaches the center of the reactor, quiescent conditions can initially be observed. Here the droplets are able to be separated from the main stream. By the time the outlet is reached, although there is a downward suction as a result of the outlet pipe, the separated droplets are largely out of range. The fact that this configuration is the highest performing of the 20 minute residence times (95.8%) confirms that this distribution along the reactor cross-section and quiescent flow conditions are more ideal for gravity separation.

WERF

The distributive plane jet configuration (Figure 5-32) designed to utilize a greater area of flow also performed favorably (though it was not as successful as the distributive/no baffle configuration). Similar to the distributive no-baffle configuration, the secondary flow patterns of the plane jet appeared to enhance the upward migration of the oil phase near the inlet. Also similar is the quiescent nature of the flow by the time it reached the outlet. The slightly poorer performance of the DPJ design compared to the distributive no baffle configuration is possibly due to the location of the outlet height. Since the DPJ outlet height is higher than the standard height, the outlet pulled more droplets out of the system than the distributive configuration and was therefore slightly less effective than the distributive no-inlet configuration.
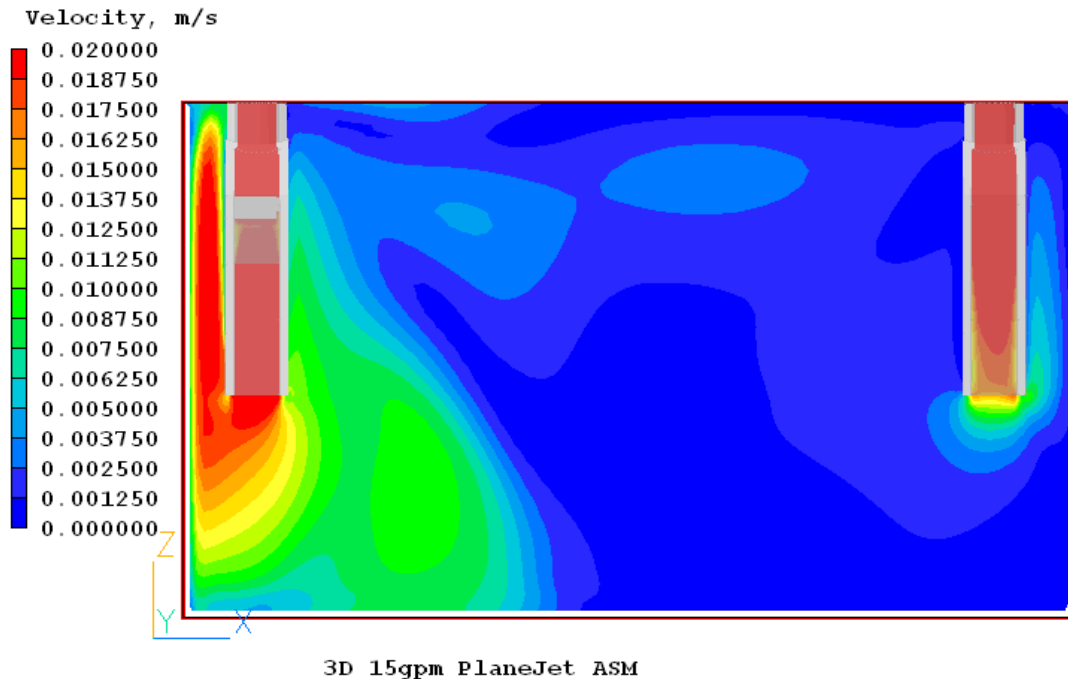
Figure 5-20. Velocity Contours Along the Center of the DPJ 15gpm Simulation.

3D 15gpm PlaneJet ASM
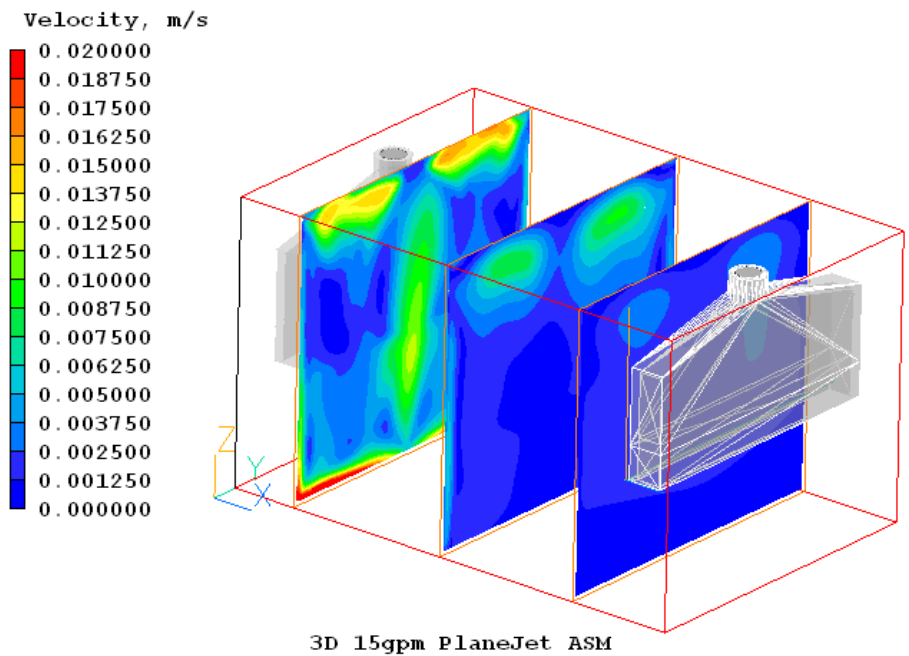
Figure 5-21. Velocity Contours in the Flow Direction for DPJ Configuration.


3D 15gpm PlaneJet ASM
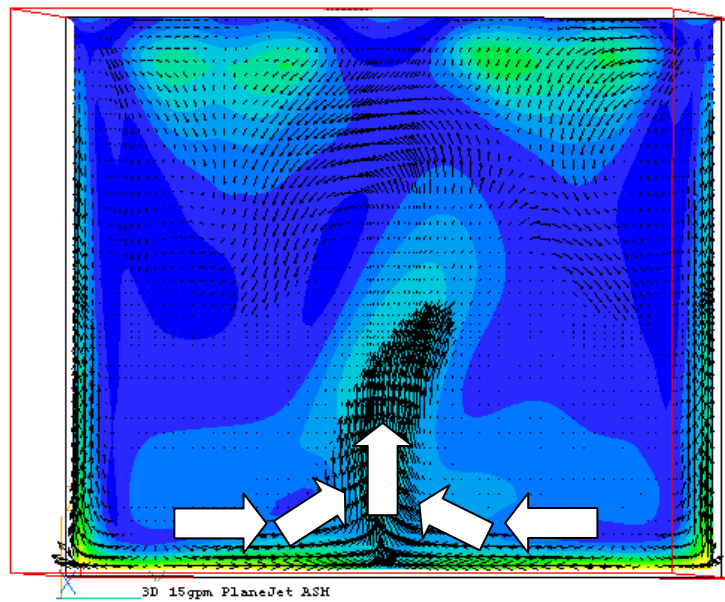
Figure 5-22. Velocity Contour Near the Inlet, Showing the Upward Flow Motion.

WERF
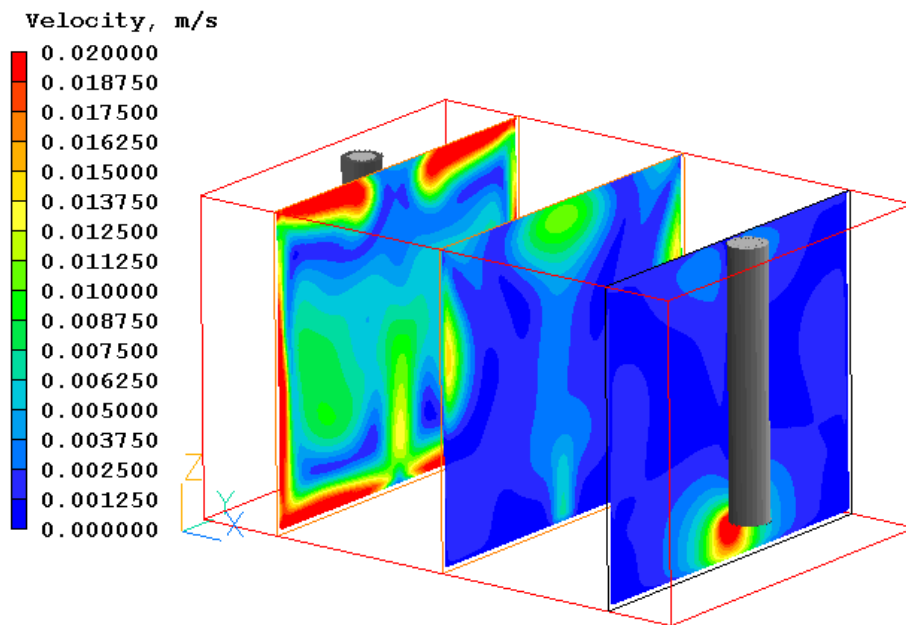
Figure 5-23. Velocity Contours for Distributive Inlet/No Baffle.
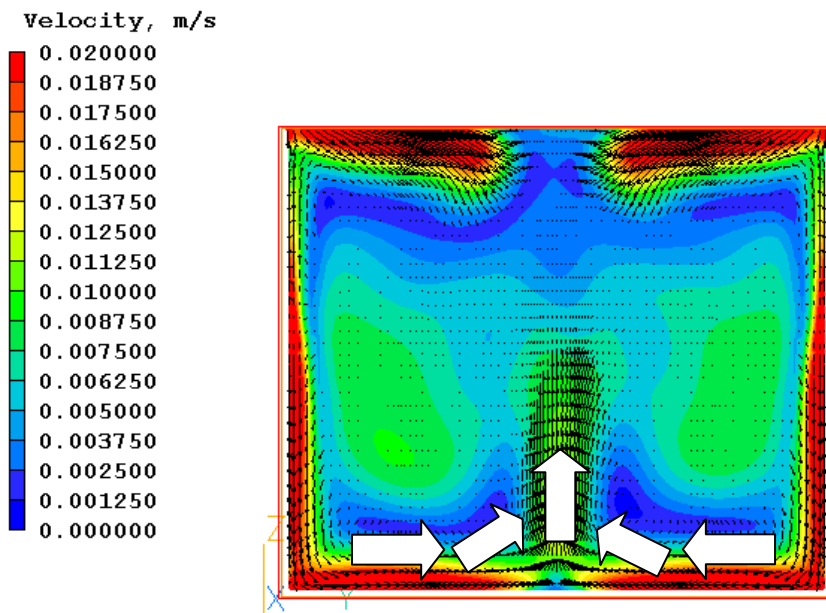
Figure 5-24. Velocity Contours for Distributive Inlet/No Baffle.
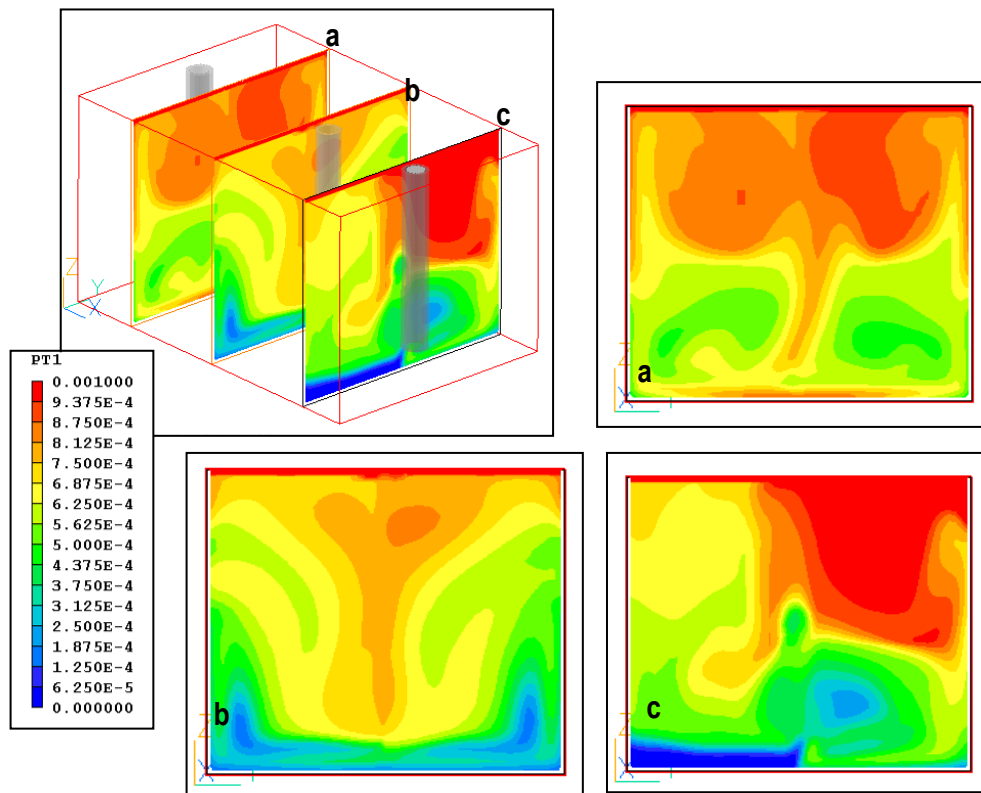
Figure 5-25. 15gpm Standard Configuration Image Showing Volume Fraction of Oil (Contours) for ASM Simulation.

WERF
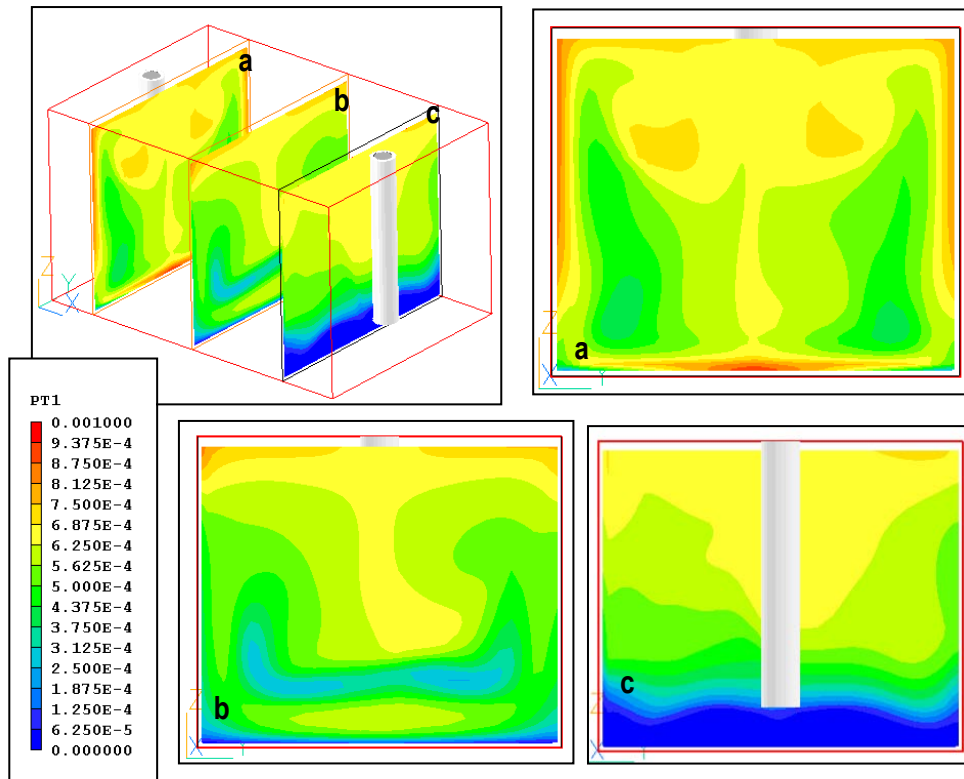
**Figure 5-26. 15gpm Short Inlet/No Baffle Configuration Image Showing
Volume Fraction of Oil (Contours) for ASM Simulation.**
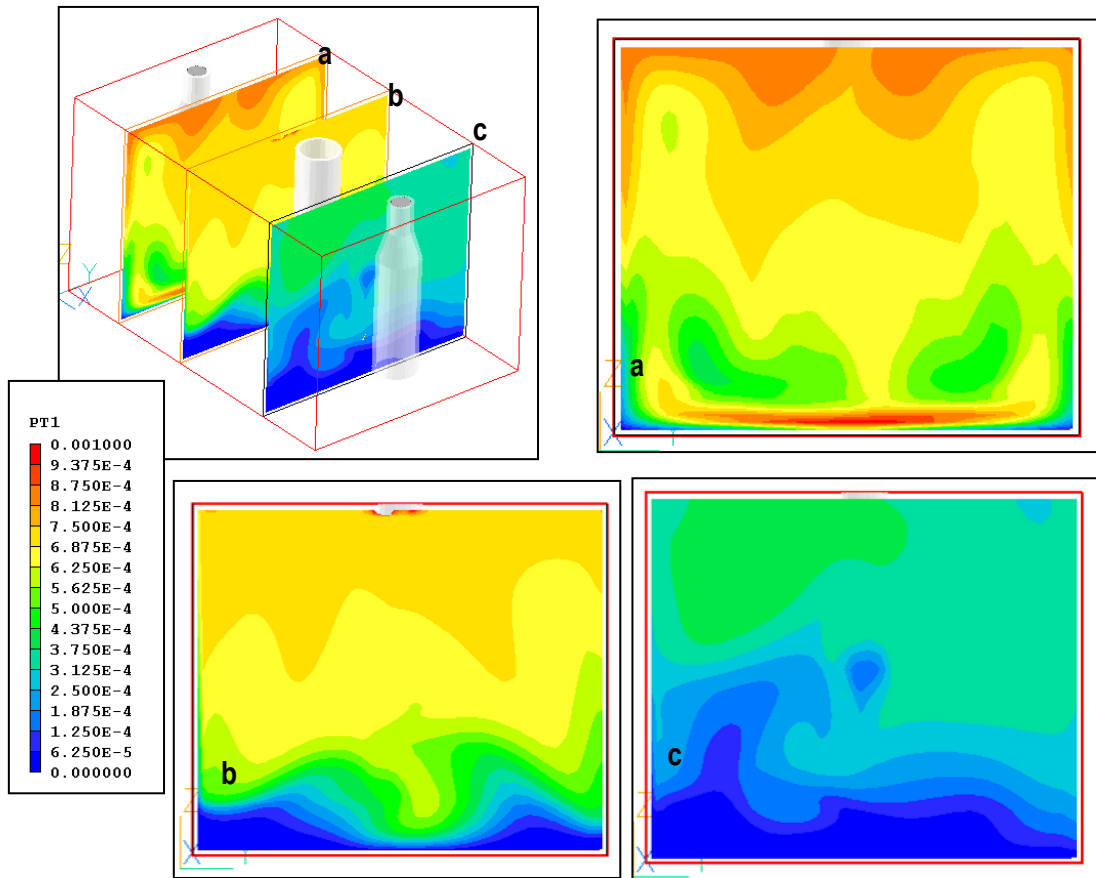
Figure 5-27. 15gpm Flared Configuration Image Showing Volume Fraction of Oil (Contours) for ASM Simulation.
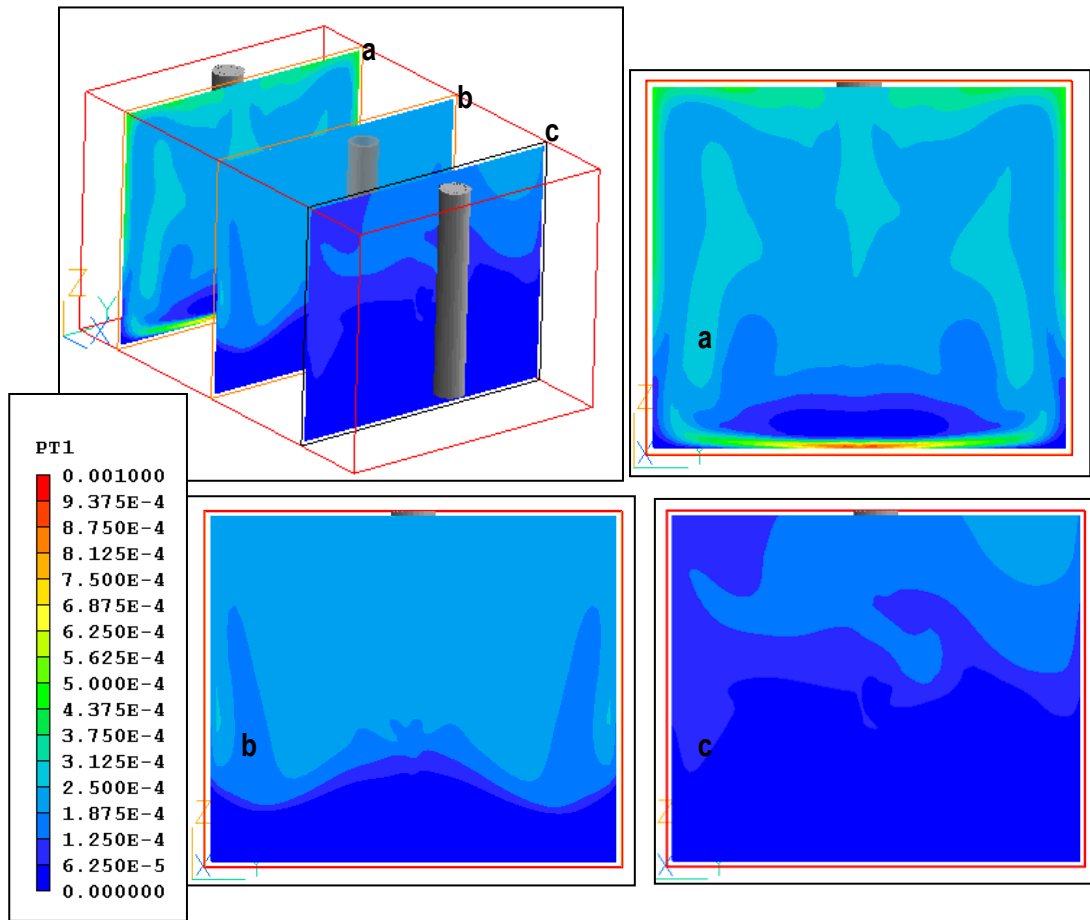
Figure 5-28. 5gpm Standard Configuration Image Showing Volume Fraction of Oil (Contours) for ASM Simulation.
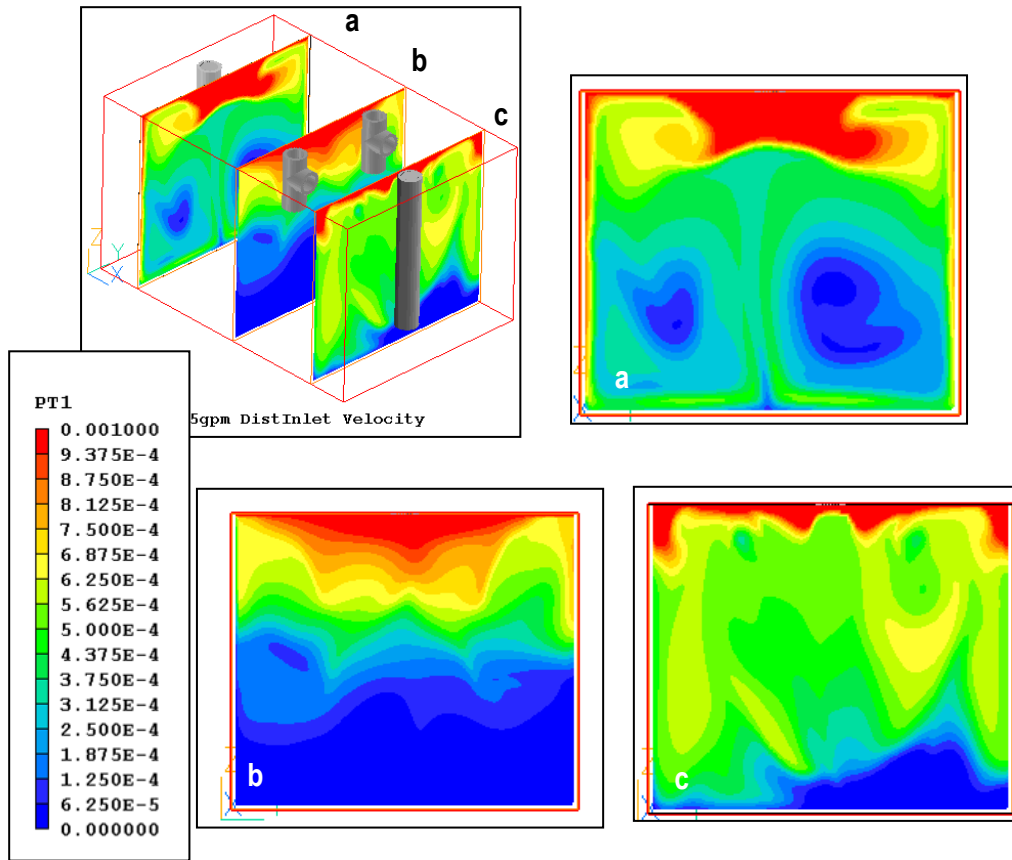
Figure 5-29. 15gpm Distributive Inlet/Distributive Baffle Configuration Image Showing Volume Fraction of Oil (Contours) for ASM Simulation.
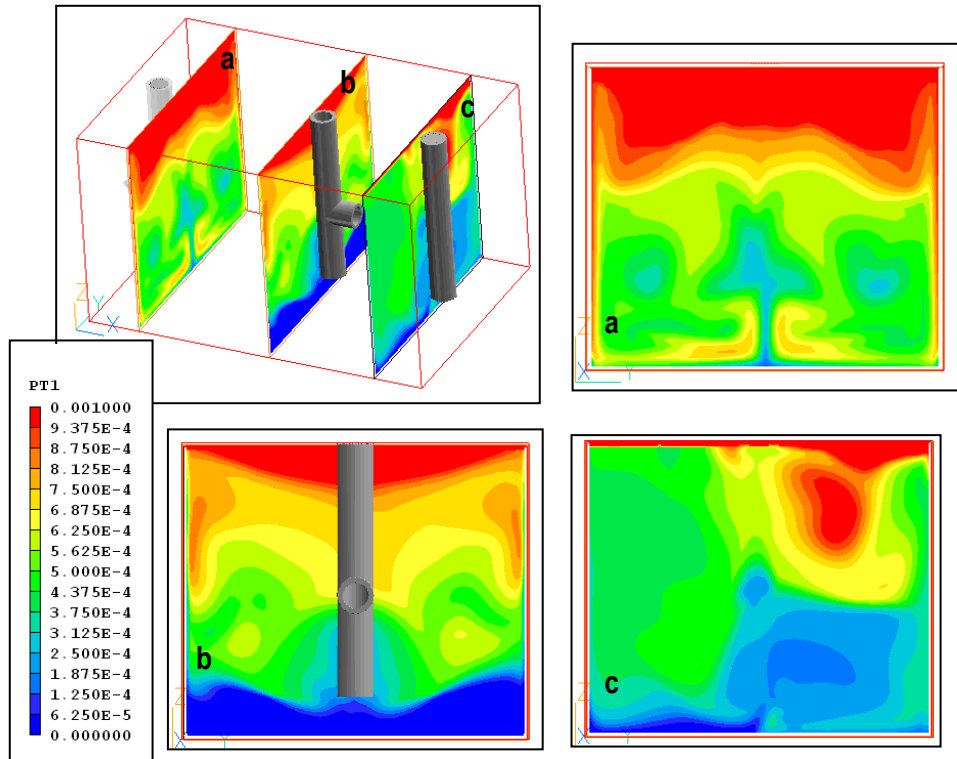
Figure 5-30. 15gpm Distributive Inlet/Standard Baffle Configuration Image Showing Volume Fraction of Oil (Contours) for ASM Simulation.
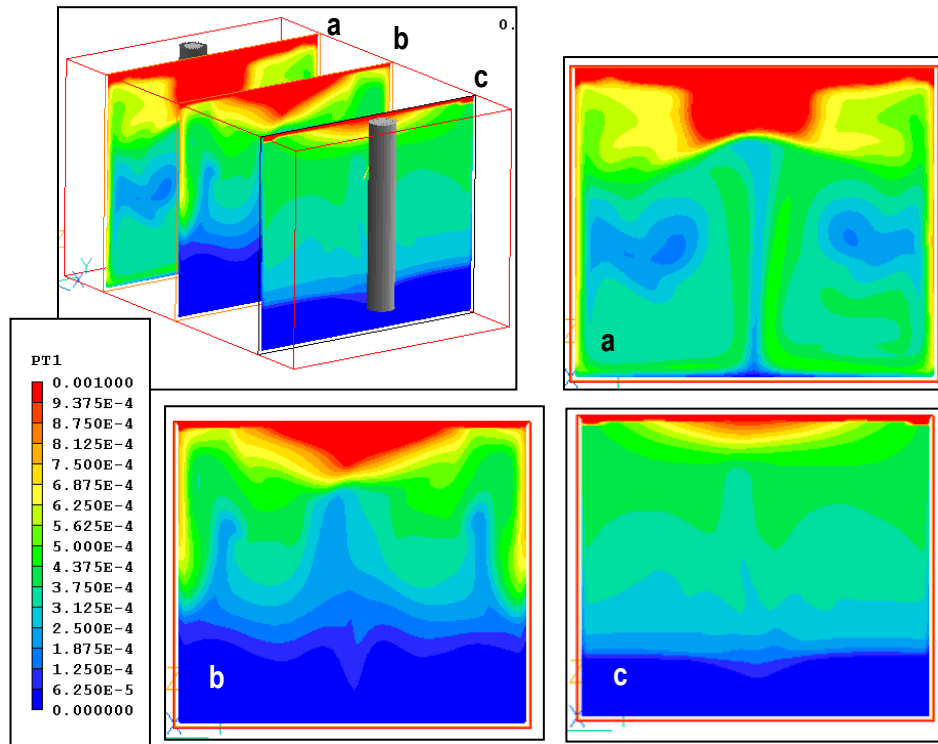
**Figure 5-31. 15gpm Distributive Inlet/No Baffle Configuration Image Showing
Volume Fraction of Oil (Contours) for ASM Simulation.**
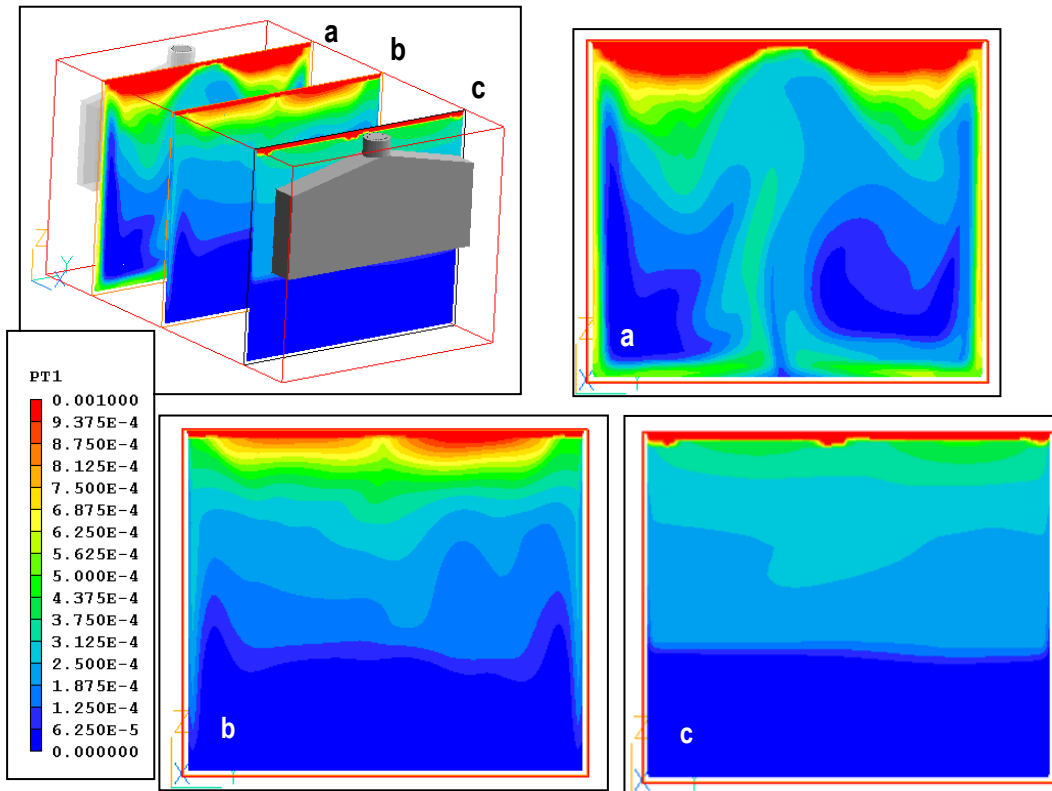
**Figure 5-32. 15gpm Plane Jet Configuration Image Showing Volume Fraction of Oil (Contours) for ASM Simulation.**

5.6   Summary of Numerical and Experimental GI tests

Some interesting comparisons can be drawn from the CFD and the experimental tests performed in this research. Table 5-10 summarizes all the results for 3D, bench and pilot tests. In Table 5-10, the bench scale experiments and the 3D CFD simulation results generally indicate similar performance for basic variations of the standard configuration (Figure 5-33).

Table 5-10. Summary of CFD, Bench, and Pilot Results.

Scenario	3D CFD % Removal	Bench % Removal	Pilot % Removal
Standard Configuration	56.7	78	50
Standard Configuration (1hr)	97.5	90	-
Short Inlet	89.3	85	-
Flared Pipe	81.6	83	-
Distributive Inlet - Standard Baffle	74.0	-	66
Distributive Inlet - No Baffle	95.8	69	-
Distributive Inlet - Distributive Baffle	75.7	87	-
Plane Jet Inlet	92.2	-	-
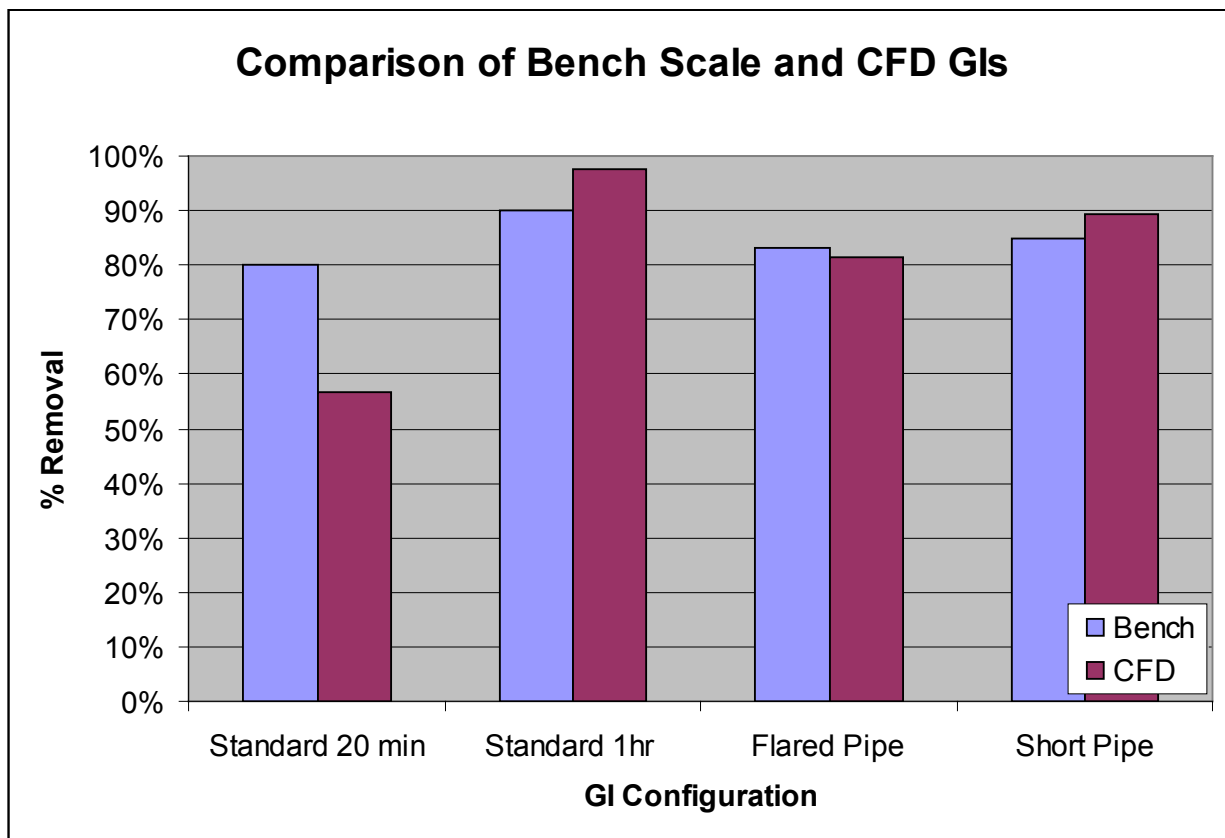
Figure 5-33. Comparison of Bench and CFD GIs.

The results of Figure 5-33 do not include comparison with the distributive inlet or DPJ configurations. As discussed earlier in the chapter, the simulation, pilot, and field distributive configuration is substantially different from the bench scale distributive configuration used. The 45º elbows featured in the pilot, CFD, and field work direct the influent flow to the back corners of the GI and may be a major cause for the difference in performance observed in those experiments.

The two pilot experiments performed during the present research had very close similarity to the CFD results (in both magnitude and change in performance as a result of inlet type change). The pilot experiments indicated a 16% increase in performance with the addition of the distributive inlet in place of the standard straight inlet tee. The 3D CFD simulations indicated a 17% increase in performance for the same change. Both of these results support the enhanced retention of FOG observed in the field for this configuration. This indicates that improvements can be made to GI performance by retro-fitting a distributive configuration to existing interceptors.

5.7   Analysis of Simulated Tracer Tests

Numerical tracer simulations were performed on several GI configurations (standard, short inlet pipe, distributed with and without mid baffle wall, flared, and plane jet). The residence time density functions (RTD) from these tracer tests are displayed in Figure 5-34. In addition to the GI tracer simulations, Figure 5-34 also display ideal RTDs from a single complete mix system and one produced by the gamma extension of the N tanks in series model with N = 2 (Clark, 1997). In Figure 5-34, the tracer results indicate that all the designs generally behave as

two tanks in series with the plane jet and distributed no baffle configurations performing slightly better than the two tanks in series RTD result.

The tracer simulations in Figure 5-34a are not surprising since GIs that contain a mid-baffle wall are essentially two compartments connected in series. The shape of the RTD did not change significantly when the standard configuration was operated at 5 instead of 15 gpm. The short inlet configuration, which utilizes no baffle wall, seems to fall between the single tank and two tanks in series RTD prediction while the plane jet, which also does not utilize a mid-baffle wall, and distributed no mid-baffle configurations seem to behave well outside of the ideal single complete mix tank RTD prediction.

The plane jet and distributed/no mid-baffle wall designs RTD departure from the single tank RTD prediction is likely due to velocity profiles that better distribute the incoming flow. Ideal single parameter RTD models are not designed to capture any inlet/outlet design changes that are incorporated to improve specific process performance such as gravity separation. Given the RTD for the different designs behaves better than a single tank, one could investigate the ideal removal performance for different oil globule sizes to understand the possible range of removal in the absence of experimentation. Such an experiment is shown in Figures 5-35 and 5-36.

In Figure 5-35, the N tanks in series RTD model (N=1.5 and N=2.0) was used to compute the fraction of removal for a range FOG globule sizes under different hydraulic residence times. The results in Figure 5-35 provide some interesting outcomes as it suggests that for GIs which behave with these types of RTDs (i.e., macro-scale mixing characteristics), free floating FOG globules (i.e., globules larger than or equal to 150 microns) can be removed by gravity separation with percent removals greater than 90% with as little time as 20 minutes. The percent removal drops off significantly for the dispersed FOG globule range (i.e., globules between 20 and 150 microns) and emulsified globule range (i.e., globules between 5 and 20 microns).

Gravity separation processes, without the use of chemical additives or other physical mechanisms such as filtration or air flotation, are well known for removing free floating globules 150 microns or larger in diameter. For that range, Figure 5-35 and more closely in Figure 5-36 when comparing free floating and dispersed size FOG globules, show that minor incremental improvement in removal will be achieved by increasing the hydraulic residence time, a result that was shown experimentally in this study. Since this study was not able to quantify the actual FOG globule sizes, the results in Figures 5-35 and 5-36 suggest that a fraction of the globule sizes was likely in the dispersed globule range and that other means of effective separation beyond simple gravity may need to be employed to achieve percent removals well beyond 90%.
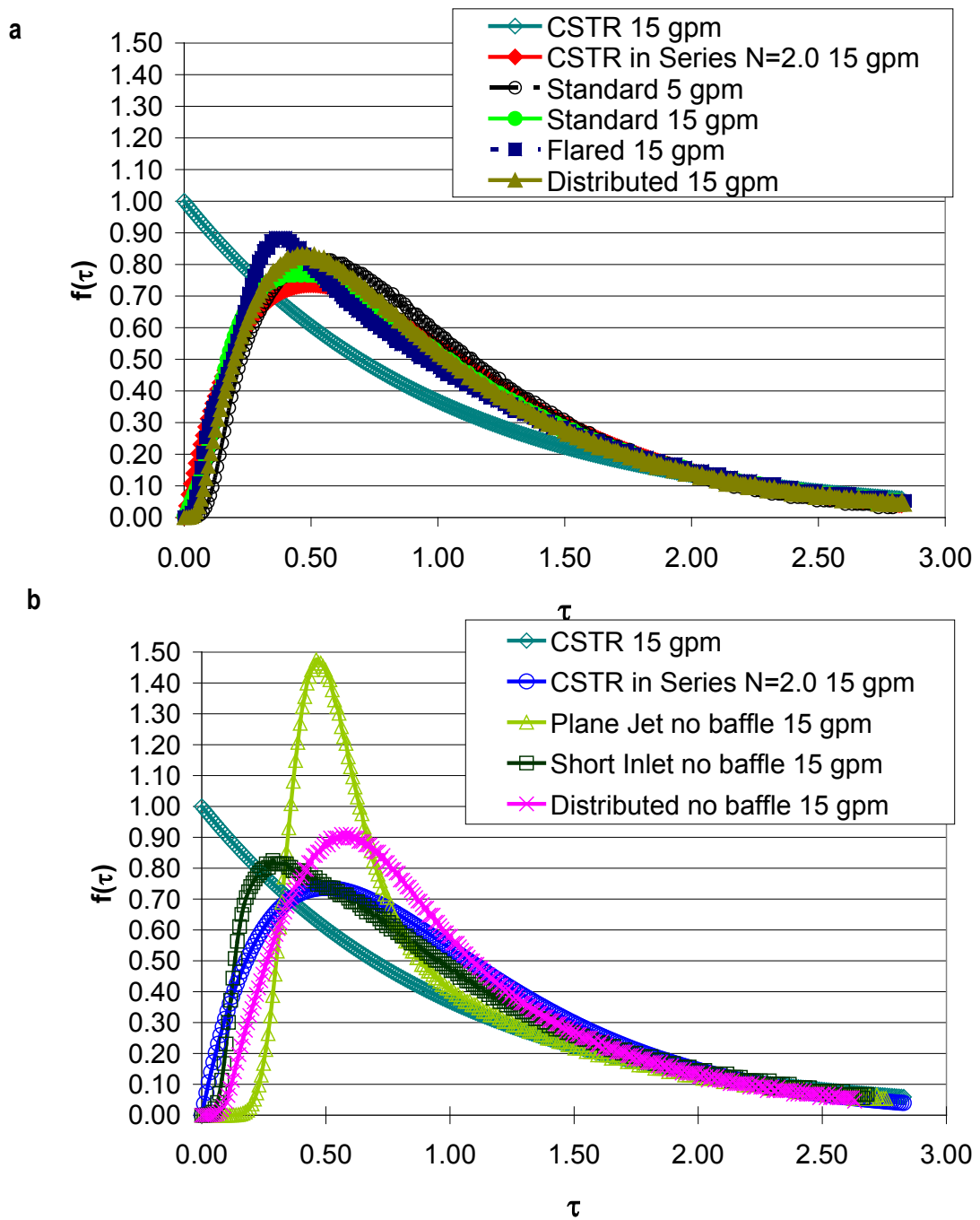
**Figure 5-34. Tracer Test Simulations for the Different Configurations:
a) Designs that Include a Mid-baffle Wall, b) Designs that Exclude a Mid-baffle Wall.**

WERF
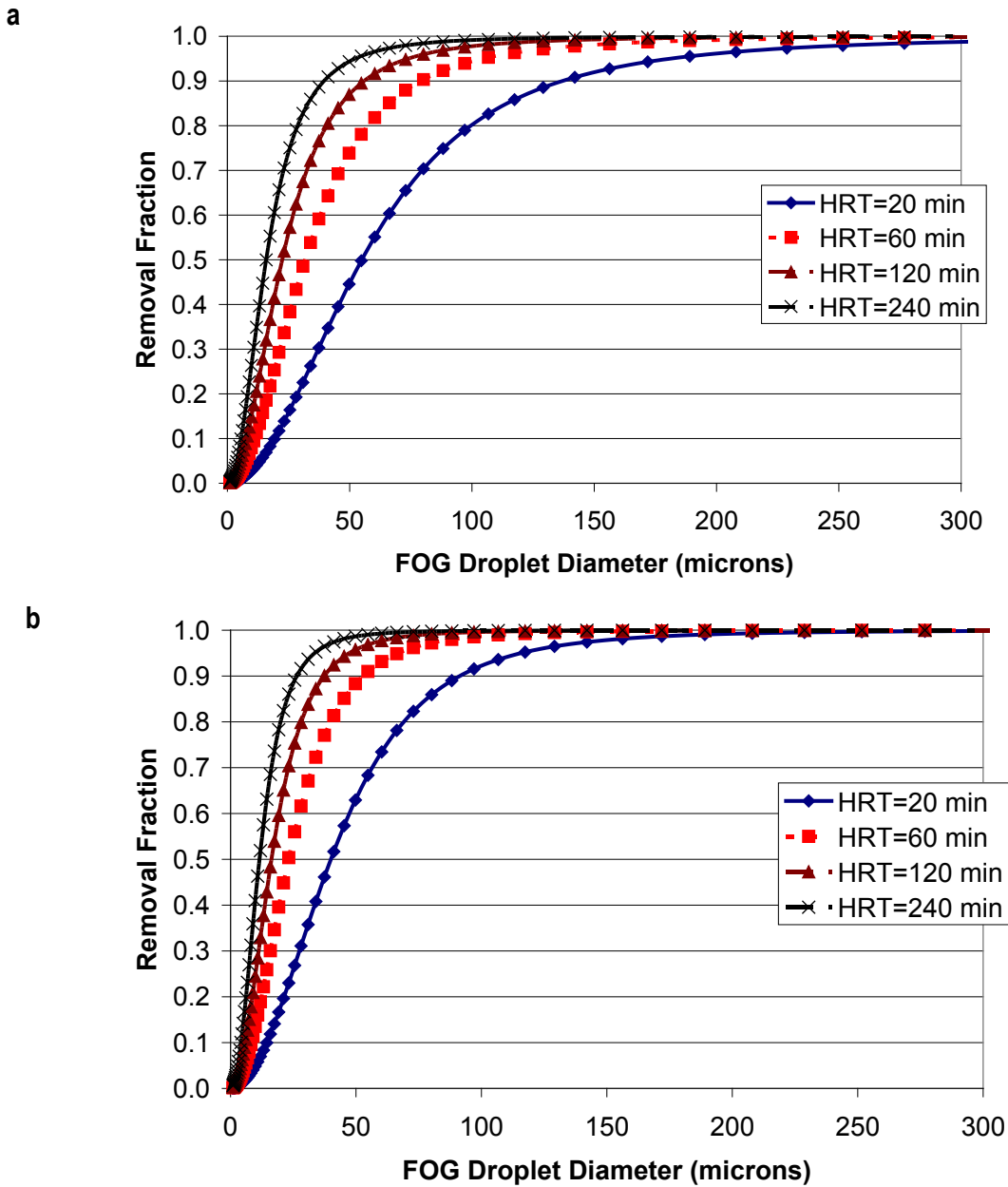
Figure 5-35. Fraction of Removal for Different FOG Globule Sizes:
a) N =1.5 for N Tanks in Series RTD Model, b) N =2.0 for N Tanks in Series RTD Model.
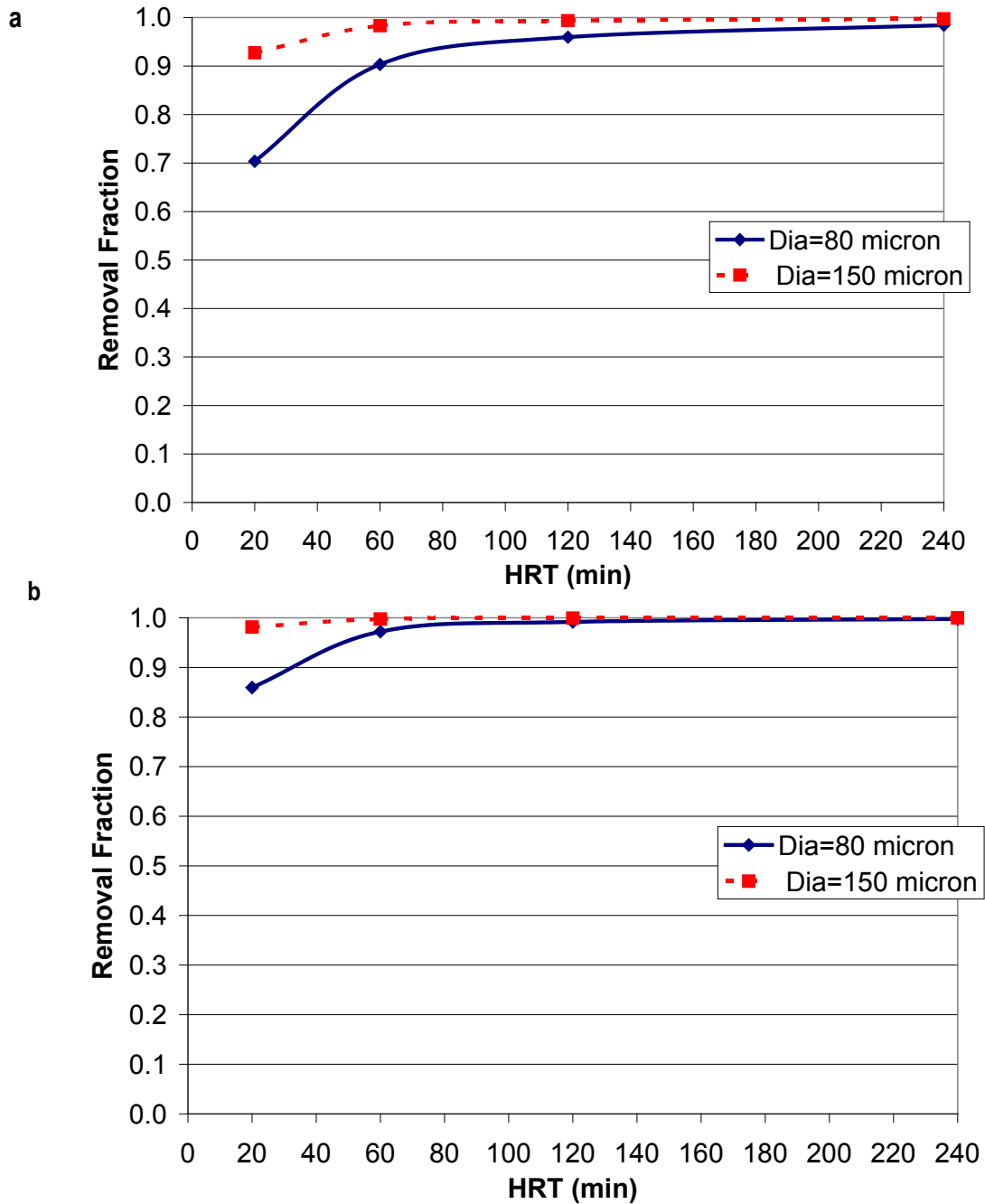
Figure 5-36. Fraction of Removal for 80 and 150 Micron FOG Globule Sizes:
a) N =1.5 for N Tanks in Series RTD Model, b) N =2.0 for N Tanks in Series RTD Model.

WERF

CHAPTER 6.0

CONCLUSIONS AND RECOMMENDATIONS

6.1   Conclusions

In this study, researchers analyzed field grease interceptors during their maturation cycle, conducted controlled laboratory experiments to assess the FOG removal performance of grease interceptors under different operating conditions and design configurations, and simulated grease interceptors to evaluate the use of numerical tools in the assessment and design of grease interceptors.

The analysis of field grease interceptors has revealed that they experience very dynamic influent conditions with time scales of fluctuations on the order of minutes for many different compounds. While peak flows of 3 to 7 times greater than average move through the grease interceptor on a daily basis, the 90% flow condition on the cumulative distribution curve reveals that average flow is 1/3 the peak flow. Consequently, a majority of the FSE waste stream, over the course of a 24-hour period, experience residence times that are on the order of hours. The field results also reveal an environment in the grease interceptor that is primarily acidic, with pH values between 4 and 6 in the bulk region, with influent pH values that are basic (i.e., pH>8). In addition, the dissolved oxygen concentration within the grease interceptor is very low (i.e., values below 0.5 mg/L) with influent values close to 4 mg/L.

The pH and DO values suggest that significant microbial activity within the grease interceptor and the environment is anaerobic. The spatial pattern of solids and FOG accumulation within the grease interceptor depends on the influent pipe configuration and the cleaning cycle of the grease interceptor. Observations of grease interceptors with inappropriate cleaning cycles have shown that solids can be transported into the second compartment and potentially into the effluent. Moreover, the standard pipe configuration can exacerbate this transfer of solids into the second compartment as this configuration generates higher velocities around the influent pipe that can scour the settled solids in the first compartment.

As a result of the analysis of grease interceptor performance, the researchers concluded:

♦ Extending the residence time in a standard GI by a factor of 3 only yielded a 10% improvement in performance, suggesting that FOG loading is only one of the factors affecting performance.
♦ FOG droplet size significantly affected FOG removal performance.
♦ Decrease in GI separation efficiency will result with the use of detergents and mixing while cleaning in-kitchen FOG wastes.
♦ Inlet/out configurations must be designed to distribute the flow.
♦ More effective FOG separation was achieved when fluid velocities near the inlet and outlet were kept below 0.015 m/s.
♦ Only include baffle walls with specific inlet/outlet configurations.
♦ Design baffle wall to distribute the flow and minimize the occurrence of high local fluid velocities.

♦ Improvement to standard GIs may be achieved by retrofitting them with better inlet and outlet tees.

Controlled laboratory experiments revealed that the removal efficiency of the standard grease interceptor configuration can be improved by making simple geometric changes. These changes can achieve percent removals similar to grease interceptors operated at three times the theoretical residence times (i.e., moving from 20 minutes to 1 hour). Influent configurations that incorporate a distributed inlet pipe allowed for more efficient separation with a greater accumulation of FOG and solids closer to the inlet part of the grease interceptor. Numerical modeling revealed complex spatial velocity profiles that clearly show why certain geometric configurations can improve FOG separation and why others can cause detrimental effects on the separation performance. Moreover, modeling results showed reasonable agreement with the controlled experiments. The results of the laboratory experiments are presented in Table 6-1.

Table 6-1. Summary of Results from the Assessment of the Performance of Grease Interceptors in Controlled Laboratory Experiments.

Experimental Configuration of a Grease Interceptor	% Removal
20 minute Standard Configuration	78
20 minute Standard Configuration (No Baffle)	86
1 hour Standard Configuration	90
20 minute Distributive Inlet/Distributive Baffle	87
20 minute Distributive Inlet (No Baffle)	69
20 minute Flared Inlet/Flared Outlet/Hanging Baffle	83
20 minute Short Inlet Pipe (No Baffle)	85

6.2   Future Research Considerations

As an indirect outcome of this study, the results showed that the U.S. EPA Method 1664 for measurement of oil and grease displayed significant variability when measuring known concentrations of total oil and grease. Variability in the measured concentration was approximately 40%, making it impossible to confirm or refute whether the grease interceptor is achieving the required effluent limit. Without a reliable analytical approach, it will be impossible for a municipality to enforce a discharge limit. Consequently, future research must develop a more reliable and valid total oil and grease analytical measurement technique.

While improvements in removal performance by grease interceptors can be achieved with geometric modifications to the inlet and outlet pipe configuration as well as modifications to the mid-baffle wall, the results of this study show that FOG removal performance did not surpass approximately 80-90%. The modifications examined were limited to designs that still allowed for ease of pump out maintenance. Consequently, additional approaches for enhancing total oil and grease removal may be necessary to help achieve better than two log removal (i.e., 99%).

The CFD simulations of grease interceptors were performed in this study only with the FOG and water phases due to computational requirements of the 3D model. Actual grease interceptors remove solids along with FOG. These solids may impact the FOG removal process and change the fluid flow pattern within the grease interceptor. More advanced models should include three phases: FOG, water, and solids.

WERF

REFERENCES

Ahrens, J.F.; Leonard, O.A.; Townley N., 1970, Chemical Control of Tree Roots in Sewer Lines. *Water Pollution Control Federation,* 42**,** 1643.

AOAC., 1995, Method 996.06 – Fat (Total, Saturated, and Monounsaturated) in Foods. Hydrolytic Extraction Gas Chromatographic Method. Chapter 41 in *Official Methods of Analysis of AOAC International*; 16th edition. Volume II. AOAC International: Arlington, VA.

AOAC, 1995, AOAC Official Method 983.23 - Fat in Foods. Chapter 45 in Official Methods of Analysis of AOAC International 16th edition, Volume II. AOAC International. Arlington, VA.

API, 1969, *Manual on Disposal of Refining Wastes;* American Petroleum Institute, Division of Refining: New York, NY.

ASAE, 2003, Moisture Measurement - Forages. S358.2. American Society of Agricultural and Biological Engineers. St. Joseph, MI 49085.

ASTM, 1999, Standard for Measuring Contact Angle. *American Society for Testing and Materials,* West Conshohocken, PA.

American Society Plumbing Engineers (ASPE) ,1999, Page 63.

Bloechle, W, 2004, *Measuring Surface Roughness with an Optical Sensor*. Hohner Corporation.

Chu, W. and Ng, F., 2000, Upgrading the conventional grease trap using a tube settler, Environment International, 26, pp. 17-22.

Code of Federal Regulations, 2002, Title 40 Part 122.42. (f). US Government Printing Office, Washington, D.C.

Cutler, D.F. and Richardson, B.K., 1989, *Tree roots and buildings, 2nd Ed*., Longman Scientific and Technical, Harlow, U.K.

Danielson, R.E. and Southerland, P.L., 1986, *18-2.2 Gas Pycnometer Method.* In *Methods of Soil Analysis. Part 1, Physical and Mineralogical Methods.* Second Edition. Klute, A. Ed.; American Society of Agronomy and Soil Science Society of America Inc.; Madison, WI.

Duke's Root Control Inc., 2007, Company Website. http://www.dukes.com/whyRootControl/howitworks.html.

Diemer, R.B. and Olson, J.H., 2002. A moment methodology for coagulation and breakage problems: Part 3-generalized daughter distribution functions. *Chemical Engineering Science*, vol.5**7** no.19, pp 4187-4198.

Fletcher, C.A.J., 1991, *Computational Techniques for Fluid Dynamics Vol. I: Fundamentals and General Techniques*, Springer-Verlag, Berlin, Germany.

Fankel, M., 2004. Recommendations for Designing Grease Interceptors. National Precast Concrete Association. May 2004.

Gardner, W.H., 1986; *21-2.2 Gravimetry with Oven Drying.* In *Methods of Soil Analysis. Part 1, Physical and Mineralogical Methods.* Second Edition. Klute, A. Ed.; American Society of Agronomy and Soil Science Society of America Inc.; Madison, WI.

Gordon, R.G., 1968, Errors bounds in equilibrium statistical mechanics. *Journal of Mathematical Physics, 9*(5), 655-663.

Harris, R. V., Clark, J. R., and Matheny, N. P., 1999, *Arboriculture, integrated management of landscape trees, shrubs, and vines*. 3rd Ed., Prentice-Hall, Upper Saddle River, N.J.

Hee, C., Martyn, Paul C., Kremer, Jay G., 2006, Removal of Oil and Grease in Oil Processing Wastewaters.

Infracal User Manual

 IAMPO (2004). Uniform Plumbing Code, Appendix H: Recommended Procedures for Design, Construction, and Installation of Commercial Kitchen Grease Interceptors, IAMPO - UPC. 2007.

Levitt, B., 1951, *Oil, Fat, and Soap*; Chemical Publishing Company Inc.: New York, NY.

Martin, G., 1931, *The Modern Soap and Detergent Industry. Volume I – Theory and Practice of Soapmaking*; Technical Press Ltd.: London, England.

Matsui, T., Miura, A., Iiyama, T., Shinzato, N., Matsuda, H, and Furuhashi, K., 2005, Effect of fatty oil dispersion on oil-containing wastewater treatment. *J. Haz. Mat.*, B118, 255–258.

McGraw, R.,1997, Description of aerosol dynamics by the quadrature method of moments. *Aerosol Science and Technology, 27*, 255-265.

Mohr, M., 1979, *The Art of Soap Making*; Firefly Books Ltd.: Willowdale, Ontaria.

Morgan, B., 1995, Separate Sanitary Overflows: What Do We Currently Know? *Association of Metropolitan Sewerage Agencies*, January 9.

NPCA, 2007, Design Considerations and Discussion of Large Outdoor Grease Interceptors, National Precast Concrete Association.

Pericleous, K.A. and Rhodes, N., 1986, The Hydrocylone Classifier-a Numerical Approach, International Journal of Mineral Processing, 17, pp 23-43.

Pericleous, K.A., 1987, Mathematical Simulation of Hydrocyclones, Applied Math and Modeling, Vol. II (4), pp 242-255.

Prins et. al., 1999, *Sewer Benchmarking Study Provides Operation and Maintenance Guidelines,* Proceedings of WEFTEC '99.

Randrup, T.B., 2001, *Occurrence of tree roots in Danish municipal sewer systems. Int. Workshop on Tree Root Devel. in Urban Soils*, Landscape Below. Arboricultural J., Hereford, U.K

Russell, R.S., 1977, *Plant root systems: Their function and interaction with the soil,* McGraw-Hill, New York.

SAS., 1996, Statistical Analysis Software. Version 6.12. SAS Institute Inc: Cary, NC.

Schrock, B.J., 1994, *Existing sewer evaluation and rehabilitation. Prepared by Joint Task Force of Water Envir. Fedn. and ASCE*, WEF Manual of Pract. FD-6, ASCE Manuals and Rep. on Engrg. Pract. No. 62, 2nd Ed., ASCE, New York.

WERF

Southerland, R. 2002. *Sewer Fitness: Cutting the Fat*. American City and Country. 117(15): 27-31.

Stoll, U. and Gupta, H. 1997. Management Strategies for Oil and Grease Residue, Waste Management & Research, Vol.15, pp. 23-32.

Stauffer, C.E., 1996, *Fats & Oils*. Eagan Press: St. Paul, MN.

U.S. EPA., 2001, Method 200.7: Determination of Metals and Trace Elements in Water and Wastes by Inductively Coupled Plasma- Atomic Emission Spectrometry; Revision 5.0. EPA-821-R-01-010; U.S. Environmental Protection Agency: Washington, D.C., January.

U.S. EPA., 1994, Method 9071A: Oil and Grease Extraction Method for Sludge and Sediment Samples; Revision 1.0; U.S. Environmental Protection Agency: Washington, D.C., September.

U.S. EPA., 2007, Why Control Sanitary Sewer Overflows? http://www.epa.gov/npdes/sso/control/index.htm; U.S. Environmental Protection Agency: Washington, D.C.; 2003. Last accessed February 3.

U.S. EPA, 1995, *Method 1664: N-Hexane Extractable Material (HEM) and Silica Gel Treated N-Hexane Extractable Material (SGT-HEM) by Extraction and Gravimetry (Oil and Grease and Total Petroleum Hydrocarbons)*; EPA Method; United States Environmental Protection Agency: Washington, D.C. 20460; EPA-821-V-94-004b.

U.S. EPA., 2001, Fact Sheet: *EPA Takes Action to Protect the Nation's Beaches from Health Threats Posed by Raw Sewage Overflows*, Available online at: http://www.epa.gov/npdes/pubs/sso-pressrelease.pdf.

Warsi, Z.U.A., 1993, *Fluid Dynamics: Theoretical and Computational Approaches*, CRC Press Inc., Boca Raton, FL.

Wakelin, N.G. and Forster, C.F. "Bioresource Technology." An Investigation into Microbial Removal of Fats, Oils and Greases 59.1 (1997): 37-43.

WERF

WASTEWATER UTILITY

Alabama
Montgomery Water Works & Sanitary Sewer Board

Alaska
Anchorage Water & Wastewater Utility

Arizona
Glendale, City of, Utilities Department
Mesa, City of
Peoria, City of
Phoenix Water Services Dept.
Pima County Wastewater Management
Safford, City of
Tempe, City of

Arkansas
Little Rock Wastewater Utility

California
Central Contra Costa Sanitary District
Corona, City of
Crestline Sanitation District
Delta Diablo Sanitation District
Dublin San Ramon Services District
East Bay Dischargers Authority
East Bay Municipal Utility District
Eastern Municipal Water District
El Dorado Irrigation District
Fairfield-Suisun Sewer District
Fresno Department of Public Utilities
Inland Empire Utilities Agency
Irvine Ranch Water District
Las Virgenes Municipal Water District
Livermore, City of
Los Angeles, City of
Los Angeles County, Sanitation Districts of
Napa Sanitation District
Orange County Sanitation District
Palo Alto, City of
Riverside, City of
Sacramento Regional County Sanitation District
San Diego Metropolitan Wastewater Department, City of
San Francisco, City & County of
San Jose, City of
Santa Barbara, City of
Santa Cruz, City of
Santa Rosa, City of
South Bayside System Authority
South Coast Water District
South Orange County Wastewater Authority

Stege Sanitary District
Sunnyvale, City of
Union Sanitary District
West Valley Sanitation District

Colorado
Aurora, City of
Boulder, City of
Greeley, City of
Littleton/Englewood Water Pollution Control Plant
Metro Wastewater Reclamation District, Denver

Connecticut
Greater New Haven WPCA
Stamford, City of

District of Columbia
District of Columbia Water & Sewer Authority

Florida
Broward, County of
Fort Lauderdale, City of
Jacksonville Electric Authority (JEA)
Miami-Dade Water & Sewer Authority
Orange County Utilities Department
Reedy Creek Improvement District
Seminole County Environmental Services
St. Petersburg, City of
Tallahassee, City of
Tampa, City of
Toho Water Authority
West Palm Beach, City of

Georgia
Atlanta Department of Watershed Management
Augusta, City of
Clayton County Water Authority
Cobb County Water System
Columbus Water Works
Fulton County
Gwinnett County Department of Public Utilities
Savannah, City of

Hawaii
Honolulu, City & County of

Idaho
Boise, City of

Illinois
Decatur, Sanitary District of
Greater Peoria Sanitary District
Kankakee River Metropolitan Agency
Metropolitan Water Reclamation District of Greater Chicago
Wheaton Sanitary District

Iowa
Ames, City of

Cedar Rapids Wastewater Facility
Des Moines, City of
Iowa City

Kansas
Johnson County Wastewater
Unified Government of Wyandotte County/ Kansas City, City of

Kentucky
Louisville & Jefferson County Metropolitan Sewer District
Sanitation District No. 1

Louisiana
Sewerage & Water Board of New Orleans

Maine
Bangor, City of
Portland Water District

Maryland
Anne Arundel County Bureau of Utility Operations
Howard County Bureau of Utilities
Washington Suburban Sanitary Commission

Massachusetts
Boston Water & Sewer Commission
Massachusetts Water Resources Authority (MWRA)
Upper Blackstone Water Pollution Abatement District

Michigan
Ann Arbor, City of
Detroit, City of
Holland Board of Public Works
Saginaw, City of
Wayne County Department of Environment
Wyoming, City of

Minnesota
Rochester, City of
Western Lake Superior Sanitary District

Missouri
Independence, City of
Kansas City Missouri Water Services Department
Little Blue Valley Sewer District
Metropolitan St. Louis Sewer District

Nebraska
Lincoln Public Works and Utilities Department

Nevada
Henderson, City of
Las Vegas, City of
Reno, City of

New Jersey
Bergen County Utilities Authority
Ocean County Utilities Authority

Passaic Valley Sewerage Commissioners

New York
New York City Department of Environmental Protection

North Carolina
Charlotte/Mecklenburg Utilities
Durham, City of
Metropolitan Sewerage District of Buncombe County
Orange Water & Sewer Authority
University of North Carolina, Chapel Hill

Ohio
Akron, City of
Butler County Department of Environmental Services
Columbus, City of
Metropolitan Sewer District of Greater Cincinnati
Montgomery, County of
Northeast Ohio Regional Sewer District
Summit, County of

Oklahoma
Oklahoma City Water & Wastewater Utility Department
Tulsa, City of

Oregon
Albany, City of
Clean Water Services
Eugene, City of
Gresham, City of
Portland, City of Bureau of Environmental Services
Water Environment Services

Pennsylvania
Hemlock Municipal Sewer Cooperative (HMSC)
Philadelphia, City of
University Area Joint Authority

South Carolina
Charleston Water System
Mount Pleasant Waterworks & Sewer Commission
Spartanburg Water

Tennessee
Cleveland Utilities
Knoxville Utilities Board
Murfreesboro Water & Sewer Department
Nashville Metro Water Services

Texas
Austin, City of
Dallas Water Utilities
Denton, City of
El Paso Water Utilities
Fort Worth, City of
Houston, City of
San Antonio Water System

Trinity River Authority

Utah
Salt Lake City Corporation

Virginia
Alexandria Sanitation Authority
Arlington, County of
Fairfax County
Hampton Roads Sanitation
District
Hanover, County of
Henrico, County of
Hopewell Regional
Wastewater Treatment
Facility
Loudoun Water
Lynchburg Regional WWTP
Prince William County
Service Authority
Richmond, City of
Rivanna Water & Sewer
Authority

Washington
Everett, City of
King County Department of
Natural Resources
Seattle Public Utilities
Sunnyside, Port of
Yakima, City of

Wisconsin
Green Bay Metro
Sewerage District
Kenosha Water Utility
Madison Metropolitan
Sewerage District
Milwaukee Metropolitan
Sewerage District
Racine, City of
Sheboygan Regional
Wastewater Treatment
Wausau Water Works

Australia
ACTEW (Ecowise)
South Australian Water
Corporation
South East Water Limited
Sydney Water Corporation
Water Corporation of
Western Australia

Canada
Edmonton, City of/Edmonton
Waste Management Centre
of Excellence
Lethbridge, City of
Regina, City of,
Saskatchewan
Toronto, City of, Ontario
Winnipeg, City of, Manitoba

New Zealand
Watercare Services Limited

STORMWATER UTILITY

California
Fresno Metropolitan Flood
Control District
Los Angeles, City of,
Department of Public Works
Monterey, City of
San Francisco, City & County of
Santa Rosa, City of
Sunnyvale, City of

Colorado
Aurora, City of
Boulder, City of

Florida
Orlando, City of

Georgia
Griffin, City of

Iowa
Cedar Rapids Wastewater
Facility
Des Moines, City of

Kansas
Overland Park, City of

Kentucky
Louisville & Jefferson County
Metropolitan Sewer District

Maine
Portland Water District

North Carolina
Charlotte, City of,
Stormwater Services

Pennsylvania
Philadelphia, City of

Tennessee
Chattanooga Stormwater
Management

Texas
Harris County Flood Control
District, Texas

Washington
Bellevue Utilities Department
Seattle Public Utilities

STATE

Connecticut Department of
Environmental Protection
Kansas Department of Health
& Environment
New England Interstate
Water Pollution Control
Commission (NEIWPCC)
Ohio River Valley Sanitation
Commission
Urban Drainage & Flood
Control District, CO

CORPORATE

ADS Environmental Services
Advanced Data Mining
International
Alan Plummer & Associates
Alpine Technology Inc.
Aqua-Aerobic Systems Inc.
Aquateam–Norwegian Water
Technology Centre A/S
ARCADIS
Associated Engineering
Black & Veatch
Blue Water Technologies, Inc.

Boyle Engineering
Corporation
Brown & Caldwell
Burgess & Niple, Ltd.
Burns & McDonnell
CABE Associates Inc.
The Cadmus Group
Camp Dresser & McKee Inc.
Carollo Engineers Inc.
Carpenter Environmental
Associates Inc.
Carter & Burgess, Inc.
CET Engineering Services
CH2M HILL
CRA Infrastructure &
Engineering
CONTECH Stormwater
Solutions
D&B/Guarino Engineers, LLC
Damon S. Williams
Associates, LLC
Earth Tech Inc.
Ecovation
EMA Inc.
Environmental Operating
Solutions, Inc.
Environ/The ADVENT Group,
Inc.
Fay, Spofford, & Thorndike Inc.
Freese & Nichols, Inc.
ftn Associates Inc.
Gannett Fleming Inc.
Garden & Associates, Ltd.
Geosyntec Consultants
GHD
Golder Associates Ltd.
Greeley and Hansen LLC
Hazen & Sawyer, P.C.
HDR Engineering Inc.
HNTB Corporation
Hydromantis Inc.
HydroQual Inc.
Infilco Degremont Inc.
Jacques Whitford NAWE, Inc.
Jason Consultants LLC Inc.
Jordan, Jones, & Goulding Inc.
KCI Technologies Inc.
Kelly & Weaver, P.C.
Kennedy/Jenks Consultants
KMK Consultants
Larry Walker Associates
Limno-Tech Inc.
The Low Impact Development
Center Inc.
Malcolm Pirnie Inc.
Material Matters
McKim & Creed
Metcalf & Eddy Inc.
MPR Engineering
Corporation, Inc.
MWH
O'Brien & Gere Engineers Inc.
Odor & Corrosion Technology
Consultants Inc.
Paradigm Environmental
Technologies, Inc.

Parametrix Inc.
Parsons
Post, Buckley, Schuh & Jernigan
Praxair, Inc.
Ring Industrial Group
RMC Water & Environment
Ross & Associates Ltd.
SAIC
Siemens Water Technologies
The Soap & Detergent
Association
Smith & Loveless, Inc.
Stantec Consulting Inc.
Stearns & Wheler, LLC
Stone Environmental Inc.
Stratus Consulting Inc.
Synagro Technologies Inc.
Tetra Tech Inc.
Trojan Technologies Inc.
Trussell Technologies, Inc.
Uni-Bell PVC Pipe Association
URS Corporation
Westin Engineering Inc.
Weston Solutions Inc.
Woodard & Curran
Zoeller Pump Company

INDUSTRY

American Electric Power
American Water
Anglian Water Services, Ltd.
ChevronTexaco Energy
Research & Technology
Company
The Coca-Cola Company
Dow Chemical Company
DuPont Company
Eastman Chemical Company
Eli Lilly & Company
Merck & Company Inc.
Procter & Gamble Company
Suez Environnment
United Utilities North West
(UUNW)
United Water Services LLC

Note: List as of 8/11/08

WERF Product Order Form

As a benefit of joining the Water Environment Research Foundation, subscribers are entitled to receive one complimentary copy of all final reports and other products. Additional copies are available at cost (usually $10). To order your complimentary copy of a report, please write "free" in the unit price column. WERF keeps track of all orders. If the charge differs from what is shown here, we will call to confirm the total before processing.

_____

Name   Title

_____

Organization

_____

Address

_____

City   State   Zip Code   Country

_____

Phone   Fax   Email

Stock #	Product	Quantity	Unit Price	Total
			Postage & Handling	
			VA Residents Add 5% Sales Tax	
			Canadian Residents Add 7% GST	

Method of Payment: (All orders must be prepaid.)

❑ Check or Money Order Enclosed

❑ Visa   ❑ Mastercard   ❑ American Express

_____

Account No.   Exp. Date

_____

Signature

TOTAL ▶ [   ]

Shipping & Handling:

Amount of Order	United States	Canada & Mexico	All Others
Up to but not more than:	Add:	Add:	Add:
$20.00	$7.50*	$9.50	50% of amount
30.00	8.00	9.50	40% of amount
40.00	8.50	9.50	
50.00	9.00	18.00	
60.00	10.00	18.00	
80.00	11.00	18.00	
100.00	13.00	24.00	
150.00	15.00	35.00	
200.00	18.00	40.00	
More than $200.00	Add 20% of order	Add 20% of order	

*minimum amount for all orders

Note: Please make checks payable to the Water Environment Research Foundation.

To Order (Subscribers Only):

Log on to www.werf.org and click on "Publications."

Phone: (703) 684-2470
Fax: (703) 299-0742

WERF
Attn: Subscriber Services
635 Slaters Lane
Alexandria, VA 22314-1177

To Order (Non-Subscribers):

Non-subscribers may be able to order WERF publications either through WEF (www.wef.org) or IWAP (www.iwapublishing.com).Visit WERF's website at www.werf.org for details.